AD-A136 957 MICRODOSIMETRIC MEASUREMENTS ON NUCLEAR REACTIONS(U) 1/2
CLARKSON COLL OF TECHNOLOGY POTSDAM N Y DEPT OF PHYSICS
P J MCNULTY 1983 SBI-AD-E001 638 N00014-81-K-2011
UNCLASSIFIED F/G 20/8 NL

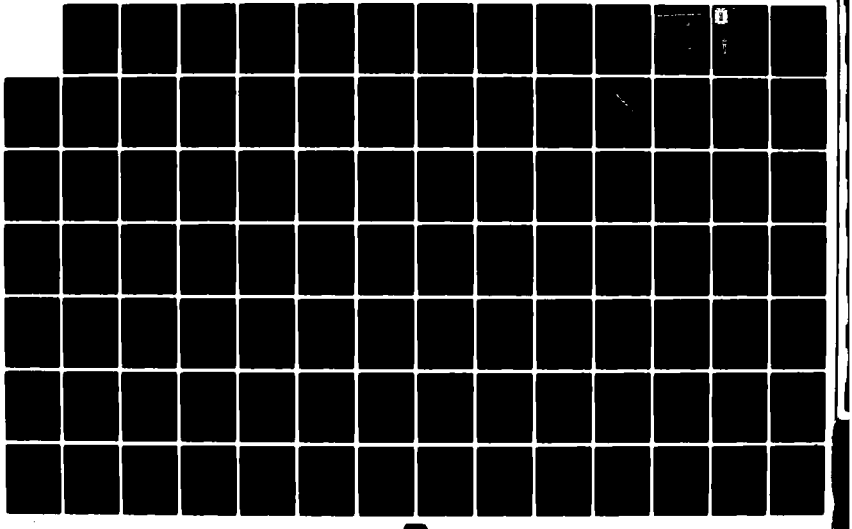

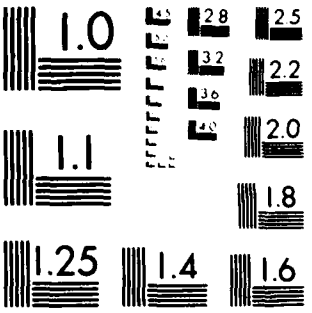

(12)

FINAL TECHNICAL REPORT

Submitted to

Naval Research Laboratory

MICRODOSIMETRIC MEASUREMENTS ON NUCLEAR REACTIONS

Prepared by

Peter J. McNulty
Professor of Physics
Soc. Sec. No.: 087-32-9340
(315) 268-2344

NAVAL RESEARCH LABORATORY
Contract No.: N0014-81-K-2011

TABLE OF CONTENTS

I. INTRODUCTION

The major effort on this one year contract was to develop a computer simulation model of nuclear interactions induced by energetic protons. The effort funded by the DNA-DARPA Program through NRL was the earliest stage of this program. A no-cost extension of the work allowed us to continue this effort until the completion of G. Farrell's Ph.D. thesis. A portion of our continued effort was funded by RADC.

The thesis is included as Appendix C and represents the results of the theoretical program initiated with NRL support.

Our analysis indicates that the recoiling nuclear fragment is the dominant contributor to large-energy depositions in small volume elements.

This knowledge may allow considerable simplification in calculating proton-induced error rates.

II. PAPERS PUBLISHED AND STUDENTS AND THESES SUPPORTED

A. PAPERS PUBLISHED

1. P.J. McNulty, G.E. Farrell, and W.P. Tucker, "Proton-Induced Nuclear Reactions in Silicon", IEEE Trans. Nucl. Sci. NS-28, 4007-4012 (1981).

2. P.J. McNulty, "Charged Particles Cause Microelectronics Malfunction in Space," Physics Today (Guest Comment) 36, 9 (1983).

B. STUDENT AND THESIS SUPPORTED

G.E. Farrell (Ph.D., 1983) Energy Deposition by Nuclear Interactions in Microscopic volumes.

IEEE Transactions on Nuclear Science, Vol. NS-28, No. 6, December 1981

PROTON-INDUCED NUCLEAR REACTIONS IN SILICON*

Peter J. McNulty and Gary E. Farrell
Department of Physics
Clarkson College of Technology
Potsdam, New York 13676

William P. Tucker
Physics Department
Florida A and M University
Tallahassee, Florida 32307

ABSTRACT

Measurements of the energy deposited in silicon surface-barrier detectors as a result of proton-induced nuclear reactions were carried out at the Harvard Cyclotron for protons with incident energies ranging from 50 to 158 MeV and detectors with thicknesses of 2.5, 4.2, 24.1, 100, and [illegible] μm. The number of events in which a given thre[illegible]mount of energy is deposited in a 4.2 μm det[illegible]ried with incident proton energy in a manner sim[illegible]to previous measurements of the proton-induced s[illegible]-error cross section. The number of events in whic[illegible].t least a threshold amount of energy was deposited in the detector fell off in a near exponential manner with increasing threshold energy. The data were found to be in reasonable agreement with a computer simulation model developed in our laboratory. The model is used to illustrate how the mass spectra of the residual nuclear fragments shifts towards lower masses with increasing recoil energy. Lighter recoils have longer ranges and a greater chance of leaving a microscopically thin sensitive volume element before coming to their end of range.

Introduction

The nuclear interaction provides a mechanism whereby an energetic lightly ionizing particle or non-ionizing neutron can deposit a large amount of energy within a volume element that has microscopic dimensions. The incident particle interacts with one of the nuclei of the material in or about the target volume. Most of the energy deposition takes the form of ionization loss along the trajectories of the charged secondary particles emerging from the "struck" nucleus and along the trajectory of the recoiling residual nuclear fragment. Large numbers of electron-hole pairs are generated as a result of this ionization loss. If such a nuclear event takes place within or near one of the sensitive elements on a large scale integrated (LSI) RAM memory device and sufficient charge is generated, the result can be a change in the logic state of the memory element. The alteration of information stored at some location in memory without observable physical damage to the device is called a soft error or bit upset.

Energetic protons have been shown to induce soft errors in a number of LSI dynamic and static RAM devices, [1-5] presumably through (p,α) reactions at low proton energies[1,6,7] and more complex reactions at higher energies.[2,5,8] Besides providing a potential mechanism for soft errors in space, proton-induced nuclear reactions have been proposed to explain anomalous signals observed in Defense Meteorological Satellite Program (DMSP)[9] and LANDSAT satellite systems[10] as well as the light flashes observed by astronauts on Skylab.[11,12]

This paper describes a study of nuclear interactions using silicon surface-barrier detectors of varying thickness ranging from 2.5 to 200 μm. The objective of the study is to provide data on the deposition of energy in volume elements having microscopic dimensions as an aid to developing models capable of predicting event rates to be expected for devices of different geometries exposed to protons with a given energy distribution. Some preliminary results on 24.1 μm thick detectors were included in last year's paper.[5]

Surface Barrier Detectors

Figure 1 shows a schematic cross section of a section of a thin transmission-type silicon surface-barrier detector. The front and back surfaces are 400 μgm/cm^2 layers of gold and aluminum, respectively. They provide the electrical contacts of the detector, and voltage applied across them (bias) results in a uniform field through the silicon slab. Each detector used in this study was run at sufficient bias to ensure that the detector volume was fully depleted. The charge generated within the slab from ionization-loss processes is swept by the applied field to the electrodes. The silicon slab portions of the detector varied in thickness from 2.5 to 200 μm. Energetic protons incident normal to the detector may interact with nuclei in the silicon slab, in one of the contacts or in the air. Only in the thinnest detectors do a significant fraction of the interactions occur outside the silicon slab.

Table 1. Thickness and Areas of Silicon Layers of the Surface Barrier Detectors Exposed.

Thickness (μm)	2.5	4.1	24.1	100	200
Area (mm^2)	25	25	25	25	200

Only those segments of the trajectories of the secondary particles emerging from the interactions that traverse the silicon slab or generate charges that migrate to the slab contribute to the observed signal. Most of the secondary particles emerging from a nuclear interaction in a thin detector leave the silicon slab before depositing significant energy (> 1 MeV). This is shown schematically in Fig. 1. The exception is the nuclear recoil. The recoiling nuclear fragments have short range and most can be expected to deposit their entire energy within all but the thinnest detectors.

* Supported in part by the Defense Nuclear Agency through Naval Research Laboratory contract N00014-81-K-2011. The help of A. Koehler and the staff of the Harvard Cyclotron are gratefully acknowledged.

0018-9499/81/1200-4007$00.75©1981 IEEE

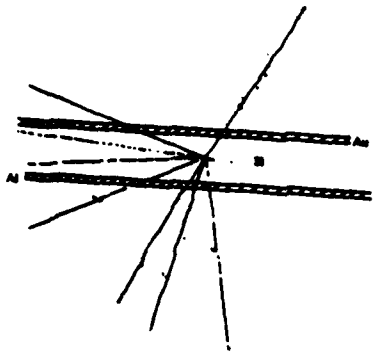

Figure 1. Schematic of a nuclear reaction occurring in a thin transmission-type silicon surface barrier detector.

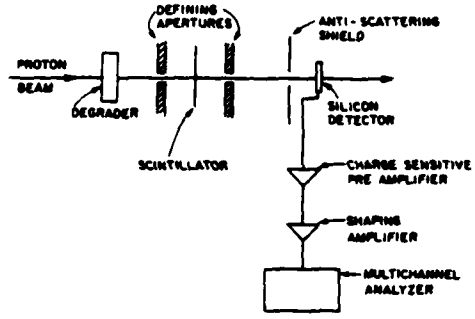

Figure 2. Experimental configuration for exposures carried out at the Harvard Cyclotron. Scintillators mounted behind the detector and upstream between the collimators were used to monitor the beam.

The question arises as to whether energy-deposition measurements using these detectors with their relatively large sensitive areas (25 mm^2) provide data that are relevant to energy deposition in the sensitive volumes of LSI devices where three dimensions are microscopic instead of one. First, the data obtained with detectors can be directly compared with models[13,14] which attempt to calculate the energy deposition spectra for volume elements of arbitrary size and shape. These models can then be used to calculate for volumes with dimensions appropriate for a given device. Second, many LSI devices have sensitive volumes whose lateral dimensions are high multiples of their thickness. The reader is referred to Bradford's paper[15] for a detailed discussion of the distribution of track segments in volume elements and the approximations involved. Because our own calculations suggest that the nuclear recoil with its short range is an increasingly important contributor as the dimensions of the volume element decrease and the threshold energy increases, we feel that the energy deposition data from the thinnest detectors may be a reasonable approximation for LSI devices with comparable thicknesses and lateral dimensions at least five times the thickness.

Irradiations

The proton exposures were carried out at the Harvard Cyclotron. The experimental configuration used for these exposures is shown in Fig. 2. The beam energy was selected by inserting appropriate degraders upstream. This report includes data from exposures to protons at 51, 91, 131, and 158 MeV. The beam incident on the detector was collimated by the two defining apertures. It was collimated to 2 mm in diameter for all but the 2.5 μm thick detector. For the latter the beam was uniform over dimensions considerably larger than the detector. When the beam is collimated to 2 mm, most of the beam protons emerging from the cyclotron interact in the collimator walls or the degrader blocks. This generates a considerable background of secondary particles. After each exposure was completed a second run was carried out with the downstream aperture replaced by a beam plug. The plug prevents any primaries from reaching the detector. The plug-in runs were used to provide an estimate of background due to interactions that occur outside the detector.

The 2 mm beam exposures were monitored by two scintillators, one just downstream of the detector (not shown) and a second upstream between the first and second apertures. The upstream counter did not cover the central portion of the proton beam. Plug-in and plug-out runs were carried out for the same number of counts on the upstream scintillator. The data presented in the paper have the plug-in spectra subtracted.

The 2.5 μm detector was monitored by a ionization chamber upstream of the detector. This allowed us to increase the beam count rate from slightly less than 10^6 protons/minute to about 10^9 protons/minute. This was advantageous because of the sharp decrease in event rate in which more than a few MeV are deposited as the detectors become thinner.

Pulses in the bias voltage across the detector were shaped and suitably amplified in an Ortec 172B charge-sensitive preamplifier and an Ortec 572 amplifier before being recorded in a multichannel analyzer. The pulses should be proportional to the energy deposited by the beam protons entering the detector and any secondary particles generated through interactions inside or outside the detector. The detecting systems were calibrated before and after the experiment with a ^{241}Am alpha source and its linearity tested with a pulser. The pulse-height spectra obtained with the surface-barrier detectors minus plug-in background should then represent the spectra of energies deposited in the slab of silicon as a result of nuclear interactions.

Pulse-Height Spectra

The standard models [16-18] of soft errors in RAMs assume that if an amount of energy exceeding some critical or threshold value is deposited within a sensitive volume element an upset will occur and the deposition of less than a threshold amount of energy will not upset the element. This makes it instructive to plot pulse-height spectra as integral spectra, i.e., number of events in which the energy deposited in the slab is greater than or equal to E versus E. Typical integral spectra are plotted in Fig. 3 for 131 MeV protons. The 100 μm detector data are plotted for an exposure of 10^7 scintillation counts.

The 200 μm data represent 10^6 counts with the numbers multiplied by a factor of 2. The 4.2 μm data were multiplied by a factor of about 25 to fit them on the scale. The 2.5 μm data were obtained with an ionization chamber monitor but we estimate a scale factor of about 25. No corrections have been made for deadtime or other losses in the scintillation counters and the ordinate scale may underestimate the true fluence. The 24.1 μm detector was only monitored by the upstream scintillator and no absolute estimate of fluence was possible. It was arbitrarily normalized in Fig. 3 for convenient plotting. Squeezing the spectra onto one plot as we did in Fig. 3 facilitates comparison of the shapes and ranges of the spectra, the important parameters for the soft-error problem.

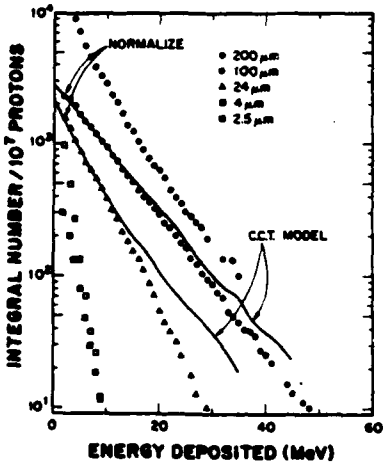

Figure 3. Integral spectra for energy deposition in thin detectors of various thicknesses for 131 MeV protons. The solid curves are the results of computer simulations carried out at Clarkson College of Technology (CCT) to roughly the same statistics. The 2.5 and 4.2 μm data were obtained for fluences 25 x 10^7 protons.

The integral spectra for the 2.5, 4.2, 24.1 and 100 μm spectra in Fig. 3 all appear to fall off near exponentially with the energy deposited. The 200 μm thick detector, on the other hand, exhibits a sharp decrease at low energies and parallels the 100 μm spectra at large energies. The 200 μm detector had a larger area (200 mm^2) than the other detectors (25 mm^2). Plug-in runs showed it to be subject to much greater background from interactions upstream, probably because it presented a larger cross-sectional area for secondaries generated upstream. These secondaries would generate low-energy pulses upon traversing the detector.

The 100 μm and 200 μm spectra illustrate the energies available from nuclear interactions. The data points beyond 10 events are not shown because of the poor statistics. The largest events for the 100 and 200 μm detectors were 76 and 90 MeV, respectively. The last 10 events would appear to gradually fall off to these end-point energies. Significant fractions of the events deposit 10, 20, 30, and even 40 MeV in the thick detectors. However, most of this energy is deposited over a volume that is considerably larger than a typical sensitive volume element on an LSI device. Reducing the thickness of the sensitive volume results in a corresponding reduction in large energy events. This is clearly illustrated in Fig. 3. Only one event with greater than 40 MeV deposited was obtained with the 24 μm detector. Reducing the thickness further results in a dramatic reduction in large-energy depositions. No events of greater than 20 MeV were seen in an exposure of the 4.2 μm detector to $1x10^7$ protons. There is, therefore, a sharp reduction in energy deposition when the thickness of the element is reduced. This will also be true for circuit elements on devices which have similar thickness and considerably smaller lateral dimensions.

Variation with Proton Energy

The integral spectra of Fig. 3 provide the number of events in which at least some threshold energy E is deposited in each of the detectors as a result of exposure to 10^7 protons incident at 131 MeV. The corresponding number of events exceeding this threshold value can similarly be obtained for the other incident proton energies. The number of events exceeding threshold per 10^7 protons (scintillation counts) is plotted versus incident proton energy for different values of the threshold for the 4.2 μm thick detector in Fig. 4a and for the 100 μm thick detector in Fig. 4b, respectively. In the case of the 100 μm detector the number of events for a given threshold increases with beam energy for threshold values from 2 to 45 MeV. Small changes in threshold result in correspondingly small changes in the number of events. The 4.2 μm data in Fig. 4a, on the other hand, shows evidence of peaking at 131 MeV for threshold energies from 5 to 8 Mev. Moreover, small changes in threshold result in substantial changes in the number of events - an increase in threshold of 1 MeV reduces the number by a factor of 2. The variation with incident beam energy exhibited by the 4.2 μm detector in Fig. 4a is similar in shape to the curves for soft-error cross sections versus proton energy presented in Ref. 2 for LSI dynamic and static RAMs. The considerable variation among devices of the same type reported in Ref. 2 may according to this analysis be due to relatively small variations in the critical charge (or energy) necessary for an upset.

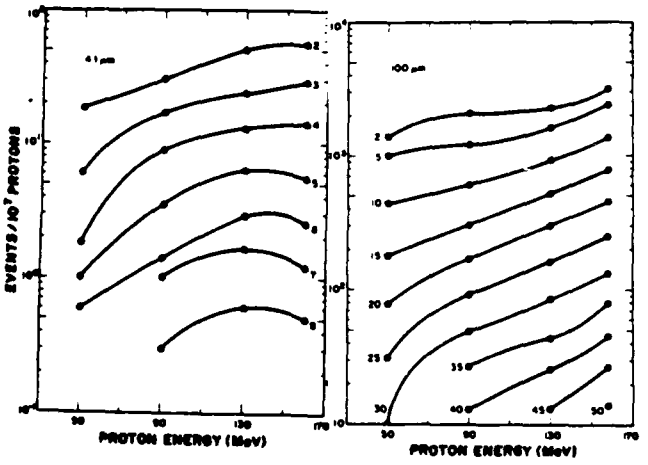

(a) (b)

Figure 4. Number of events per 10^7 incident protons in which at least a threshold amount of energy is deposited in the detector. (a) Curves for threshold energies of 2 to 8 MeV deposited in a 4 μm thick detector. (b) Curves for 2 to 50 MeV deposited in the 100 μm thick detector.

Model Calculations

We have recently developed a computer code for calculating the energy deposited in parallelpiped volume elements of arbitrary dimensions. It is based on the simulation model of nuclear interactions developed by Metropolis et al.[19] and Dostrovsky et al.[20]

The primary protons and all struck nucleons are followed by Monte Carlo routines through a series of interactions within the nucleus. All secondary particles that emerge from the excited residual nucleus during the cascade and evaporation processes are followed to their end of range. The numbers of each type of secondary particle and their energy spectrum, were compared with Refs. 19 and 20 to test the program and found to be in agreement. The mass-number spectrum of the residual nuclei were compared with Silberberg and Tsao[21] for 130 MeV protons incident on silicon and found to predict similar mass spectra within ± 1 AMU. Their recoil energy spectra were found to agree with an earlier empirical model of the recoiling residual fragments which uses the Silberberg and Tsao mass spectra[21] and Goldhaber's[22] parameterization of the recoil fragment momenta of the data of Heckman et al.[23] The program then determines the points at which any particles enter the sensitive volume element and where they leave (see Fig. 5). Interactions may occur inside or outside the sensitive volume element. The difference in residual range between the exit point and entry point is used to determine the energy loss within the volume element. For the larger volume elements the assumption is made that the energy loss within the volume element equals the energy deposited in that element. The program totals all energies deposited in the volume element by the primary proton, all charged secondaries, and the recoiling nuclear fragment.

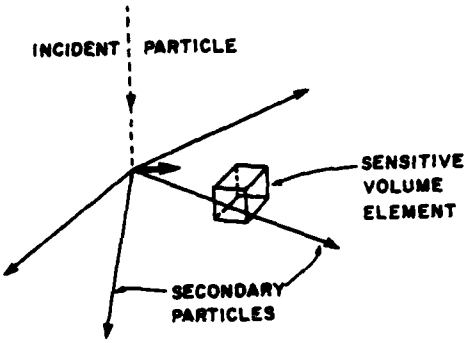

Figure 5. Schematic of a nuclear interaction occurring near a sensitive volume element. The C.C.T. model calculates the energy deposited in volume elements of arbitrary dimensions.

Theoretical integral energy deposition spectra for protons incident on slabs of silicon with areas of 25 mm^2 and thicknesses of 24.1 and 100 μm are plotted as solid curves in Fig. 3. The simulation plots are normalized to the lowest energy data points in both cases. The programs continued to run until the number of simulated events roughly matched the experimental number. As a result the high deposition-energy portions of the theoretical as well as experimental spectra have limited statistical significance which can be estimated from the ordinate scale. Within the statistics the fits at both 24.1 and 100 μm are quite encouraging.

We have previously shown that the 24.1 μm spectrum has a shape similar to the energy spectrum of recoiling residual nuclear fragments.[5] The shallower slope of the 100 μm spectrum relects the larger contribution from other charged secondary particles to the energy deposited. As the thickness of the detectors decrease, the secondaries contribute a correspondingly smaller fraction of the energy. For the very thin detectors even some of the recoiling nuclear fragments leave the detector before reaching their end of range.

Residual Nuclear Fragments

The large mass of the recoiling residual nuclear fragment implies that it has a very short range. For RAM memory elements, as for the very thin detectors, the nuclear recoil provides a mechanism for depositing energies larger than the threshold values for upsets. However, according to our computer calculations, not all recoils reach their end of range within a few microns of the interaction. The more energetic nuclear recoils tend to occur in interactions where the number of secondary particles emitted from the nucleus is large. This implies that the residual fragments with less mass, i.e., the more energetic residual nuclei would tend to be lighter than the average and, therefore, have longer ranges. This is illustrated in Fig. 6 which shows the mass spectra of the residual nuclear fragments predicted for nuclear fragments having recoil kinetic energies above 0, 10, 20, and 30 MeV. The spectra are plotted for 90 and 350 MeV protons incident on silicon. At both incident energies the predicted spectra shift towards lower masses as the minimum energy is increased. The largest shift occurs for values between 0 and 10 MeV.

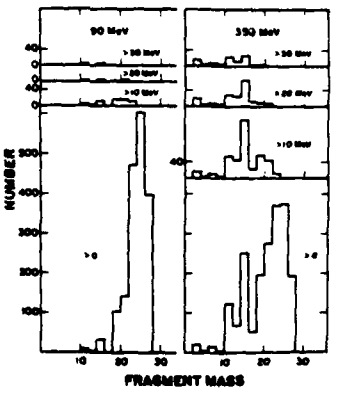

Figure 6. Mass spectra of residual nuclear fragments as calculated by the C.C.T. model for 90 and 350 MeV proton interactions with silicon. Spectra are shown for recoils having greater than 0, 10, 20, and 30 MeV for both incident proton energies.

The interactions at an incident proton energy of 350 MeV are more energetic than at 90 MeV. This is reflected in Fig. 6 by the larger number of energetic fragments. There also appears to be a significant shift towards lower masses for the same threshold energy. A fragment with a mass of 16 AMU and a kinetic energy of 10 MeV would have a range of about 4 μm in silicon; if the kinetic energy was 30 MeV the range would be increased to roughly 13 μm.

Summary and Conclusions

The measurements described in this report provide data on the energy deposition in slabs of silicon of a variety of thicknesses ranging from 2.5 to 200 μm. The data are relevant to the soft error problem because the data for a given silicon thickness provides an upper limit to the energy-deposition spectra to be expected for circuit devices with sensitive elements of the same thickness. Moreover, the data provides a clear test of computer simulation models. Once such a model is thoroughly tested, it can be used to predict the energy-deposition spectra for sensitive elements of arbitrary dimensions and calculations can be performed for specific devices. This will provide a means of quantitative estimates of the soft-error rates to be expected for LSI and VLSI devices to be exposed to energetic particles in space.

The total cross section for nuclear interactions tends to fall over the range of incident proton energies studied (50 - 158 MeV). However, our measurements show that the cross section for interactions which deposit more than a few MeV in either a 4.1 μm or a 100 μm thick detector increase with the incident proton energy over this energy range. One would expect the soft-error cross section for LSI devices to increase with incident proton energy in a manner similar to that shown in Fig. 4a for the 4.1 μm thick detector. In fact, earlier measurements of the soft-error cross section in LSI RAMs increase with proton energy in a manner quite similar to the 4.1 μm data. The sizable decrease in event rates with increasing threshold requirement evident in Fig. 4a may explain the variation in sensitivity observed even for LSI devices from the same batch.[2]

Decreases in the thickness of the sensitive volume were shown to greatly reduce the range of energies deposited. This suggests that devices with thinner sensitive elements for the same threshold may have greatly reduced soft-error sensitivity to proton interactions. Such a correlation between sensitivity to soft errors and thickness of the sensitive volume is also apparent for exposures to heavy ions.[17,18,24]

A computer code for calculating the energy deposition in volume elements of arbitrary dimensions as a result of nuclear interactions has been developed at Clarkson and shown to agree in shape within statistics with the integrated spectra obtained for 24.1 and 100 μm thick detectors exposed to 131 MeV protons. The model needs improvements before fitting to thinner detectors. The model suggests that recoiling nuclear fragments with kinetic energies above 10 MeV have lighter masses and correspondingly longer residual ranges. This may somewhat reduce the effectiveness of the recoil nucleus in inducing upsets in very small sensitive volume elements.

References

1. C.S. Guenzer, E.A. Wolicki, R.G. Allas, "Single Event Upsets of Dynamic RAMs by Neutrons and Protons", IEEE Trans. Nucl. Sci. NS-26, 5048-5052 (1979).

2. R.C. Wyatt, P.J. McNulty, P. Toumbas, P.L. Rothwell, and R.C. Filz, "Soft Errors Induced by Energetic Protons", IEEE Trans. Nucl. Sci. NS-26, 4905-4910 (1979).

3. C.S. Guenzer, R.G. Allas A.B. Campbell, J.M. Kidd, E.L. Petersen, N. Seeman, and E.A. Wolicki, "Single Event Upsets in RAMs Induced by Protons at 4.2 GeV and Protons and Neutrons below 100 MeV", IEEE Trans. Nucl. Sci. NS-27, 1485-1489 (1980).

4. W.E. Price, D.K. Nichols, and K.A. Soliman, "A Study of Single Event Upsets in Static RAMs", IEEE Trans. Nucl. Sci. NS-27, 1506-1508 (1980).

5. P.J. McNulty, G.E. Farrell, R.C. Wyatt, P.L. Rothwell, R.C. Filz, and J.N. Bradford, "Upset Phenomena Induced by Energetic Protons and Electrons", IEEE Trans. Nucl. Sci. NS-27, 1516-1522 (1980).

6. E.L. Petersen, "Nuclear Reactions in Semiconductors", IEEE Trans. Nucl. Sci. NS-27, 1494-1499 (1980).

7. J.N. Bradford, Air Force Report RADC TR-79-109, May 1978.

8. P.J. McNulty, R.C. Wyatt, G.E. Farrell, R.C. Filz, and P.L. Rothwell, "Proton Upsets in LSI Memories in Space" in Space Systems and Their Interactions with the Earth's Space Environment, H.B. Garrett and C.P. Pike, Eds. (American Institute of Aeronautics and Astronautics, New York 1980). pp. 413-433.

9. R.C. Filz and L. Katz, "An Analysis of Imperfections in DMSP Photographs Caused by High Energy Solar and Trapped Protons", Air Force Report AFCRL-TR-74-0469, September 1974.

10. T.A. Croft, " Nocturnal Images of the Earth from Space", Stanford Research Institute Report No. 68197, March 1977.

11. P.L. Rothwell, R.C. Filz, and P.J. McNulty, "Light Flashes Observed on Skylab 4: The Role of Nuclear Stars", Science 193, 1002-1003 (1976).

12. P.J. McNulty, V.P. Pease, V.P. Bond, R.C. Filz, and P.L. Rothwell, "Particle-Induced Visual Phenomena in Space", Radiation Effects 34, 153-156 (1977).

13. J.N. Bradford, "Single Event Error Generation by 14 MeV Neutron Reactions in Silicon", IEEE Trans. Nucl. Sci. NS-27, 1480-1484 (1930).

14. G.E. Farrell and P.J. McNulty, to be published.

15. J.N. Bradford, "A Distribution Function for Ion Track Lengths in Rectangular Volumes", Journal of Appl. Phys. 50, 3799-3801 (1979)

16. D. Binder, E. C. Smith, and A.B. Homan, "Satellite Anomalies from Cosmic Rays", IEEE Trans. Nucl. Sci. NS-22, 2675-2680 (1975).

17. J.C. Pickel and J.T. Blandford, "Cosmic-Ray-Induced Errors in MOS Memory Cell", IEEE Trans. Nucl. Sci. NS-25, 1166-1167 (1978).

18. L.L. Sivo, J.C. Peden, M. Brettschneider, W. Price, and D. Pentecost, "Cosmic-Ray-Induced Soft Errors in Static MOS Memory Cells", IEEE Trans. Nucl. Sci. NS-26, 5042-5047 (1979).

19. N. Metropolis, R. Bivins, M. Storm, A. Turkevich, J.N. Miller, and G. Friedlander, "Monte Carlo Calculations on Intranuclear Cascades I. Low-Energy Studies", Phys. Rev. 185-219.

20. L. Dostrovsky, A. Fraenkel, and G. Friedlander, "Monte Carlo Calculations of Nuclear Evaporation Processes III. Applications to Low-Energy Reactions", Phys. Rev. 116, 683-702 (1959).

21. R. Silberberg and C.H. Tsao, "Partial Cross Sections in High Energy Nuclear Interactions and Astrophysical Applications I. Targets with $Z \leq 28$", Astrophysical Journal Supplement. 25, 315 (1973).

22. A.S. Goldhaber, "Statistical Models of Fragmentation Process", Phys. Lett. 53B, 306-308 (1974).

23. H.H. Heckman, D.E. Greiner, P.J. Lindstrom, and H. Shwe, "Fragmentation of ^{4}He, ^{12}C, ^{14}N, and ^{16}O Nuclei in Nuclear Emulsion at 2.1 GeV/Nucleon", Phys. Rev. 17, 1735-1747 (1978).

24. W.A. Kolasinski, J.B. Blake, J.K. Anthony, W.E. Price, and E.C. Smith, "Simulation of Cosmic-Ray-Induced Soft Errors and Latchup in Integrated-Circuit Computer Memories", IEEE Trans. Nucl. Sci. NS-26, 5087-5091 (1979).

guest comment

Charged particles cause microelectronics malfunction in space

Peter J. McNulty

Anomalies in spacecraft performance have been reported on a number of US satellites. Some take the form of satellite components suddenly turning on or off. These anomalies are believed to result from events triggered in microelectronic devices by energetic charged particles. While the anomalies have for the most part been too rare to jeopardize any mission objectives, they do show signs of increasing in severity as more sophisticated electronics are flown. They should serve as a warning to persons responsible for designing experiments or other systems to fly in space. But unfortunately discussion of the phenomena have been limited to engineering journals and government reports.

These anomalous events greatly complicate the design of experiments intended to function and survive in the harsh radiation environments found in space, particularly if the experimenter wishes to incorporate large-scale and very-large-scale integrated devices into the experiment. In addition to the traditional problems of total dose and dose-rate vulnerability, memories and microprocessors can have their logic state altered as a result of a single particle traversing the device or initiating a nuclear reaction within it. Such events are called "single event upsets," and they include both soft and hard errors:

- Soft errors appear as anomalous signals, bit upsets (that is, changes from 1 to 0 or 0 to 1 in the binary information stored in memory) and incorrect logic execution. While the device continues to function as designed after a soft error, it processes false information.
- Hard errors are permanent changes induced by the radiation that prevent the proper function of the device. Included as hard errors are "latch-ups," in which the logic state of a circuit element becomes stuck in either a 1 or a 0 state. A latch-up can produce catastrophic results by leading to strong surges of instrument currents; if the circuit was improperly designed, for example, it may simply burn up. At present, the cross section for latch-up or other hard errors is substantially smaller than for soft errors but this may change as the sizes of circuit elements decrease.

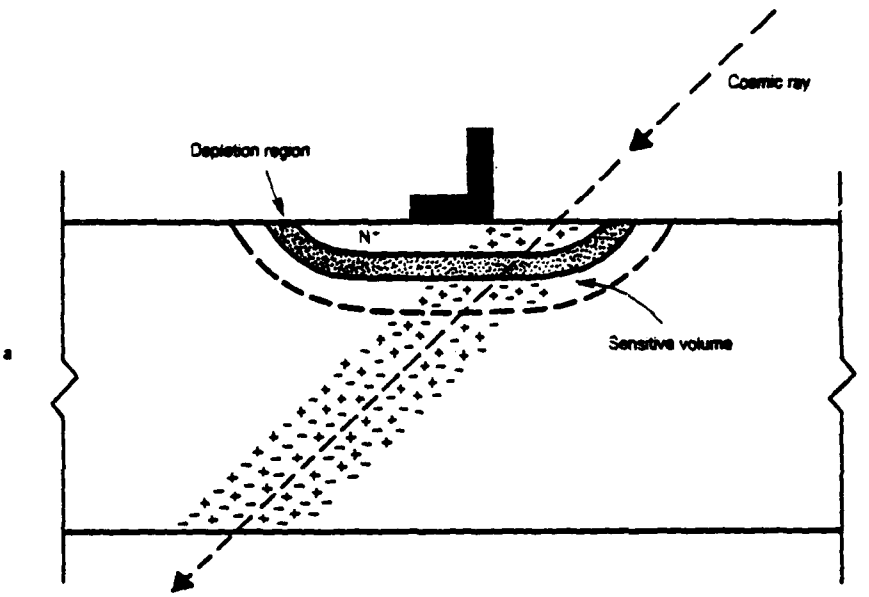

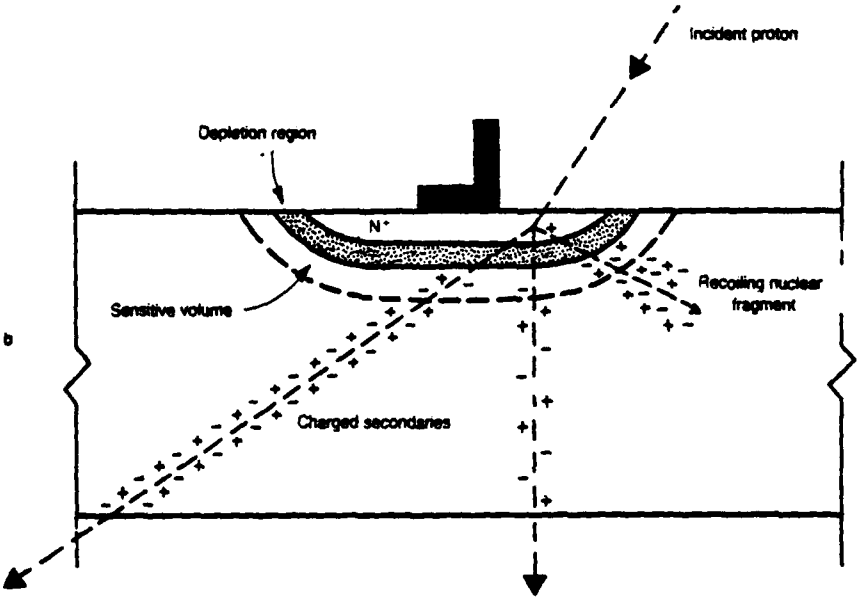

Single upset event in an electronic device may be produced by the charge generated when (a) heavy cosmic-ray nucleus traverses the depletion region of a sensitive n–p junction or (b) when a proton causes a nuclear reaction within the sensitive volume of the junction.

A bit upset in a random-access memory may significantly alter the data stored in memory or change an instruction; such a change may in turn lead to an improper switching (on or off) of a system component. The logic error introduced when a soft error occurs in one of the storage registers of a microprocessor may trigger an unanticipated loop that cannot be escaped without turning the unit off.

The upsets can be avoided altogether only by severely restricting the types of devices flown and, thereby, limiting the speed and memory capacity of the experiment. Considerable work, including the development of error-cor-

continued on page 108

Peter J. McNulty is professor of physics at Clarkson College of Technology, Potsdam, New York.

guest comment

continued from page 9

rection techniques, must be carried out before sophisticated integrated circuits—like those used routinely in such arcade games as PAC-MAN, that is, RAMs with more than 1 kbit of memory per chip—can be trusted to function reliably in space. Because of SEUs are initiated by energetic particles, physicists will have to play a significant role both in understanding and in overcoming the problems involved.

Daniel Binder and his colleagues suggested[1] as early as 1975 that the passage of a heavily ionizing cosmic-ray nucleus through the depletion region of sensitive transistor elements could charge the base–emitter capacitance of the elements to their turn-on voltage, resulting in a change of the logic state of a flip-flop circuit. In trying to explain the rare anomalies t were beginning to occur in spacecra erformance they proposed that a se ce of such bit upsets could be inter d as a command to initiate or t nate some procedure.

With the introduction of I circuits (256 bits) on space ne error rates increased consi erably. There have been reports of bit upsets in LSI devices on over a dozen American satellites including some in the Intelsat satellite data system, Tiros-N, Pioneer-Venus and the global positioning system programs.[2] Workers at the Jet Propulsion Laboratory discovered that one of the microprocessors and some of the 246×4 bit RAMs that were to be included as components on the Galileo flight to Jupiter are susceptible to soft errors. The Galileo project established a team to study the problem; various groups are testing devices with accelerators to ensure that the satellite will have proper guidance and control in Jupiter's intense radiation belts.

While SEU phenomena pose serious problems and possible limitations for space scientists, they also provide research opportunities for nuclear physicists interested in the basic physics of medium-energy nuclear reactions, particle track structure in solids and microdosimetry. Various mechanisms have been proposed to explain how a heavily ionizing cosmic-ray nucleus can induce soft errors in integrated circuits in traversing them.[3–6] All involve the generation of electron–hole pairs in or near the depletion regions formed at p–n junction having a reversed bias. The intense electric fields at the junction separate the charges, with those of the appropriate sign collected while those of the opposite sign are swept out of the depletion region; the sensitive element thus reponds like a solid-state nuclear detector. Both the primary solar or galactic cosmic-ray nuclei and the secondary particles produced by cosmic-ray interactions elsewhere in the spacecraft can give rise to tracks of electron–hole pairs, whose charge is then collected. If sufficient charge is collected, an upset occurs. Because some of the charges generated outside the depletion region will also be collected, the effective sensitive volume is somewhat larger than the depletion region. On dynamic RAMs the sensitive elements may include bit sense lines, sense amplifiers, and the memory storage cells themselves.[7] The sensitive volume elements on static RAMs appear to be p–n junctions on the flip-flop circuits that form the memory elements.[4,5]

Calculating the size and shape of the sensitive volume element is complicated[8] by a phenomenon known as "field funneling." When the cosmic-ray particle traverses the junction, the electron–hole pairs generated distort the junction field: Field lines originally confined to the depletion region extend, for about a nanosecond, some distance along the particle's trajectory, and can therefore attract or funnel carriers from a considerable distance into the junction. The extent of field funneling is a function of doping concentration, bias voltage, and the stopping power of the primary particle. Funneling is expected to be less significant for devices where the sensitive depletion regions are dielectrically isolated—for example, by placing CMOS-type circuit elements on a saphire substrate.

Given a detailed knowledge of the device from which one can determine the effective dimensions of all the sensitive volumes, the critical charges necessary to change their logic states and the energy-deposition characteristics of the radiation to which the device is exposed, the models predict the soft-error rate for the device.

Nuclear interactions provide a second mechanism for generating a considerable amount of charge within a microscopic volume element. Moreover, they are the means by which energetic protons, by far the most numerous nuclei in space, induce soft errors. The figure also shows schematically (b) a nuclear interaction occurring within a junction. The charge collected should be proportional to the total energy deposited, and only those interactions that generate at least the critical charge for that element (that is, deposit the corresponding threshold amount of energy) will induce a soft error. Because of this threshold requirement in the localized energy deposition, the SEU cross section depends on incident proton energy in a way that is quite different from the total inelastic nuclear cross section.[9] At higher proton energies, larger energies are transferred to the struck nucleus, with

more secondary particles being emitted in the cascade and evaporation stages of the interaction. While the resulting residual nuclear fragment is lighter than at lower proton energies and has a correspondingly greater recoil energy and therefore recoils with only a small fraction of the energy released in the event, it deposits all of that energy locally.

Exposing electronic devices to accelerator beams of heavy ions and protons has produced some SEU data, but considerable work will have to be done before error rates for new device designs can be predicted with confidence. One barrier to testing the available models is the fact that the manufacturers of many devices consider detailed information, including the dimensions of sensitive volume elements, to be proprietary. Such problems have as yet precluded a rigorous test of the SEU models. We have found qualitative agreement between the sharp predicted increase in SEU cross section as the incident proton energy increases from 20 to 100 MeV and the measured rise in SEUs in a totally depleted silicon surface-barrier detector for events in which more than a few MeV are deposited.[9,10] Others have reported agreement between the thresholds measured for heavy ions incident on static RAM devices and model predictions.[4,5]

There is a considerable interest in determining how the SEU rates scale as the dimensions of the circuit elements decrease, that is, as the density of memory elements on a device increases. Reducing the size of the sensitive volume reduces the chance of its being traversed by a cosmic-ray particle and, to the extent that it also reduces the path length within the sensitive volume for those traversals that do occur, the charge collected in the depletion region is reduced. According to John N. Bradford,[11] the contribution from funneling will decrease with the size of the sensitive volume. On the other hand, smaller circuit elements require less critical charge to alter their logic state. Edward A. Burke and his colleagues have predicted[12] that as the volume elements for static RAMs decrease in size the error rate per bit will reach some maximum value and then decrease inversely with the number of bits on a chip. Of course, the total error rate may increase if one uses the increased integration to enlarge memory.

With the present state of affairs, system designers are understandably reluctant to incorporate newer and more sophisticated RAMs and microprocessors without previous flight testing. However, it will obviously not be possible to test adequately in space every device that the designers might want to consider. Device testing must, in general, be done on Earth. We must therefore develop algorithms to predict with confidence SEU rates in space from laboratory test data. A committee with representatives from the Air Force and NASA is developing plans for a project, tentatively called Chemical Release and Radiation Effects Satellite, for substantial ground-based testing and modeling, culminating in a 1986 flight to determine the adequacy in space of the algorithms. The flight will include a program of careful measurements of the fluence and energy spectra of the energetic charged particles in the ionizing radiation, together with simultaneous recording of SEU data for a wide variety of devices. Some of these devices will be flown to qualify them for use in space, but the majority will be selected to provide a range of sensitive-element geometries and device technologies for a thorough test of the algorithms developed.

An adequate test of these algorithms will, of course, require a large number and variety of devices. Many agencies are expected to contribute SEU packages, including Rome Air Development Center, the Naval Research Laboratory, and NASA–Goddard Space Flight Center, with the Air Force Geophysics Laboratory providing the instruments to characterize the radiation.

In addition to direct fluence and energy-spectra measurements for the cosmic rays, trapped protons and electrons, CRRES is also expected to conduct the first microdosimetry survey of space. (Microdosimetric measurements determine the spectra of energy deposition in microscopic volume elements.) In the past, such measurements have been carried out to investigate the biological effects of exposure to radiation and to plan radiation therapy treatments for cancer patients. Two measurements are planned for CRRES: The first will measure the pulse-height spectra in a totally depleted detector having a thickness comparable to that of the sensitive volumes on most RAMs and microprocessors (5–10 microns). The second will measure the pulse-height spectra using a gas ionization chamber, with the pressure of the gas chosen so that the spectrum simulates that generated in a sensitive layer of silicon having the dimensions of typical circuit components.

The orbit parameters for CRRES have not been announced but it is expected to be an elliptical orbit of roughly 20° inclination to the equator which will sample both the near-Earth environment within the geomagnetic cut-off, where the primary exposure will be to protons and electrons trapped in the Van Allen belts, and in deep space beyond the cut-off and the Van Allen belts, where the dominant exposure will be to the cosmic rays.

At the present time, designing an electronic system for use in space involves a trade-off between the speed and size allowed by LSI and VLSI circuits and increased SEU rates. Proper circuit design, including error-correction techniques currently being developed, may mitigate the problems posed by SEUs while maintaining adequate speed of computation. However, proper design requires quantitative understanding of the SEU mechanisms which, in turn, requires detailed information on the devices being made available, improvements in our understanding of track structure and microdosimetry and, most important, the development of algorithms by which accelerator testing can be used to predict SEU rates in space.

• • •

Conversations with J. N. Bradford and E. A. Burke of RADC, E. G. Mullen of AFGL, J. B. Blake of Aerospace Corp., W. P. Price of JPL, and E. G. Stassinopoulos of NASA–Goddard were helpful in the preparation of the report and are gratefully acknowledged. The author's research covered in this report was sponsored by DNA and the Air Force.

References

1. D. Binder, E. C. Smith, A. B. Holman, IEEE Trans. on Nucl. Sci. **NS-22**, 2675 (1975).
2. P. J. McNulty, J. B. Blake, V. Danchenko, E. Petersen, W. E. Price, J. Wilkenfeld, in *Proc. Workshop on the Earth's Radiation Belts: January 26–27, 1981*, Report No. AFGL-TR-81-0311, Air Force Geophysics Laboratory (1981), page 99.
3. J. C. Pickel, J. T. Blandford, IEEE Trans. Nucl. Sci. **NS-25**, 1166 (1978).
4. L. L. Sivo, J. C. Peden, M. Breitschneider, W. Price, P. Pentecost, IEEE Trans. Nucl. Sci. **NS-26**, 5042 (1979).
5. W. E. Price, J. C. Pickel, T. Ellis, F. B. Frazel, IEEE Trans. Nucl. Sci. **NS-28**, 3946 (1981).
6. J. C. Pickel, J. T. Blandford, IEEE Trans. Nucl. Sci. **NS-28**, 3962 (1981).
7. D. S. Yaney, J. T. Nelson, L. L. Vanskike, IEEE Trans. Electron Devices **ED-26**, 10 (1979).
8. C. M. Hsieh, P. C. Murley, R. R. O'Brien, Trans. Electron Devices **ED-2**, page 103 (1981).
9. R. C. Wyatt, P. J. McNulty, P. Toumbas, P. L. Rothwell, R. C. Tilz, IEEE Trans. Nucl. Sci. **NS-26**, 4905 (1979).
10. P. J. McNulty, G. E. Farrell W. P. Tucker, "Proton-Induced Nuclear Reactions in Silicon", IEEE Trans. Nucl. Sci. **NS-28**, 4007 (1981).
11. J. N. Bradford, Charge Collection for Ion Track Plasma Column in Silicon Devices, Report RADC-TM-81-ES-07, US Air Force (1981).
12. E. A. Burke, Effects of Size Reduction on Cosmic-Ray Induced Errors in RAMs, Rome Air Development Center, Report RADC-TM-31-EF-03, US Air Force (1981).

APPENDIX C

CLARKSON COLLEGE OF TECHNOLOGY

DEPARTMENT OF PHYSICS

ENERGY DEPOSITION BY NUCLEAR INTERACTIONS IN MICROSCOPIC VOLUMES

A Thesis

by

GARY E. FARRELL

Submitted in partial fulfillment of the requirements

for the degree of

DOCTOR OF PHILOSOPHY

Physics

May 1983

Accepted by the Graduate School

_____ _____

Date Dean

ABSTRACT

A computer simulation has been developed which calculates the energy deposited in a small sensitive volume by nuclear interactions. A Monte Carlo approach is used. The energy deposited by the incident particles, by the cascade and evaporation particles, and by the residual nuclei from the interactions is calculated. The small sensitive volume can be embedded in a large volume, and energy deposited in the sensitive volume by interactions taking place in the large volume can be calculated.

The nuclear model used in the simulation is shown to be in agreement with experiment and with other models. The predicted energy deposition spectra are shown to be in good agreement with results obtained by exposing silicon surface barrier detectors to proton beams at the Harvard Cyclotron. The recoiling residual nuclei were found to play a major role in the energy deposition in thin detectors.

The simulation can be used to predict the soft error rate of microelectronic devices exposed to protons or neutrons. It will be particularly useful for devices flown in space, where protons are present in the radiation belts and are the most abundant component of the cosmic rays.

ACKNOWLEDGEMENTS

I wish to express my deep gratitude to Dr. Peter J. McNulty for suggesting this study and for his constant guidance and encouragement. I wish also to thank Dr. Herman W. Chew, Dr. John F. Dicello, Dr. Henry Domingos, and Dr. Herbert F. Helbig for their helpful assistance. Thanks are due to Dr. Stephen D. Druger and Dr. David J. Kaup for useful discussions.

Very special thanks are due to Cynthia L. Davis for her tireless efforts, without which the manuscript would never have been completed on time. Eleanor Doyle assisted with some last-minute typing.

GLOSSARY

RAM	random access memory
CCD	charge coupled device
PMOS	p-channel metal-oxide-semiconductor
NMOS	n-channel metal-oxide-semiconductor
CMOS	complementary symmetry metal-oxide-semiconductor
SOS	silicon on sapphire
MSI	medium scale integration
LSI	large scale integration
VSLI	very large scale integration
soft error	an anomalous change in the information stored on a chip without physical damage to the chip itself
latch-up	the effect of a transistor remaining in saturation after the driving signal is removed

TABLE OF CONTENTS

I. INTRODUCTION

Charged particles, in passing through matter, deposit energy along their path. The spectrum of the energy deposited in a small volume is a complicated function to calculate in view of the nuclear reactions which can be induced. Recently a knowledge of this energy spectrum has proven to be of considerable importance, especially in analyzing the charged-particle-induced soft-error phenomena in microelectronic circuits flown in space[1-54], the light flash phenomena experienced by Skylab astronauts[55-70] and mutations induced in biological cells.[71,72]

Energy is deposited by several means. The incoming charged particle itself will ionize the medium through which it passes. Several other mechanisms come into play if the primary particle strikes a nucleus and causes a reaction. From the struck nucleus will emerge high energy protons and neutrons known as cascade particles, as well as slower and occasionally more massive evaporation particles. The cascade and evaporation particles, as well as the recoiling remnant of the struck nucleus, will also ionize the medium.

In this computer simulation, the location and dimensions of a sensitive volume within a large volume are specified. If sufficient energy is deposited in the sensitive volume, an effect will be produced. On a microelectronics chip, this volume might correspond to a sensitive junction with linear dimensions of microns. In a

biological cell the sensitive volume may be the cell's nucleus or the volume occupied by a single gene. On the retina of the human eye, the sensitive volume may be a summation area in the layer of photoreceptors.

The effect produced by sufficient energy deposition in a sensitive microvolume on a device would be a hard or soft error.[1] A soft error is an anomalous change in the information stored on a chip without physical damage to the device itself.[9] Permanent damage would be classed as a hard error. Sufficient energy deposition in a retinal receptor would result in a visual effect, while the effect in a cell nucleus could be a mutation. This small sensitive volume is embedded in a large volume, which can represent the surrounding material. For microelectronics, it would represent the rest of the chip.

A large number of incident protons or neutrons is sent through the large volume. The program is set up for rectangular geometry. The incident beam can be omnidirectional or unidirectional. Each particle is followed to determine if it passes through the sensitive volume. If it deposits any energy there, this is calculated from range-energy tables. Nuclear reactions induced in the large volume can also send particles through the sensitive volume. The incident particles, depending on their type and energy, have a certain probability per unit distance of undergoing a nuclear reaction. If this occurs, any cascade particles (neutrons and protons) are identified. Then the evaporation particles, which can be

neutrons, protons, deuterons, tritons, He^3's, or alphas are identified. Lastly the identity and momentum of the residual nucleus is calculated. The paths of all of these are followed to see if any cross the sensitive volume. For those that do, the energy they deposit there is found from range-energy tables. In the case of electronics, where the medium is silicon, electron-hole pairs are generated at the rate of 3.6 eV of deposited energy per pair.[1]

Figure 1 illustrates a high LET particle passing through the sensitive region of a microelectronics device. Linear energy transfer, or LET, is the amount of energy a particle loses per unit distance. Figure 2 shows a nuclear interaction taking place in a device. The proton which caused the interaction was lightly ionizing, but the particles from the interaction have a much higher LET and are much more likely to result in a device error. Figures 3 and 4 show schematically the wake of electron-hole pairs generated by the particles shown in the previous two figures.

Monte Carlo techniques are used to follow the entire course of the nuclear reaction. Starting from distributions which are either known or calculated by the program, a random number choice determines a particular value of such things as the impact point of a proton on a silicon nucleus, the distance traveled inside the nucleus before undergoing a collision, the identity of the struck particle, the scattering angle, and many others.

The code has two distinct types of calculations to

perform. One is to model the nuclear reactions accurately. The other is to trace the path of all of the particles and to determine how much energy each deposits in the sensitive volume. A large number of nuclear reactions must be followed through to ensure statistical accuracy. There exist computer codes which model nuclear reactions,[73,74] but they consume large amounts of computer time. To balance the need for accuracy with the limitations on computer time, a new nuclear code was written. Over the course of this work, the speed of the available computer was substantially improved. Each time this occurred, further refinements to the program became possible.

This work was done with the microelectronics problem in mind. It was predicted as far back as 1962[2] that as devices were miniaturized to dimensions of a few microns they would be susceptible to energetic charged particles. Such effects were reported in 1975,[3] and by 1978 the problem had grown to major significance.[1,4,5] The trend for such devices has been toward constant miniaturization. The basic unit of microelectronics is the chip, a silicon wafer a few millimeters on a side. Such chips, in the early 1960's, had about ten transistors. At the present time, one may have over 10^5.[6]

As a check on the computer simulation, silicon surface barrier detectors have been exposed to proton beams at the Harvard Cyclotron. These detectors had thicknesses of 2.5, 4.2, 8.7, 15, 24.1, 97, and 200 um and the proton energies

used were 18, 25, 32, 37, 51, 86, 91, 125, 127, 131, and 158 MeV. Although thin in only one dimension, it has been shown by Bradford[7,8] that they provide a reasonable approximation to devices in which all three dimensions are small.

Other areas in which this work will have relevance are the study of the light flashes observed by the astronauts and the study of radiation induced biological mutations. A variety of visual phenomena were reported by the Skylab and Apollo astronauts. These are believed to be caused by energetic particles passing through the eye. Studies with particle beams on the ground have confirmed that light flashes can be induced by pions, muons, neutrons, and heavy ions. Nuclear star production is also believed to play a role. Here the relevant sensitive volume is a retinal receptor about 30 um thick and 300 um in diameter.[55-70]

Genetic mutations can also be induced by charged particles. If sufficient energy is deposited in a sensitive volume then a chemical bond in a DNA molecule can be broken. If the molecule does not repair itself, and if the damage does not kill the cell, genetic changes may be seen. In some models the sensitive volume is taken to be a sphere one micron in diameter.[71,72]

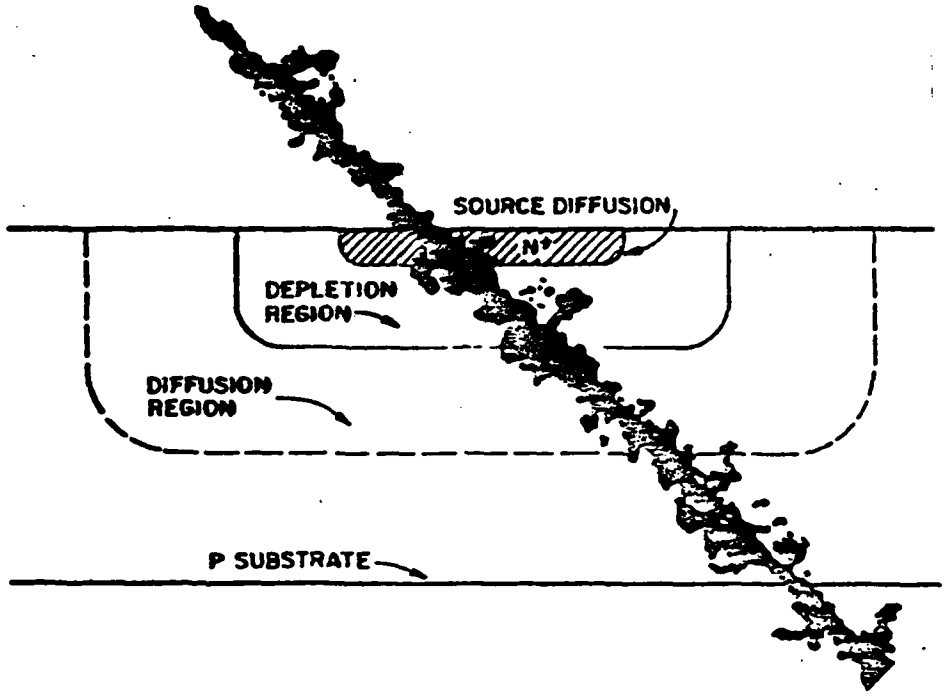
SOURCE DIFFUSION
N+
DEPLETION REGION
DIFFUSION REGION
P SUBSTRATE

FIGURE 1

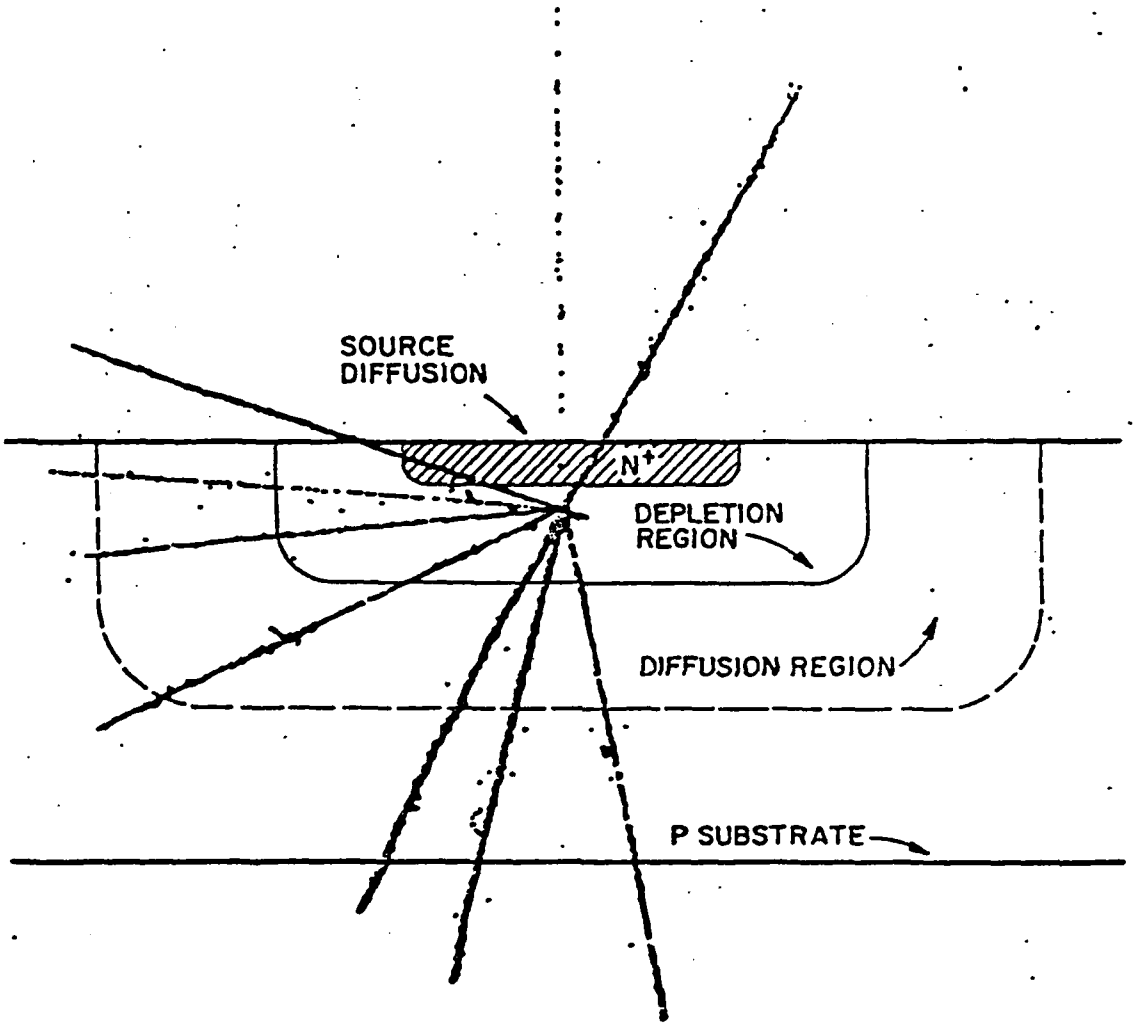
SOURCE
DIFFUSION
N+
DEPLETION
REGION
DIFFUSION REGION
P SUBSTRATE

FIGURE 2

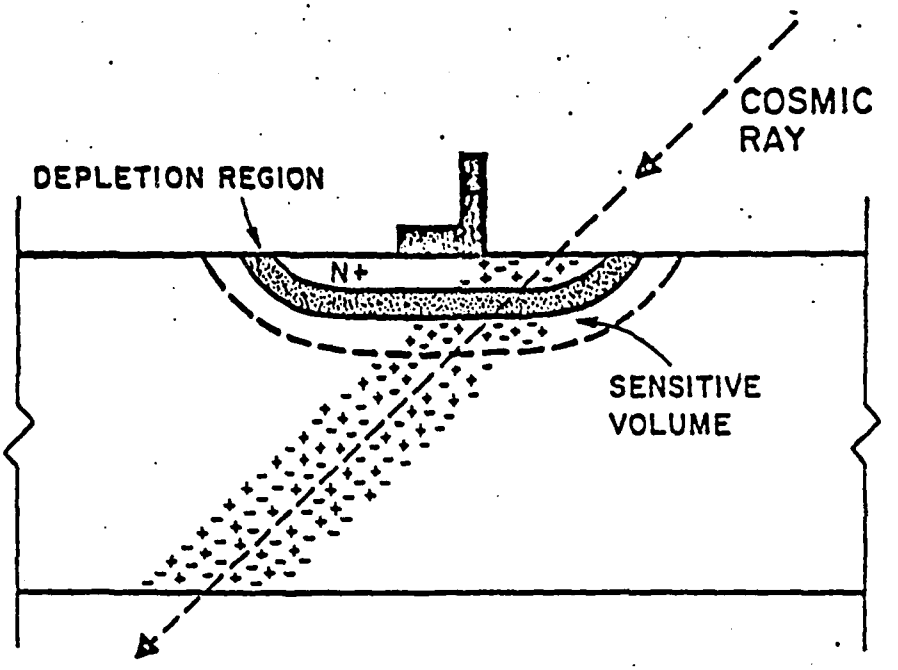

FIGURE 3

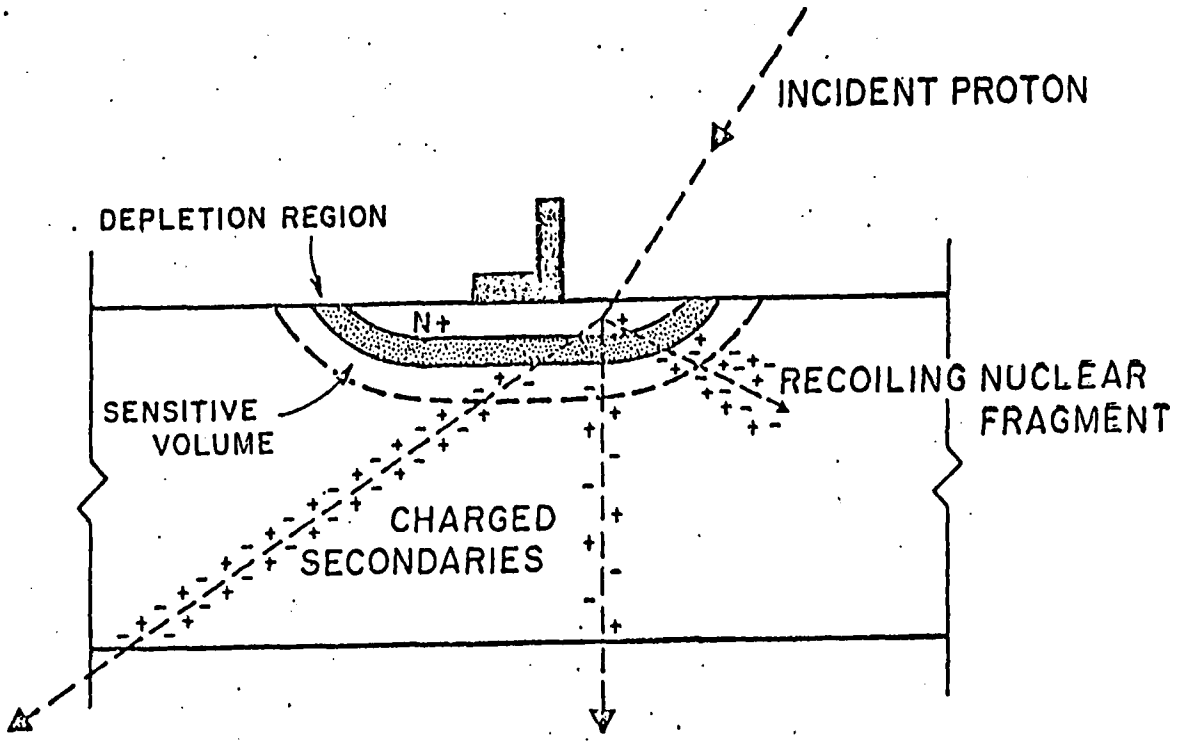
INCIDENT PROTON
DEPLETION REGION
N+
SENSITIVE VOLUME
RECOILING NUCLEAR FRAGMENT
CHARGED SECONDARIES

FIGURE 4

II. PREVIOUS INVESTIGATIONS

A. ELECTRONICS EFFECTS

In a 1962 paper by Wallmark and Marcus[2] it was pointed out that microelectronic semiconductor memories have device size limits. Both the effect of primary cosmic rays and the effect of secondary particles from silicon nuclei struck by cosmic rays were considered. Then the matter was largely forgotten for over a decade.

In 1975, soft errors in communication and computer hardware brought the radiation problem to the attention of the semiconductor manufacturers. Binder, Smith, and Holman[3] investigated anomalous errors caused by the triggering of J-K flip-flops on communications satellites. The assumed mechanism was the charging of the base-emitter capacitance of sensitive transistors to the turn-on voltage. The effect could be duplicated by exposing the circuit to the beam from a scanning electron microscope. It was assumed that iron cosmic rays were responsible for errors in the satellites. Performance calculations based on the cosmic ray flux predicted an error rate of 3.1×10^{-3} per transistor per year, close to the observed rate of 1.5×10^{-3}.

In 1978, three important papers appeared. May and Woods[1] published the first of their investigations in the field of soft errors. After 25 million device hours of testing, they concluded that quantities of uranium and thorium, present in parts per million levels in the

packaging materials of commercial chips, were causing soft errors. These radioactive materials emit alpha particles, which deposit energy along their path. This energy results in the production of electron-hole pairs, up to 2.5×10^6 along the entire track of the alpha within several picoseconds. These electrons (or holes) are swept into potential wells in the device. Typically an empty potential well represents a '1' and a full potential well a '0'. Enough electrons can be generated to fill an empty potential well, resulting in a memory change. For one chip an error rate of 1.5×10^{-3} errors/hour was calculated and compared to the observed rate of 2.0×10^{-3}.

Bradford[4] (1978) pointed out that with the advent of VLSI devices the range of the electrons generated by a passing cosmic ray would be comparable to the device dimensions. This would cause nonuniform distribution effects to show up, making possible large local doses.

In the same year, Pickel and Blandford[5] published a report on a satellite system with 24 4K NMOS RAM's. The system had been showing roughly one error per day. From the device specifications, it was determined that 5.6 MeV was the minimum energy required for a soft error. It was then calculated which of the cosmic rays could deposit this amount in the required volume. The cosmic ray spectrum is known, and this led to a theoretical error rate of .62/day.

In early 1979 an important paper by Yaney, Nelson, and Vanskike[9] noted that alphas striking sense amplifiers and

bit lines also caused soft errors. These authors also studied the efficiency with which the charge generated by the particle would be collected.

An article by Capece[10] noted that alpha induced errors were being seen even in static RAM's. Previously only dynamic RAM's were known to be affected. The sensitive static RAM's contained polysilicon load resistors. The small current in them could be overpowered by the charge flow from a passing alpha.

Up to this time errors were only expected from alpha particles and heavier nuclei in the cosmic rays. Bradford[11] noted that protons should also be able to affect microcircuitry. While the ionization by the proton itself would be insufficient to cause a soft error, these protons are capable of inducing nuclear interactions. A proton striking a nucleus leaves it in an excited state. The nucleus rids itself of this excess energy by "evaporating" other particles. Some of these particles will be alphas or heavier fragments, which can cause errors.

Bradford[7] developed analytic expressions for the event rate due to cosmic radiation. These expressions were based on track length distributions in rectangular volumes. The probability of multiple hits was also examined.

Kirkpatrick[12] developed a model for the diffusion and collection of charge along a particle track, and applied this to the soft-error problem. An important

prediction was that devices of dimensions of .5 um or less would be susceptible to soft errors from alpha particles.

Ziegler and Lanford[13] investigated the effects of cosmic rays on RAM's and CCD's. Interactions with electrons, protons, neutrons, and muons were considered. In addition to electron-hole pairs produced by the incident particle, those from secondary alphas and those from elastically recoiling silicon nuclei were counted. Their calculations indicated that the neutron component of cosmic rays would be the main soft error mechanism for 64K dynamic RAM's, through the production of secondary alphas. In 64K and 256K CCD devices (the latter was a hypothetical device) the dominant mechanism was predicted to be the ionization wake of muons.

Wyatt et al.[14] and McNulty et al.[15] examined the effects of protons, He^3's, and alphas on two types of 4K dynamic RAM's. The proton energies used were 131, 91, 51, 32, 18, 1.8, 1.3, and .95 MeV. The He^3's were of 4.3 MeV energy and the alphas were from an Am^{241} source (5.5 MeV). Errors were seen with all incident particles at all energies. The cross section for soft errors was seen to rise with proton energy, although ionization by the incident particle decreases with increasing proton energy. This pointed to inelastic nuclear reactions as a soft error mechanism, as the inelastic cross section rises with proton energy. In Wyatt et al.[14], as an early result of the work presented in this thesis, a major role for the residual recoiling nucleus was first postulated.

The first model of soft error upsets in static MOS memory devices was developed by Sivo et al.[16] Calculations were done for CMOS and PMOS devices, and compared to spacecraft data. Ionization from heavy ion cosmic rays was assumed to be the mechanism, and the predictions agreed well with observed error rates.

The energy deposited by a heavy ion passing through silicon was studied by Hamm et al.[17] An important observation was that the lateral extent of an ion track was very small compared to the dimensions of semiconductor memory cells. Ion tracks could thus be accurately modeled as mathematical lines.

Brucker et al.[18] conducted a series of experiments with SOS devices exposed to krypton and argon beams of about 2 MeV/nucleon. The observation of a greater number of 0 --> 1 changes than 1 --> 0 changes was explained in terms of the geometry of the memory element and the nodal capacitances of the element. An error rate in space of 2.6×10^{-9} errors per day-bit was predicted.

Kolasinski et al.[19] tested various static RAM's by exposure to 600 MeV/nucleon iron nuclei and to argon and krypton nuclei of about 2 MeV/nucleon. Latch up was observed in several cases. Good agreement was obtained with predictions from the model of Sivo et al.[16]

Guenzer et al.[20] irradiated 16K dynamic RAM's with 6.5, 9, and 14 MeV neutrons and with 32 MeV protons. Upsets were found, and they were attributed to (n,α) and (p,α) reactions. Both 1 --> 0 and 0 --> 1 changes

occurred. As the Pickel and Blandford model[5] only explained one type of change, a new theory involving hits on floating bit lines was presented.

Another paper by Bradford[8] pointed out that an analytic expression for the distribution of chords through a rectangular parallelepiped was known, and that this could be coupled with the LET distribution of cosmic rays to give the number of particles depositing more than a threshold amount of energy in such a volume.

Pickel and Blandford[21] conducted experiments on a variety of device types, exposing them to 115 MeV argon and 150 MeV krypton ions. A model was developed which used the LET spectrum from cosmic rays together with the exact expression for the path length distribution within a parallelepiped. The model compared favorably with data from devices on several orbiting satellites.

McNulty et al.[22] exposed static RAM's to a beam of 18 to 130 MeV protons, and obtained error rates two to three orders of magnitude lower than those observed with dynamic RAM's. The static devices were also found to be less sensitive than the dynamic in exposures to short bursts of 10 MeV electrons. A model of nuclear recoil energies was developed by applying a parameterization of Goldhaber's[75] data to the cross sections of Silberberg and Tsao.[76] This was shown to be in reasonable agreement with data from silicon surface barrier detectors exposed to 130 MeV protons.

Price et al.[23] exposed nine types of CMOS static

RAM's to a 50 MeV proton beam and a neutron beam of energy range 5 to 30 MeV. No errors were seen, implying that nuclear reactions were an ineffective upset mechanism at these energies.

Peterson[24] studied the various nuclear reactions induced by protons and neutrons from 5 to 75 MeV. The reactions that produced upset causing alphas were identified, and other reaction products were examined to determine if they could produce upsets. Reactions in which the target nucleus splits into two heavy fragments were postulated to be a potential source of error.

In a later paper, Bradford[25] (1980) used several known cross sections for reactions resulting from 14 MeV neutron bombardment of silicon in conjunction with chord length distributions in a rectangular volume to determine soft error upset rates. A sensitive volume of 1.3 um x 5.1 um x 7.6 um was assumed with a threshold energy of 280 keV. A prediction of 96 electronic upsets was made for 10^8 neutrons/cm^2 incident on 10^6 such cells.

Brucker et al.[26] exposed three versions of a CMOS/SOS 4K static memory device to 2 MeV/nucleon beams of krypton and argon. The results were interpreted in terms of the geometry of the device, and a predicted error rate for the device in space was calculated.

Campbell and Wolicki[27] observed that soft errors could be induced in 16K dynamic RAM's by the bremsstrahlung radiation from 40 MeV electrons. The reaction $^{28}Si(\gamma,\alpha)^{24}Mg$ was assumed to be responsible.

Guenzer et al.[28] tested several RAM's for soft errors using thermal neutrons, protons of 23.0, 33.4, 52.3 MeV and 4.2 GeV, and neutrons of 14 MeV. Upsets were seen with all but the thermal neutrons.

An important finding by Hsieh et al.[29] was that the electron-hole pairs produced by an ionizing particle distort the field around a p-n junction causing the field to extend far down into the bulk silicon around the track of the ionizing particle. The field reverts to normal after a few nanoseconds, but during that time a large number of charge carriers are funneled to the junction. For a typical junction struck by a 4.3 MeV alpha particle, the effect was equivalent to the total collection of all charge within 10 um of the depletion layer.

McNulty et al.[30] (1981) measured the energy deposited in silicon surface-barrier detectors by protons of 51, 91, 131, and 158 MeV. The detector thicknesses used were 2.5, 4.2, 24.1, 100, and 200 um. The results were found to be in good agreement with the computer simulation model described in this thesis.

Hamm et al.[31] applied their Monte Carlo computer code to the case of 130 MeV protons incident on silicon, and obtained values for nuclear recoil which were substantially below those predicted by McNulty et al.[22] Even with the inclusion of the energy carried off by the evaporation particles, the energy spectrum fell below the nuclear recoil spectrum of McNulty et al.

Price et al.[32] exposed three types of I^2L devices

to 144 MeV krypton and 102 MeV oxygen ions. Errors were observed in all of the devices, and the error rate was found to be in reasonable agreement with a theoretical model. This enabled the authors to make error rate predictions for the chips in a galactic cosmic ray environment.

Guenzer et al.[33] exposed three microprocessors to 14 MeV neutrons. Errors were observed, many of which caused the microprocessor to stop execution of the program. The assumed mechanism was alpha production from nuclear interactions.

Myers et al.[34] developed a model which accurately predicted the relative soft error rates of several RAM's. Their experimental data came from exposures to 95 MeV oxygen, 120 MeV krypton and argon, and protons of energies from 15 to 200 MeV.

Pickel and Blandford[35] reported the results of the exposure to krypton ions of up to 152 MeV and argon ions of up to 210 MeV of three CMOS RAM's. Both hardened and unhardened devices were exposed. A comparison and analysis was done with the previously developed Cosmic Ray Induced Error Rate (CRIER) model.

Peterson[36] examined the various means of depositing energy in semiconductor devices by protons in the radiation belts. Direct ionization by the incident protons, evaporation of a struck nucleus, elastic and inelastic scattering of the nucleus, and spallation reactions were considered. Given the altitude of a satellite, a plot of

soft error rate versus critical charge was obtainable from the analysis.

Kolasinski et al.[37] examined the soft upsets caused by 150 MeV krypton ions incident on two types of CMOS RAM's. The error rate was measured as a function of bias voltage and of beam angle. Using these results with a simple model, estimates of soft fail rates in a galactic cosmic ray environment were made.

Knudson and Campbell[38], using an alpha particle beam as small as 2.5 um diameter, exposed different areas on a 16K NMOS dynamic RAM chip. The alphas were of 1.6 to 3.5 MeV. The sense amplifier area was found to be the most sensitive. Dynamic RAM's store data as the presence or absence of a certain amount of charge. Areas where a '1' was stored by a cell depleted of electrons had a higher tolerance to soft upsets than cells where a '1' was stored as the presence of a certain charge.

Woods et al.[39] tested several types of MSI devices for soft errors using a 120 MeV krypton beam. No errors were observed with CMOS devices, while low-power TTL, standard TTL, low-power Schottky, and Schottky devices all proved to be sensitive.

Hu[40] developed a model of the field funneling phenomenon which predicted the funneling depth and the resulting current. This was shown to be in good agreement with experiment.

Farrell and McNulty[41] used a computer simulation model to predict the spectra of energy deposited in various

silicon surface barrier detectors. For the thicker detectors the agreement between experiment and theory was excellent. Energy spectra of the recoiling nuclei from nuclear interactions in the silicon were presented, and the tail of the distribution was shown to be in substantial disagreement with the tail of the distribution of Hamm et al.[31], who used the Oak Ridge codes.

McLean and Oldham[42] developed a field funneling model somewhat different from that of Hu[40], and obtained good agreement with experiment. They predicted the effective funnel length to be 2.0 to 2.5 times the depletion layer width, whereas Hu predicted 1.35 to 1.5 times the width.

Messenger[43] also studied the motion of charges resulting from a charged particle passing through silicon. The funneling phenomenon was taken into acount, and analytic expressions for the current were derived.

Diehl et al.[44] modeled the circuit response to energetic heavy ions passing through the device. This was compared to experimental results from 150 MeV krypton ion bombardment of two static RAM's. The effect of varying the device parameters was studied. It was found that adding a resistance between the inverter pair of the RAM cell decreased the sensitivity to soft errors, although at some sacrifice of speed.

Andrews et al.[45] also reported on the design, fabrication, experimental results, and theory of one of the devices studied by Diehl et al.

Kolasinski et al.[46] studied the effects of 140 MeV krypton, 160 MeV argon, and 33 MeV oxygen ions on several CMOS RAM's. Estimates of the critical charge were made for two types of SOS devices, where field funneling should not be important. Computer circuit simulations also yielded values of the critical charge for an error, but these were not found to be in particularly good agreement with the experiment.

Pickel[47] investigated the effects of scaling on CMOS memory cells, making projections for devices of .4 um geometry. Computer circuit simulations were used. Predictions of error rate where made for a geosynchronous satellite.

Peterson et al.[48] also looked at scaling in VLSI circuitry. The effects of cosmic rays in particular were studied, and predictions were made for the soft error rate for several environments. It was also noted that protons in the radiation belts would be able, through either nuclear reactions or direct ionization, to affect devices of sufficiently small geometry.

Price et al.[49] exposed low power Schottky technology devices to protons of 56 and 130 MeV, 33 MeV carbon, 38, 47, and 109 MeV oxygen, 40 MeV chlorine, 108 and 212 MeV argon, and 130 MeV krypton. The intent was to see how such devices would perform in the proton radiation belts and in the cosmic ray environment. Two of the six devices tested were found to be susceptible to protons, although it was noted that shielding would be effective in this case. All

were to some extent susceptible to heavy ions, where shielding would make little difference.

Campbell and Knudson[50] fabricated both MOS and diffused junction test structures to test the field funneling effect. The structures were exposed to 2.5 MeV alphas and 1.3 MeV protons. Microbeams of 2.5 um and 25 um diameter were used for the irradiation, and the charge generated was measured. The diffused junction structure showed evidence of field funneling for both the protons and alphas, while the MOS structure only gave evidence of it for thin gate oxide thicknesses.

Shapiro et al.[51] reported the results of exposing NMOS microprocessors to 40 MeV protons. Secondary particles from nuclear reactions were suspected to be the cause of the observed upsets. The proton fluence per upset was roughly an order of magnitude less than that required in an earlier experiment using 14 MeV neutrons.

Nichols et al.[52] tested several 1K bipolar static RAM's with protons of 15 to 590 MeV. The error rate rose with proton energy, and the threshold for upsets appeared to be about 15 MeV. The protons in the radiation belt have similar energies.

Bradford[53] derived the energy deposited in microvolumes by protons in the 100-1000 MeV range. Nuclear reactions, including heavy recoil fragments, were taken into account. The Oak Ridge code was used to provide reaction product cross sections.

Magno et al.[54] reported the effects of alpha

particles from an Am^{241} source on superconducting Josephson junctions. These devices also were vulnerable to single event upsets. It was theorized that an alpha striking a portion of the junction's area would cause it to revert from the superconducting to the normal state. This would cause an increase in the current flowing through the part of the junction that was still superconducting. If the current exceeded a certain critical value, the junction would switch states.

To summarize, over the past eight years the effects of radiation on microcircuitry have proven to be extremely important. The focus was initially on soft errors induced by the heavy ion component of cosmic rays. Alphas from natural radioactivity, alphas from proton and neutron induced nuclear reactions, and residual nuclear fragments ware eventually found to cause problems as well. Different device technologies show greatly different sensitivities to radiation induced soft errors. The field funneling effect complicates efforts to determine the dimensions of the sensitive volume on a given device.

B. NUCLEAR MODELS

Nuclear reactions can be viewed as taking place in two stages. In the first, or cascade stage, an incoming nucleon enters the nucleus, collides with another nucleon, and these in turn strike others. This sets up a cascade within the nucleus which ends with some nucleons being ejected from the nucleus, which is left in an excited state. As was pointed out by Serber,[77] this approach is valid as long as the de Broglie wavelength of the nucleons is much less than the nuclear radius.

In the second, or evaporation stage, the nucleus is viewed as a Fermi gas of neutrons and protons confined in a potential well with some excitation energy. The excitation energy is shared by the nucleons in the well, and the system can be characterized by a nuclear temperature. Occasionally a nucleon, near the edge of the nucleus and moving in the right direction, will have enough energy to escape from the potential well. This process was studied in detail by Weisskopf.[78] The cascade and evaporation stages are shown in Figures 5 and 6.

The Monte Carlo technique has been applied to both stages of the nuclear interaction, and gives reasonable agreement with experiment. The earliest application of the technique to the cascade stage was by Goldberger.[79] He examined 100 cascades of 86.6 MeV neutrons on a lead nucleus. This satisfied the Serber criterion, because the wavelength of an incident neutron was 18 times smaller than

the nuclear radius. The nucleus was pictured as a mixture of two non-interacting Fermi gases (neutrons and protons) in a potential well of 26 MeV depth. The Fermi energy was taken to be 18 MeV, leaving a binding energy of 8 MeV. All of the energy levels up to the Fermi energy were filled. In momentum space, this corresponded to a sphere of radius $P_F = h(3\pi^2 N/V)^{1/3}$, where V was the nuclear volume and N was the number of neutrons or protons. Upon entering the nucleus, a path length for the incident neutron was chosen as $\lambda \ln(1/p_n)$, where λ was the mean free path in nuclear matter and p_n was a random number between 0 and 1. The Fermi momentum sphere was divided into twenty regions of equal volume. The probability of making a collision with a particle in a given region was proportional to $p\bar{\sigma}(p)$, where p was the relative momentum and $\bar{\sigma}(p)$ was the total cross section for a collision with relative momentum p. This quantity was calculated for each region, and a region was selected through the choice of a random number. The kinematics of the collision were worked out, and it was determined if the final state satisfied the Pauli principle. If not, a new path length was calculated. To escape from the nucleus, a particle was required to have 14.5 MeV, or the average of the proton and neutron barriers.

A similar set of Monte Carlo calculations were performed by Bernardini et al.,[80] who studied 90 incident 400 MeV nucleons on an A = 100 nucleus. The distinction between neutrons and protons was not made, only average

nucleons were used. The Fermi energy was taken to be 22 MeV and the binding energy to be 9 MeV. A Coulomb barrier of 4 MeV (half the proton value) was used. An isotropic cross section equal to the average of the p-p and n-p cross sections was used. It was assumed that the average cross section over the Fermi sphere was the same as the mean cross section for the incident energy. The Fermi sphere was divided into 1000 sample regions. If the energy of a nucleon fell below 35 MeV it was assumed to be thermally captured. The thermal excitation energy was calculated from $U = 400 - \sum_{n=1}^{N} E_n - \alpha(N-1)$ where U is the excitation energy, $\sum_{n=1}^{N} En$ is the sum of the kinetic energies of the outgoing N nucleons, and α is the binding energy per nucleon. This model gave results which were in fair agreement with experiment.

These early calculations had been tediously worked out by hand. Metropolis et al.[81] used a computer to work through a much larger number of cascades. The incident particles were protons of from 82 to 365 MeV, with a later paper examining incident protons of up to 1800 MeV and incident pions of up to 1500 MeV. A more accurate nuclear radius was used, with $r_0 = 1.3 \times 10^{-13}$cm. instead of 1.4×10^{-13}cm.(used by Bernardini et al.[80]) or 1.5×10^{-13}cm.(used by Goldhaber[79]). Bernardini had approximated both the n-p and p-p cross sections by a $1/E^{\alpha}$ expression. Metropolis et al. used the far more accurate

$$\sigma_{ii} = \left(\frac{10.63}{\beta^2} - \frac{29.2}{\beta} + 42.9\right) \text{mb}$$

$$\sigma_{ij} = \left(\frac{34.10}{\beta^2} - \frac{82.2}{\beta} + 82.2\right) \text{mb}$$

Here β is the relative velocity of the nucleons divided by the velocity of light. Bernardini et al. had assumed isotropic center of mass scattering, while Metropolis et al. used $d\sigma/d\Omega = k(A\cos^4\theta + B\cos^3\theta + 1)$ where values of A and B were given at eight energies and interpolation used. Bernardini et al. had to settle for three place random numbers, while Metropolis et al. used 38 place random numbers. For each target, the average binding energy per nucleon and the Fermi energy were calculated. A wide range of quantities were calculated, usually with 1000 cascades per run, and checked against experiment and against previous calculations. The agreement was generally good.

A modification of the Metropolis program by Chen et al.[74,82,83] forms the VEGAS cascade code, which is used today. In this code refraction and reflection of nucleons, a non-uniform nuclear density distribution, a velocity dependent potential, and nucleon correlations are included.

Another code still in use was developed by Bertini et al.[84-87] at Oak Ridge. The Bertini model divided the nucleus into regions of different densities. In each

nucleus into regions of different densities. In each region a separate Fermi energy and nuclear potential were calculated. Pion production was taken into account using the Lindenbaum-Sternheimer isobar model. This program (MECC-7) worked well for incident nucleons of energy < 3.5 GeV. A later model[88] incorporated a localized reduction in nuclear density due to cascade development, the sequencing of events with time, and a higher energy pion production model. This gave fair results to 1000 GeV, and is known as HECC-1.

In the evaporation stage, the nucleus is viewed as being in thermal equilibrium. Weisskopf derived an expression for the probability for the emission of particle j with kinetic energy between ε and $\varepsilon+d\varepsilon$ as

$$P_j(\varepsilon)d\varepsilon = \gamma_j \sigma \varepsilon [W(f)/W(i)]d\varepsilon$$

where $\gamma_j = g_j m_j/\pi^2 h^3$, g is the number of spin states of particle j, m_j is the mass of particle j, σ is the cross section for the inverse reaction, and W(f) and W(i) are the level densities of the final and initial nuclei.

Dostrovsky et al.,[89] were the first to apply the Monte Carlo technique to nuclear evaporation. Using the Weisskopf expression they approximated the inverse cross section by $\pi R^2 \alpha (1+\beta/\varepsilon)$ for neutrons, and by $\pi R^2(1+c_j)(1-k_j V_j/\varepsilon)$ for charged particles. Here R was taken to be $(1.5\times10^{-13}\text{cm.})A^{1/3}$, $\alpha = .76+2.2A^{-1/3}$,

$\beta = (2.12A^{-2/3}-.05)/\alpha$, Vj was the classical Coulomb barrier, and c_j and k_j were chosen to give good empirical fits to theoretical cross sections.

The level density was approximated by $W(E) = C\exp\{2[a(E-\delta)]^{1/2}\}$, where $a = A/20$, E is the excitation energy of the nucleus, and δ is the pairing energy. C is a constant. This expression is Hurwitz and Bethe's[90] modification of an equation due to Weisskopf. The pairing energies were taken from the values of Cameron.[91,92] With these values, Weisskopf's equation can be integrated to yield the relative probabilities of emission of various particles from an excited nucleus, as well as their excitation energy.

A modified form of the Dostrovsky et al.[89] program, developed by Dresner[93] and by Guthrie,[94,95] and incorporating suggestions of Peelle and Aebersold,[96] is used at Oak Ridge with the Bertini code. This includes Be^8 break up, includes the recoil energy of the nucleus in the calculation of the excitation energy, and includes a pairing energy adjustment at the end of the evaporation process. Fission cross sections are also included.

Other methods of treating nuclear reactions include those of Mathews et al.,[97] which allows cascade stage emission of nucleon clusters, and the various preequilibrium models.[98] The present work does not make use of either of these.

CASCADE STAGE

INVOLVES NUCLEONS (PROTONS AND NEUTRONS)

FAST (10^{-21} SECONDS)

HIGH ENERGY

FORWARD EMISSION

NUCLEONS MAY ESCAPE OR BE CAPTURED

NUCLEUS IS LEFT WITH EXCITATION ENERGY

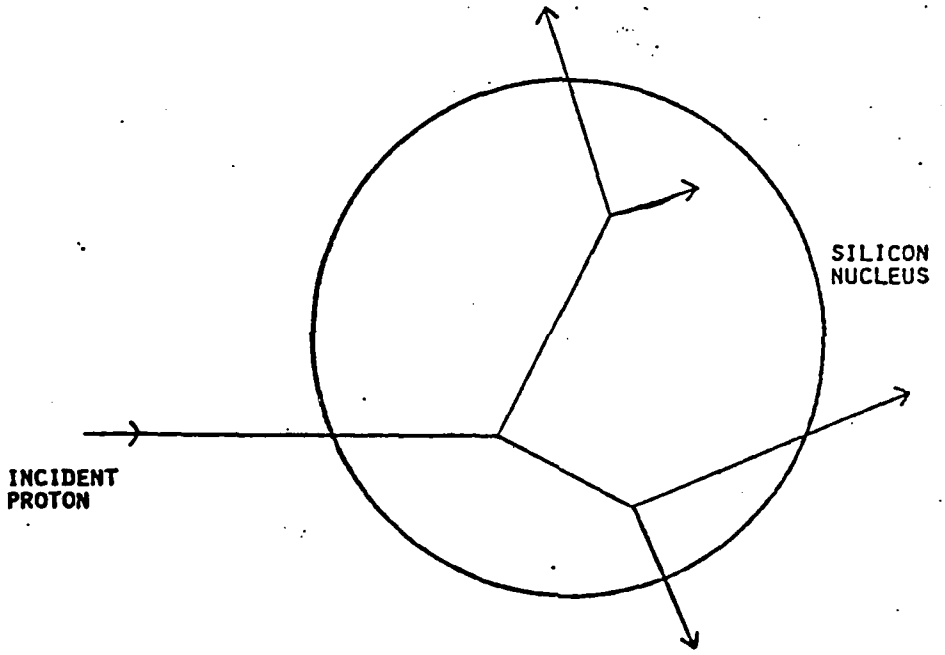

FIGURE 5

EVAPORATION STAGE

INVOLVES NUCLEONS AND CLUSTERS OF NUCLEONS

SLOW (10^{-16} SECOND'S)

LOWER ENERGY

ISOTROPIC EMISSION

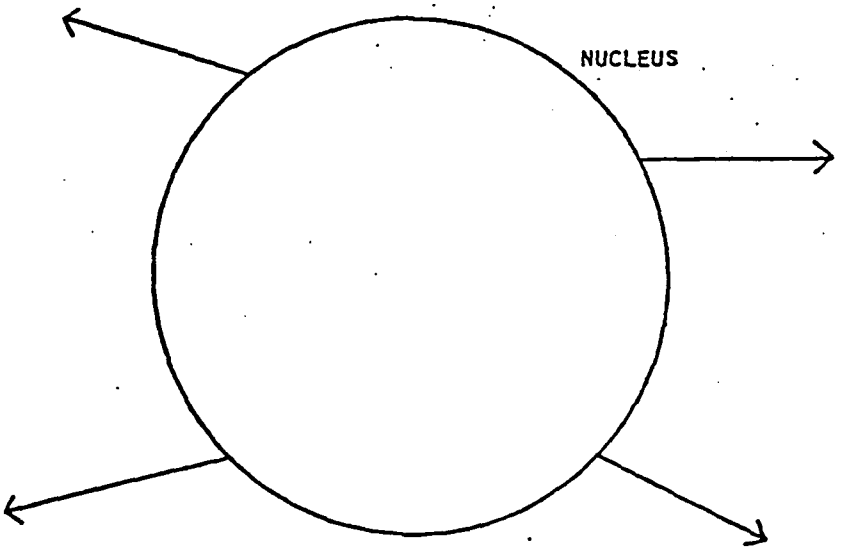

FIGURE 6

III. COMPUTER MODEL

The course of the calculation is shown in the diagram on p. 43. The dimensions of the large volume and the sensitive volume are read in. The large volume represents any surrounding material. Nuclear reactions occurring in the large volume can send particles through the sensitive volume. An energy spectrum for the incident particles is also read in. The bombarding particles can be either neutrons or protons. The particles can be either monoenergetic or of a double power law spectrum of the form E^{α} from E_1 to E_2 and E^{β} from E_2 to E_3. The constants α, β, E_1, E_2, and E_3 are also read in from the data file, as are range-energy tables. The energy and direction of the first incident particle are chosen. The range of the particle is found from the tables. The large volume is divided into segments, and the probability of the particle undergoing a nuclear reaction in each of the segments is calculated. Through the choice of a random number, it is decided whether the particle will interact and in which segment it will interact. Another random number selection determines the exact point of interaction within the segment.

Next to be calculated is the amount of energy deposited by the incident particle in the sensitive volume. Consider the x-direction first. Assume that the sensitive volume extends from $x=x_1$ to $x=x_2$. Let the incident particle path, from where it enters the large

volume to where it stops or interacts, extend from $x=x_3$ to $x=x_4$. There are six cases:

Case 1:

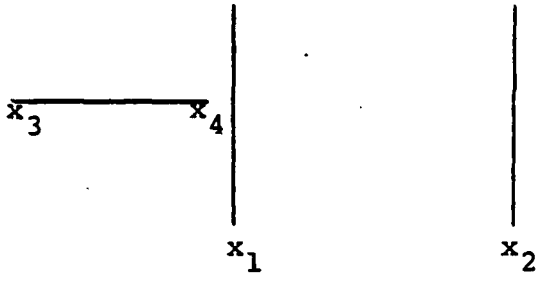

Case 2:

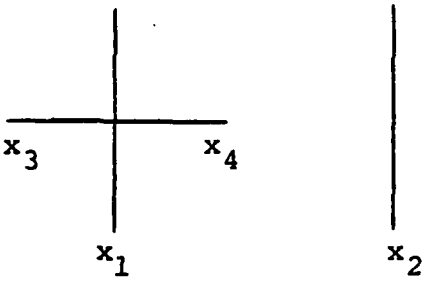

(Stopper)

Case 3:

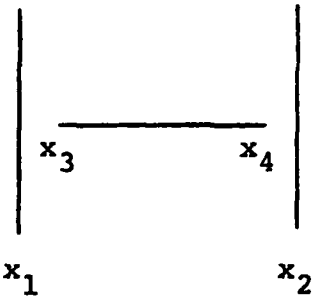

(Insider)

Case 4:

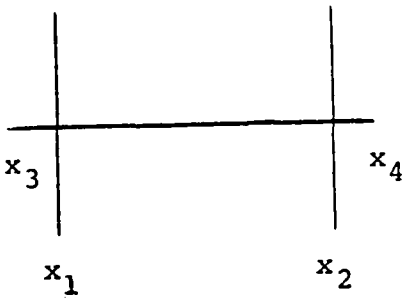

(Crosser)

Case 5:

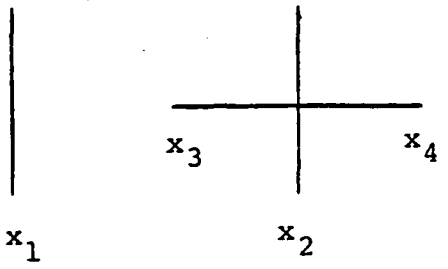

(Starter)

Case 6:

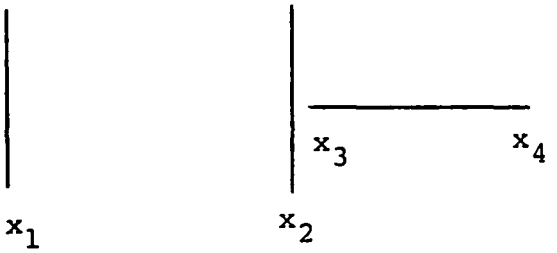

A comparison of the values of x_1, x_2, x_3, and x_4 determines the case. In case 1 and case 6 the particle does not intersect the sensitive volume. In the other four cases the x-coordinates of the sensitive volume and the particle track intersect, and it remains to be determined if the y- and z-coordinates also do. The locus of intersection in the x-dimension is a line segment with two endpoints. In case 2, for example, these endpoints are $x=x_1$ and $x=x_4$. The path of the incident particle defines a line, the equation of which is known. Knowing the x-coordinates of the endpoints, the y-coordinates of

these points can be found from the equation of the line. Call these y-coordinates y_3 and y_4. Let the sensitive volume extend, in the y-direction, from y_1 to Y_2. Run through the six cases again:

Case 1:

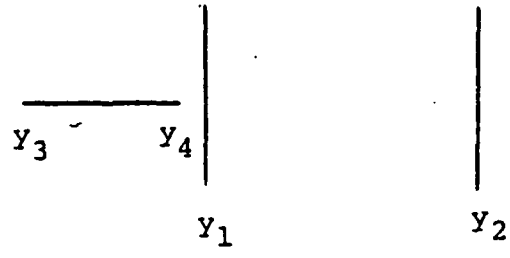

Case 2:

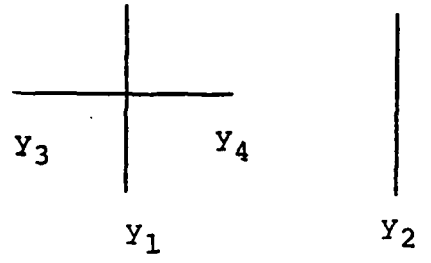

(Stopper)

Diagrams for the other cases will be omitted. Once again if there is a locus of intersection, it will define a line segment with endpoints which are readily found. On this segment, both the x- and y-coordinates of the particle track and the sensitive volume intersect. From the equation of the line, the z-coordinates of the endpoints of the line segment are found. Call them z_3 and z_4, and let the sensitive volume extend from z_1 to z_2. Again run through the six cases, and find the locus of intersection. This defines a final line segment, on which the x-, y-, and z-coordinates of the particle track and the

sensitive volume intersect. Thus, this section of track is within the sensitive volume. The endpoints of this track segment are found, and are labeled A and B. Let R be the point where the incident particle comes to its end of range, or where it would have had it not interacted. Two residual ranges are defined by $\overline{AR}$ and $\overline{BR}$. The energy corresponding to each residual range is calculated, and the difference in these energies is the amount deposited in the sensitive volume.

If there is an interaction, the incident particle's energy at the interaction site is found from the range-energy tables. The struck nucleus is treated as a sphere of radius $1.3A^{1/3}$ fermis, where A is the mass number. A random impact point on the surface of the sphere is chosen. Upon entering the nucleus, the particle picks up the nuclear potential in addition to its kinetic energy. The nuclear potential is taken to be the sum of the Fermi energy and the binding energy. This potential is the depth of the well within which the nucleons in the nucleus are confined. The nucleons in the nucleus have energies up to a certain maximum energy, the Fermi energy.

In passing through the nucleus, the incident particle may or may not collide with other nucleons. The program uses empirical relations for p-p, n-n, and n-p cross sections devised by Metropolis et al.[81] An average cross section is found from $\sigma_{av} = [(A-Z)\sigma_{ni}+Z\sigma_{pi}]/A$, where i denotes the identity of the incident particle. The mean free path is then $\lambda = 1/\rho\sigma_{av}$, where ρ is the nuclear

density. A particular path length is then chosen as $-\lambda \cdot \ln(RAN)$, where RAN is a random number between 0 and 1. If the chosen path length, measured from the impact point on the nuclear surface, carries the particle outside the nucleus, then there is no collision. If the incident particle's path leaves it within the nucleus, a potential nuclear collision takes place.

The kinematics of the collision are worked out relativistically. Neutrons and protons are treated as having equal masses. The components of momentum of the incident particle are already known. To obtain the momentum of the struck nucleon, we assume that the momentum distribution of the nucleons is that of a sphere in momentum space with a radius equal to the Fermi momentum. Choosing three random numbers determines a point in this Fermi sphere, which yields the momentum of the struck nucleon.

The energies and momenta of the incident and target nucleons are transformed to the center of momentum frame. The scattering angle in the center of momentum frame is found from $d\sigma/d\Omega = K(A\cos^4\theta+B\cos^3\theta+1)$, where A and B depend on the relative velocity and the identity of the nucleons.[81] Given this distribution, a value of θ is determined by another random number choice. The momenta of the two nucleons after the collision are found and transformed back to the lab frame. If either of these is less than the Fermi momentum, then the collision is forbidden by the Pauli principle. The nucleons are

fermions, no two can occupy the state, and all states up to the Fermi energy are assumed to be filled.

If the collision is permitted, a path length is chosen for each of the two nucleons and the procedure is repeated. The two nucleons strike others, which in turn strike others, thus building up a nuclear cascade. Whenever a nucleon escapes from the nucleus, the nuclear potential is subtracted from the nucleon's energy.

When the energy of a nucleon falls below a certain cutoff energy, taken in this case as the sum of the nuclear potential and the Coulomb barrier for a proton, the cascade stage is terminated for that nucleon. Particles of energy less than the cutoff energy will undergo many potential collisions before the Pauli principle actually permits one to occur. A transition is therefore made to the evaporation stage, where further particle emission is handled statistically.

At the end of the cascade stage, a number of particles have been ejected from the nucleus. Their energy, momenta, angles with respect to the incident beam, and identity (proton or neutron) have been calculated. The momentum and identity of the residual target nucleus are also known. The residual nucleus has an excitation energy given by $U = T_o - \sum_{i=1}^{N} T_i - (N-1)B - T_N$ where T_o is the energy of the incident nucleon, $\sum_{i=1}^{N} T_i$ is the sum of the kinetic energies of the cascade particles ejected from the nucleus, N is the number of these particles, B is the binding energy of a nucleon, and T_N is the kinetic energy of the residual

nucleus.

The evaporation calculation closely follows the Dostrovsky et al.[89] model. Weisskopf's[78] equation for the probability per unit time of emitting particle j with kinetic energy between ε and $\varepsilon+d\varepsilon$ is $P_j(\varepsilon)d\varepsilon = \gamma_j \sigma\varepsilon \cdot [W(f)/W(i)]d\varepsilon$. The factors in the equation have been discussed in the previous section. Substituting the expressions into the equation for γ_j, σ, and W yields:

1) $$P_n(\varepsilon)d\varepsilon = \frac{g_n m_n r_o^2 A_n^{2/3}}{\pi h^3} \exp -2[a_o(E-\delta_o)]^{\frac{1}{2}} \varepsilon\alpha(1+\frac{\beta}{\varepsilon}) \cdot \exp 2[a_n(E-Q_n-\delta_n-\varepsilon)]^{\frac{1}{2}} d\varepsilon$$

This is the equation for neutron emission. For charged particles one replaces the subscript n with j, α with $(1+C_j)$, and $-\beta$ with K_jV_j. The subscripts 0 and n refer to the initial and final nucleus, respectively. The neutron separation energy is denoted by Q_n. This is calculated from tables of binding energy. The values of the pairing energy are taken from Cameron[91;92] and from Dostrovsky et al.[89] Equation 1 must now be integrated. The lower limit of integration is 0 MeV, the upper limit is $R_n = E-Q_n-\delta_n$. These limits are the smallest and greatest kinetic energies for an emitted neutron. For charged particles, the upper limit R_j $E-Q_j-K_jV_j-\delta_j$. The equation is integrated, and Dostrovsky's approximation of $\exp[2(a_nR_n)^{1/2}] >> 1$ is used. This makes a direct comparison with Dostrovsky's results possible. This yields:

$$2)\ \Gamma_n = \frac{m_n r_o^2}{2\pi h^2} \exp -2[a_o(E-\delta_o)]^{\frac{1}{2}} A_n^{2/3} \frac{g_n \alpha}{a_n^2} \exp[2(a_n R_n)^{\frac{1}{2}}] \cdot$$

$$2a_n R_n - (\tfrac{3}{2} - a_n\beta)[2(a_n R_n)^{\frac{1}{2}} - 1]$$

$$3)\ \Gamma_j = \frac{m_j r_o^2}{2\pi h^2} \exp -2[a_o(E-\delta_o)]^{\frac{1}{2}} A_j^{2/3} g_j \frac{(1+c_j)}{a_j^2} \cdot$$

$$\exp[2(a_j R_j)^{\frac{1}{2}}]\ 2a_j R_j - \tfrac{3}{2}[2(a_j R_j)^{\frac{1}{2}} - 1]$$

Equation 2 is the relative probability for neutron emission, equation 3 for charged particle emission. These quantities are calculated for n, p, d, t, He^3, and α. The identity of the evaporated particle is then found from these probabilities through the choice of a random number. The kinetic energy distribution is given by equation 1, and another random number choice determines the energy for a given particle. The evaporation particles are assumed to be emitted isotropically in the frame of the nucleus. Two more random number choices determine the angle of emission.

The excitation energy eventually falls to a level (about 10 MeV) which is too low for an additional particle to be emitted. Further de-excitation would occur by gamma emission, but this is not treated in the program.

The energy of the residual nucleus is found from momentum conservation. Its identity and direction of motion are also known. The ranges of the cascade particles, evaporation particles, and residual nucleus are found from range-energy tables. Utilizing the same geometric approach that was used to find the energy deposited in the sensitive volume by the incident particle, the energy deposited by these other particles in the sensitive volume is found. The total deposited energy for the incident particle is thus found. This procedure is repeated for a large number of incident particles with a different random number sequence each time. The spectrum of deposited energy in the sensitive volume is thus obtained. This program will give valid results up to an incident energy of 350 MeV, above which pion production begins to have an effect. Figure 7 shows a diagram of the entire nuclear reaction process.

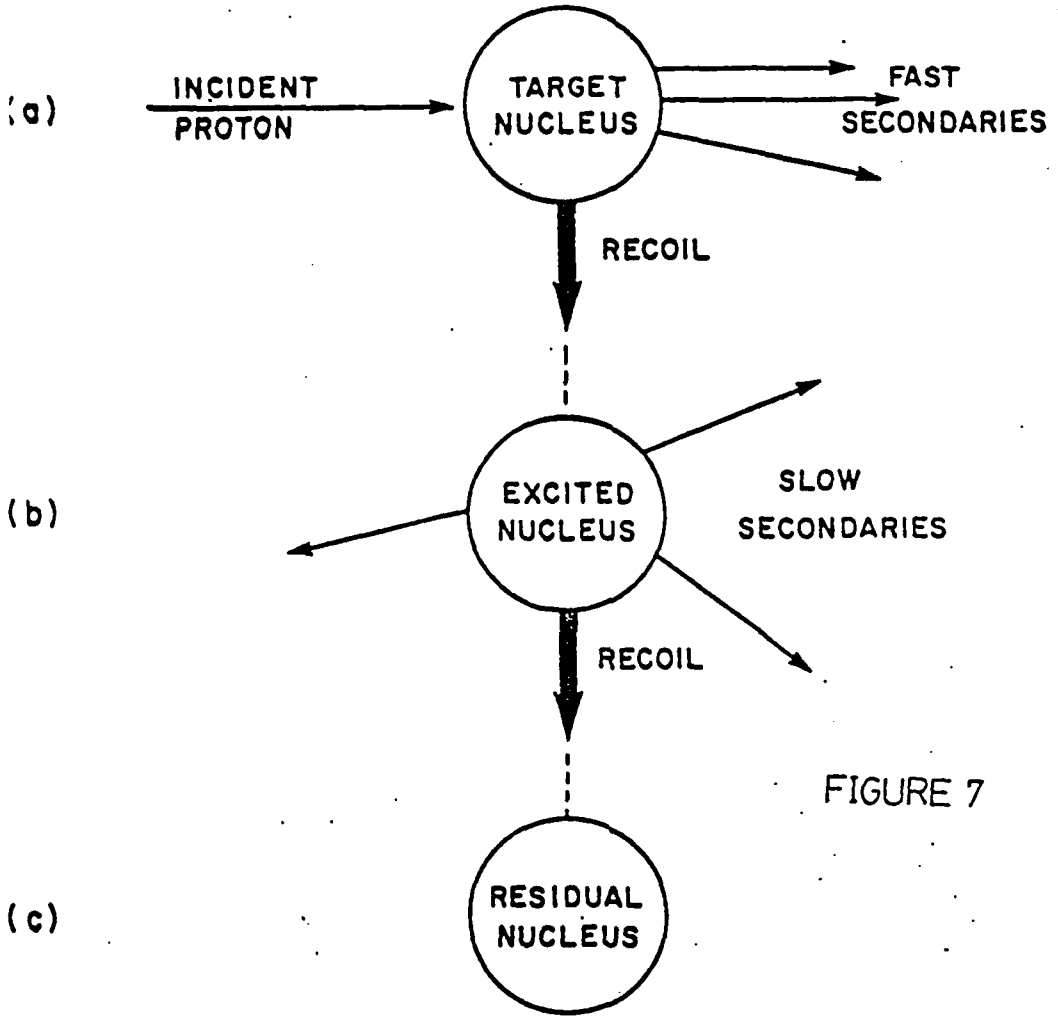
(a)
INCIDENT PROTON
TARGET NUCLEUS
FAST SECONDARIES
RECOIL
(b)
EXCITED NUCLEUS
SLOW SECONDARIES
RECOIL
(c)
RESIDUAL NUCLEUS

FIGURE 7

Course of the Calculation

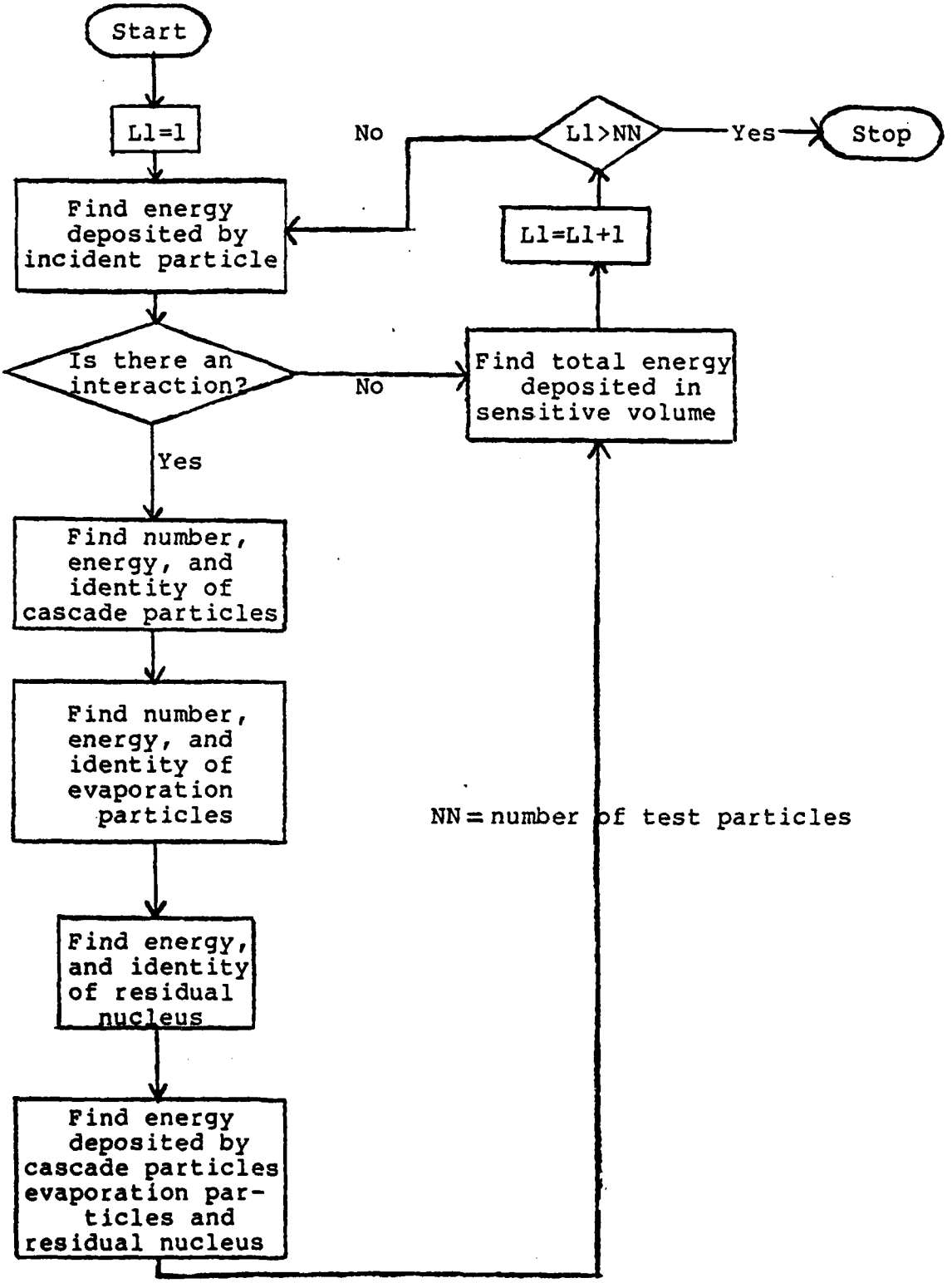

IV. COMPARISONS WITH PREVIOUS MODELS AND EXPERIMENTS

Comparisons between the nuclear reaction model developed for this thesis, other nuclear codes, and experimental results will now be shown. Currently existing codes predict well the features of some nuclear reactions, while failing to predict other reactions well. The aim in the following graphs is to show that the model used in this work gives results approximately as accurate as other codes.

The chief difference between the nuclear model used in this code and that of Bertini[84-87] is Bertini's use of a nonuniform nuclear density. A number of comparisons between experimental data, Bertini's theoretical results, and the results of this code are shown in the following figures. This code is referred to as OMNI.

In Figures 8-23 the Bertini code results are represented by a solid line, the OMNI results by a dashed line, and experiment by a dot-dashed line.

Figure 8 is a comparison for the $^{12}C(p,pn)^{11}C$ reaction. Bertini's model, which uses a larger nuclear volume, is more successful in predicting the magnitude of the cross section. In Figure 9 a comparison of the $^{12}C(p,3p3n)^{7}Be$ cross section is seen. Here the OMNI code is more successful, although the values for both codes are much lower than the experimental values. There are two reasons why ^{12}C would be expected to give difficulty to the codes. First, it is a lightweight nucleus. By the end

of the reaction there may be as little as an alpha particle left over. The evaporation process is described by a statistical model which assumes a larger number of nucleons. Second, the carbon nucleus can be viewed to a certain extent, as a collection of three alpha particles. The cascade stage views the nucleus as a collection of independent nucleons, and does not permit particles heavier than protons or neutrons to be emitted. The inclusion of heavier cascade particles would require a considerably more complex computer program. Cascade stage alpha emission could explain the large difference between theory and experiment in Figure 9.

Cascade proton spectra from 190 MeV protons on aluminum are shown in the next four figures. Figure 10 shows the spectrum in the interval from 0^{o} to 65^{o}, Figure 11 shows it from 100^{o} to 180^{o}, Figure 12 shows it from 46^{o} to 65^{o}, and Figure 13 shows it from 102^{o} to 117^{o}. Both OMNI and the Bertini code are seen to be in good agreement with experiment. As aluminum is only one atomic number removed from silicon, this suggests that the results for that element will also be good.

Figure 14 shows the angular distribution of cascade protons from 90 MeV neutrons on C. Here the Bertini model is in better agreement. Energy spectra for the same experiment are shown in Figures 15 and 16. The spectrum at 0^{o} (Figure 15) is at variance with the predictions of both models, while the OMNI model does a much better job at 45^{o} (Figure 16). The proton spectrum at 90^{o} from 240

MeV protons on C (Figure 17) is well described by both models, while the OMNI model predicts the proton spectrum at 30° from 340 MeV protons on C (Figure 18) to slightly better accuracy. The spectrum of cascade protons at 40° from 340 MeV protons on C is predicted well by both models. This is shown in Figure 19.

In Figure 20 the proton spectrum at 40° for 96 MeV protons on F is shown. Both models are in good agreement. The experimental peak at large energies is presumably due to elastic scattering, which neither program handles. In Figure 21 the angular distribution of cascade protons from 90 MeV p on Cu is plotted. The energy spectrum from the same experiment is plotted in Figures 22 and 23. At 0° (Figure 22) both models work badly, while at 45° (Figure 23) there is fair agreement in both cases.

Figures 24 and 25 compare the energy spectra of evaporation neutrons and protons obtained in the OMNI model to the spectra obtained from the evaporation code used in the Bertini model. Protons of 130 MeV were incident on Si^{28}. Plots for two different values of the level density parameter are shown, with A/8 being the value used in almost all of the calculations.

A comparison of three widely used nuclear cascade codes was made by Barashenkov et al.[99] In the simulations, Al^{27} and Ta^{181} were bombarded by 150 Mev and 300 MeV protons. The codes used were the Bertini code, the Brookhaven code, and a code developed at the Joint Institute of Nuclear Research (JINR) in the USSR. For each

code thhe energy distribution of cascade protons at 30^{o} and 80^{o}, the excitation energy distribution after the cascade stage, and the mass yields were calculated. The paper cites "excellent agreement" in the abstract and "remarkably similar results" in the conclusions, but the comparison graphs in the article show some wide disagreements. For example, for 150 MeV p on Ta^{181} and a (p,p) reaction leaving an excitation energy of 130 MeV, the Bertini and Brookhaven codes disagree by a factor of roughly 400. For the same type of reaction on Al^{27} for an excitation energy of 100 MeV they differ by a factor of 40, and if the incident energy is changed to 300 MeV the difference is a factor of 50. Other comparisons are shown, and the Bertini code is seen to predict somewhat lower excitation energies than the others. The Brookhaven code, however, is the more sophisticated. The Bertini code uses three concentric regions to model the nuclear density distribution, while the Brookhaven model uses eight. The Brookhaven model also uses a velocity-dependent potential for nucleons within the nucleus, treats reflection and refraction at potential boundaries, and approximates the effect of nucleon pair correlations by setting a minimum distance between nuclear collisions. The Bertini code does none of these, although it has the advantage of incorporating pion production, thereby extending the applicable energy range of the program.

Jastrzebski et al.[100] measured the cross sections and residual ranges of nuclei from the bombardment of

Ni^{58} and Ni^{62} by protons of 80, 136, 153, and 164 MeV. The results were compared to computer calculations using the cascade code VEGAS and the evaporation code DFF. The ranges of the recoiling nuclei were determined from their energies as given by the computer codes and the range-energy tables of Northcliffe and Schilling.[101] The theoretical values, as seen in Figures 26-29, are greater in general than the experimental values for large values of ΔA and smaller for very small values of ΔA. Here the VEGAS results are shown by a solid line, the OMNI results by a dashed line, and the experimental values as points with error bars. Part of the reason for this variance lies in the nature of the quantity tabulated by Northcliffe and Schilling. This quantity is the pathlength, or the integral of dE/dx over distance. The experiment actually measures the projected range, i.e., the projection of the pathlength along the direction of the incident particle. The OMNI simulation also uses the Northcliffe and Schilling data, and is seen to give results in good agreement with the VEGAS-DFF calculation. This is encouraging in view of the more sophisticated nature of the VEGAS program.

Kwiatkowski et al.[102] measured the mass, energy, and angular distributions of the products from the interaction of 180 MeV protons with ^{27}Al. The mass distribution of residual nuclei is shown in Figure 30, together with theoretical predictions from the VEGAS code and the OMNI code developed in this work. The VEGAS results are shown by a solid line, the OMNI results by a dashed line, and the

experimental values by points. The OMNI code gives a reasonably good fit to experiment. It was observed that the relatively large number of low mass residual nuclei, while not predicted by the cascade models, was in agreement with predictions of the pre-equilibrium model.[98].

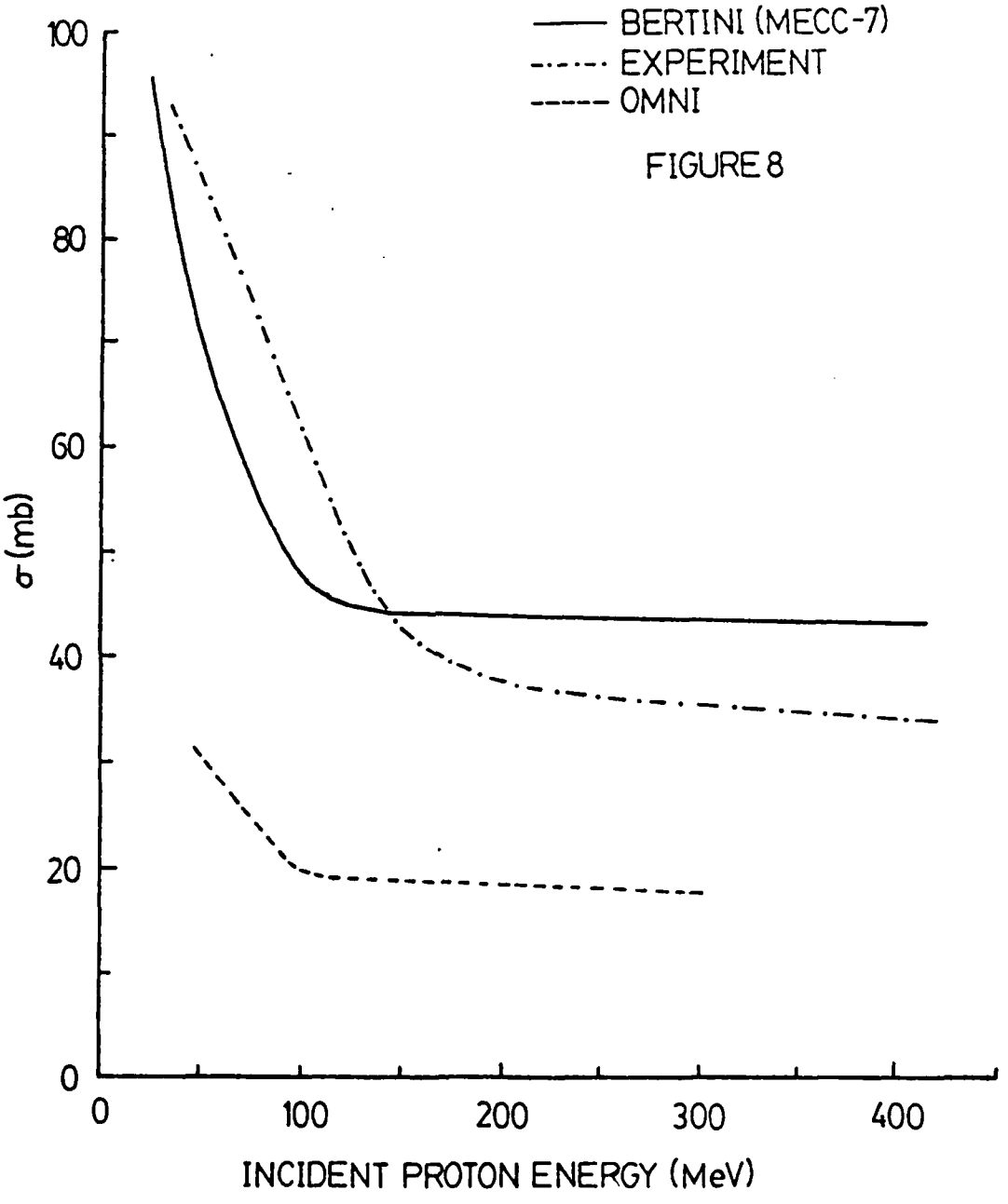
BERTINI (MECC-7)
EXPERIMENT
OMNI
100
80
60
40
20
0
σ (mb)
0
100
200
300
400
INCIDENT PROTON ENERGY (MeV)

FIGURE 8

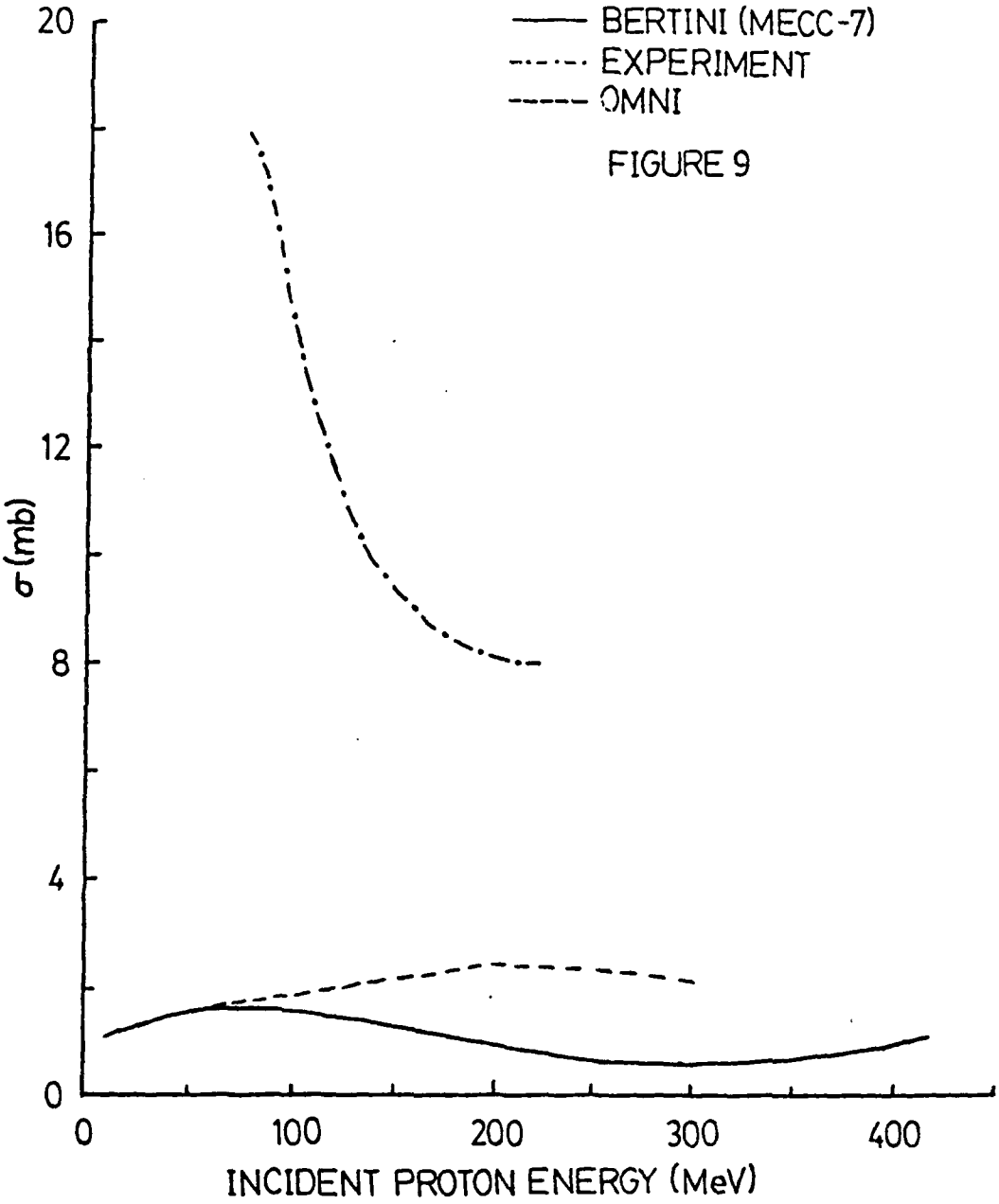
BERTINI (MECC-7)
EXPERIMENT
OMNI
20
16
12
8
4
0
σ (mb)
0
100
200
300
400
INCIDENT PROTON ENERGY (MeV)

FIGURE 9

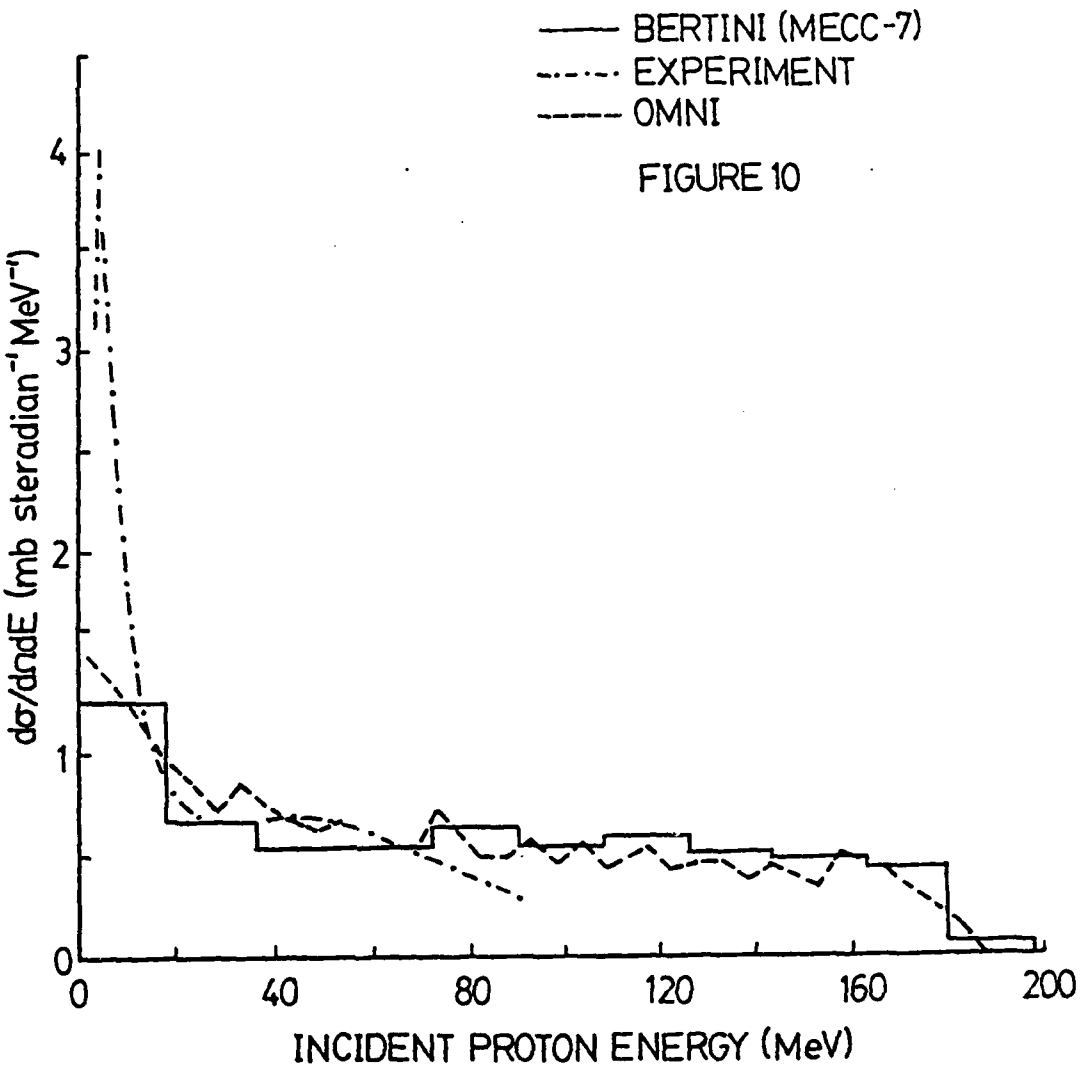
BERTINI (MECC-7)
EXPERIMENT
OMNI
dσ/dΩdE (mb steradian⁻¹MeV⁻¹)
0
1
2
3
4
0
40
80
120
160
200
INCIDENT PROTON ENERGY (MeV)

FIGURE 10

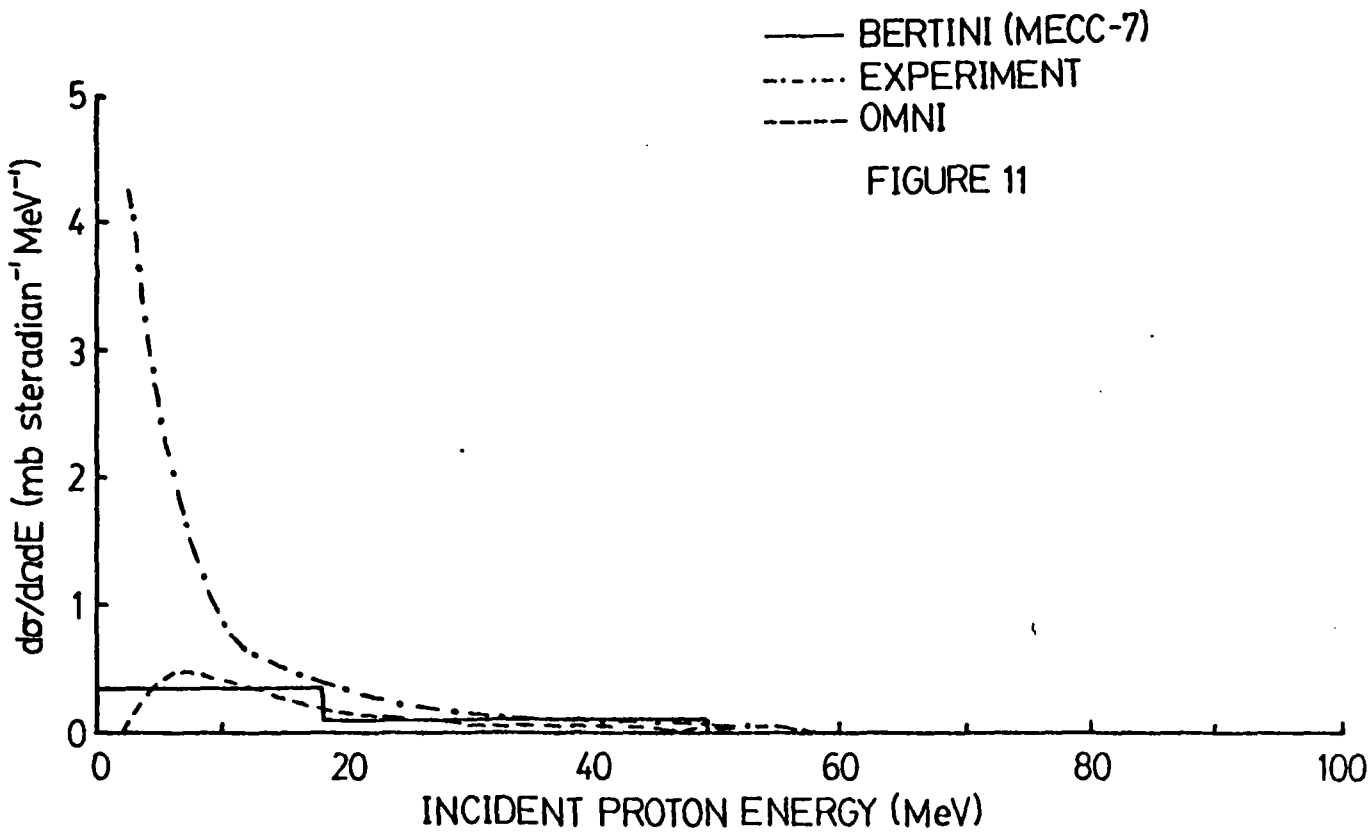
—— BERTINI (MECC-7)
-·-·-· EXPERIMENT
----- OMNI
dσ/dΩdE (mb steradian⁻¹ MeV⁻¹)
0
1
2
3
4
5
0
20
40
60
80
100
INCIDENT PROTON ENERGY (MeV)

FIGURE 11

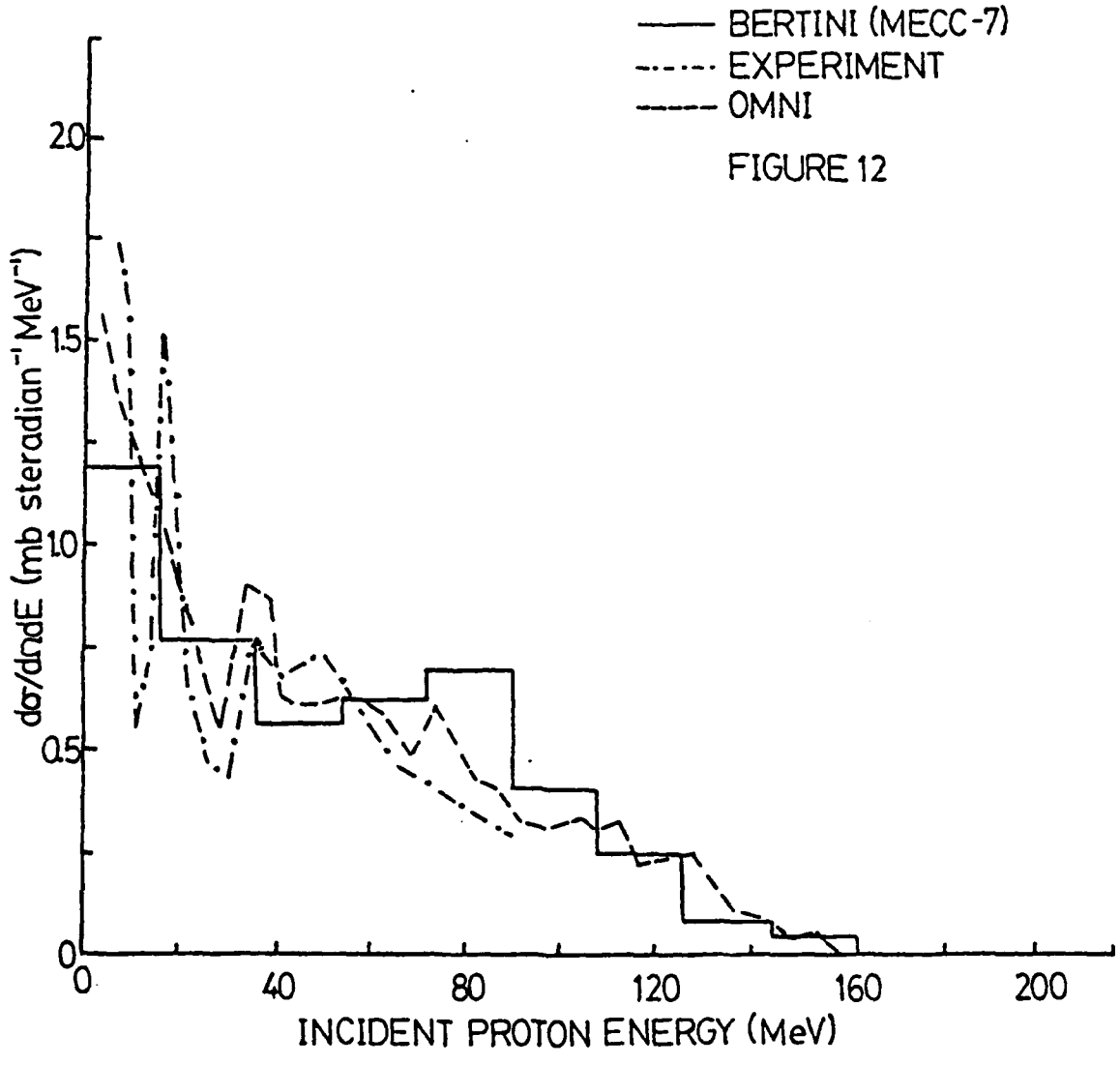
BERTINI (MECC-7)
EXPERIMENT
OMNI
2.0
1.5
1.0
0.5
0
dσ/dndE (mb steradian⁻¹ MeV⁻¹)
0
40
80
120
160
200
INCIDENT PROTON ENERGY (MeV)

FIGURE 12

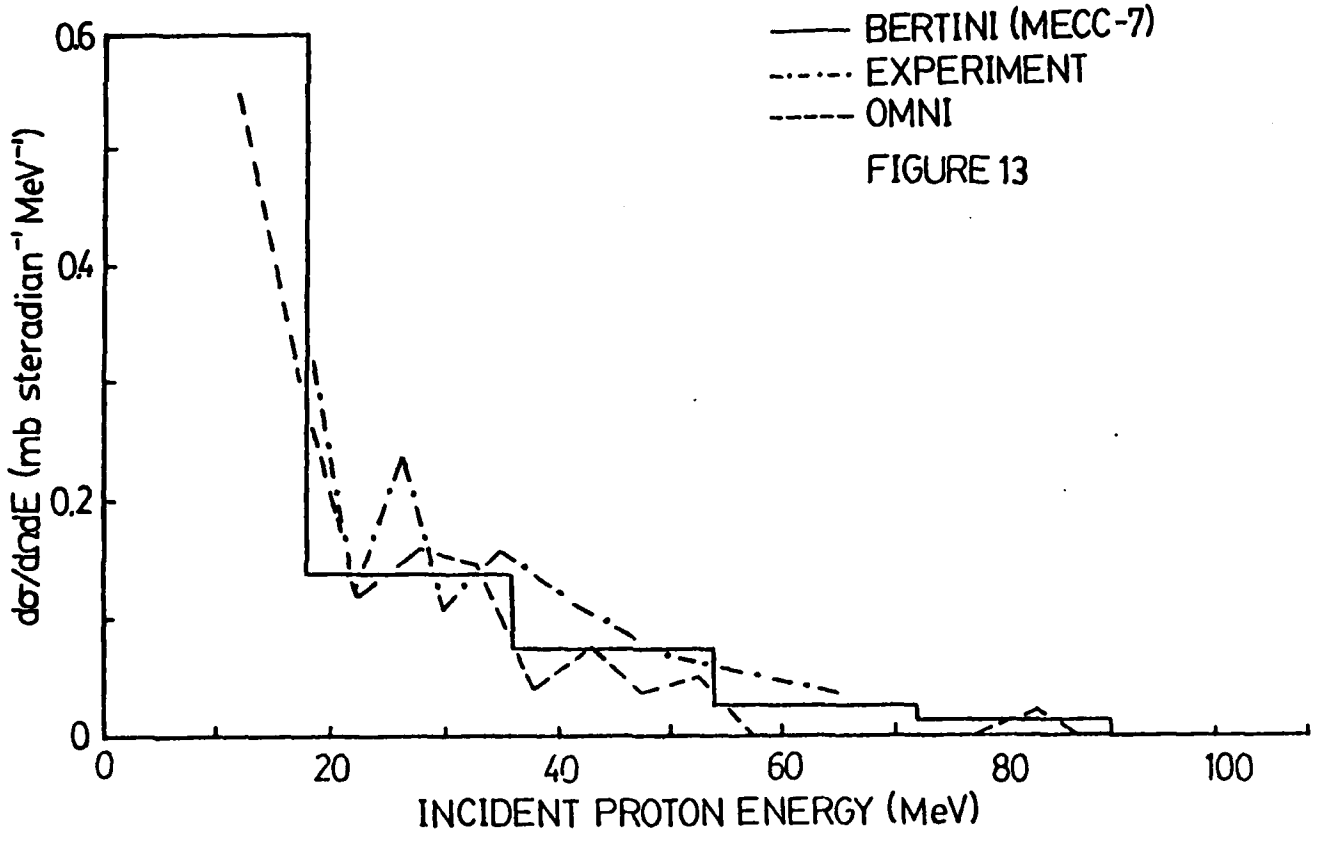
BERTINI (MECC-7)
EXPERIMENT
OMNI
0.6
0.4
0.2
0
dσ/dΩdE (mb steradian⁻¹ MeV⁻¹)
0
20
40
60
80
100
INCIDENT PROTON ENERGY (MeV)

FIGURE 13

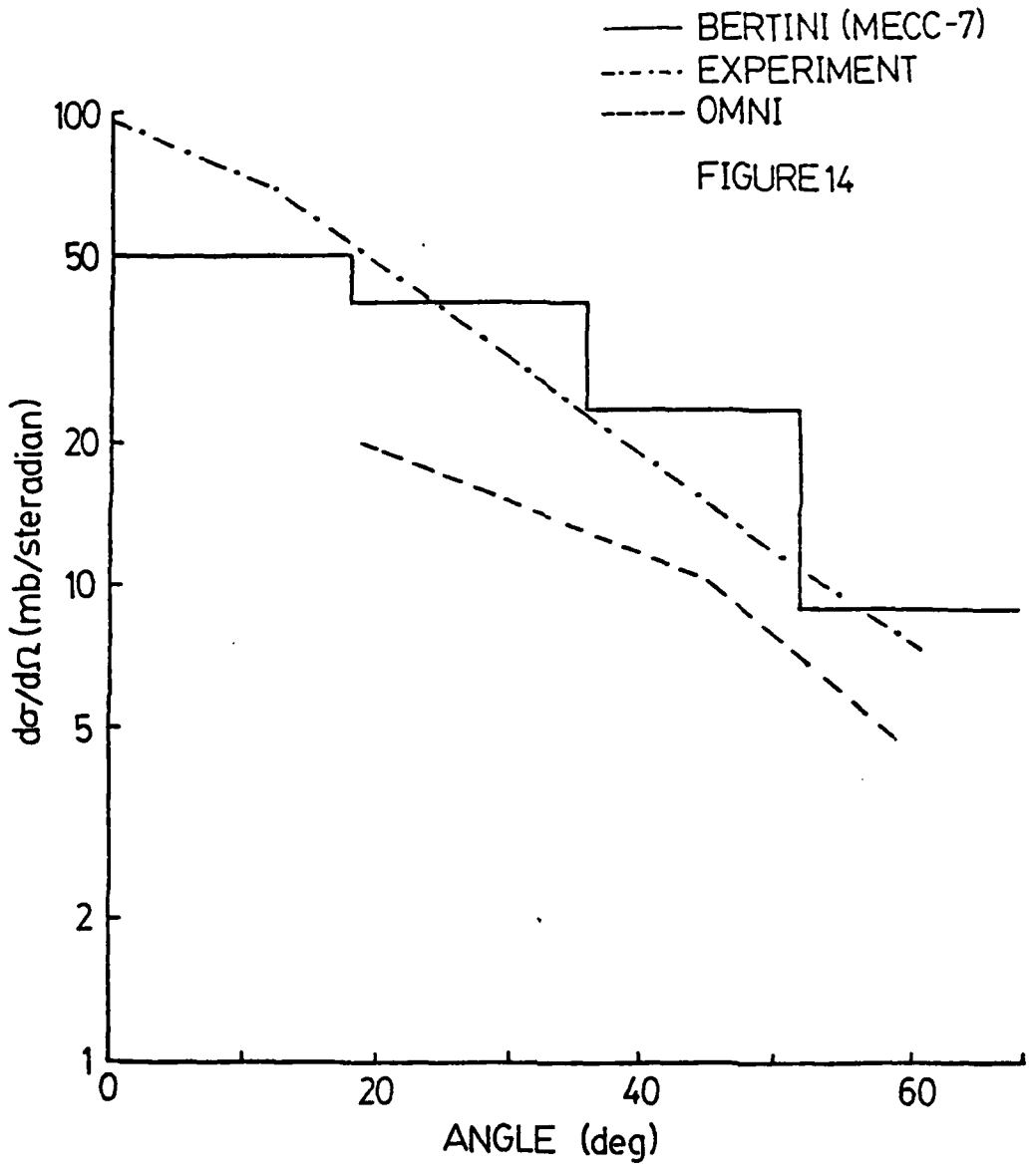
BERTINI (MECC-7)
EXPERIMENT
OMNI
100
50
20
10
5
2
1
dσ/dΩ (mb/steradian)
0
20
40
60
ANGLE (deg)

FIGURE 14

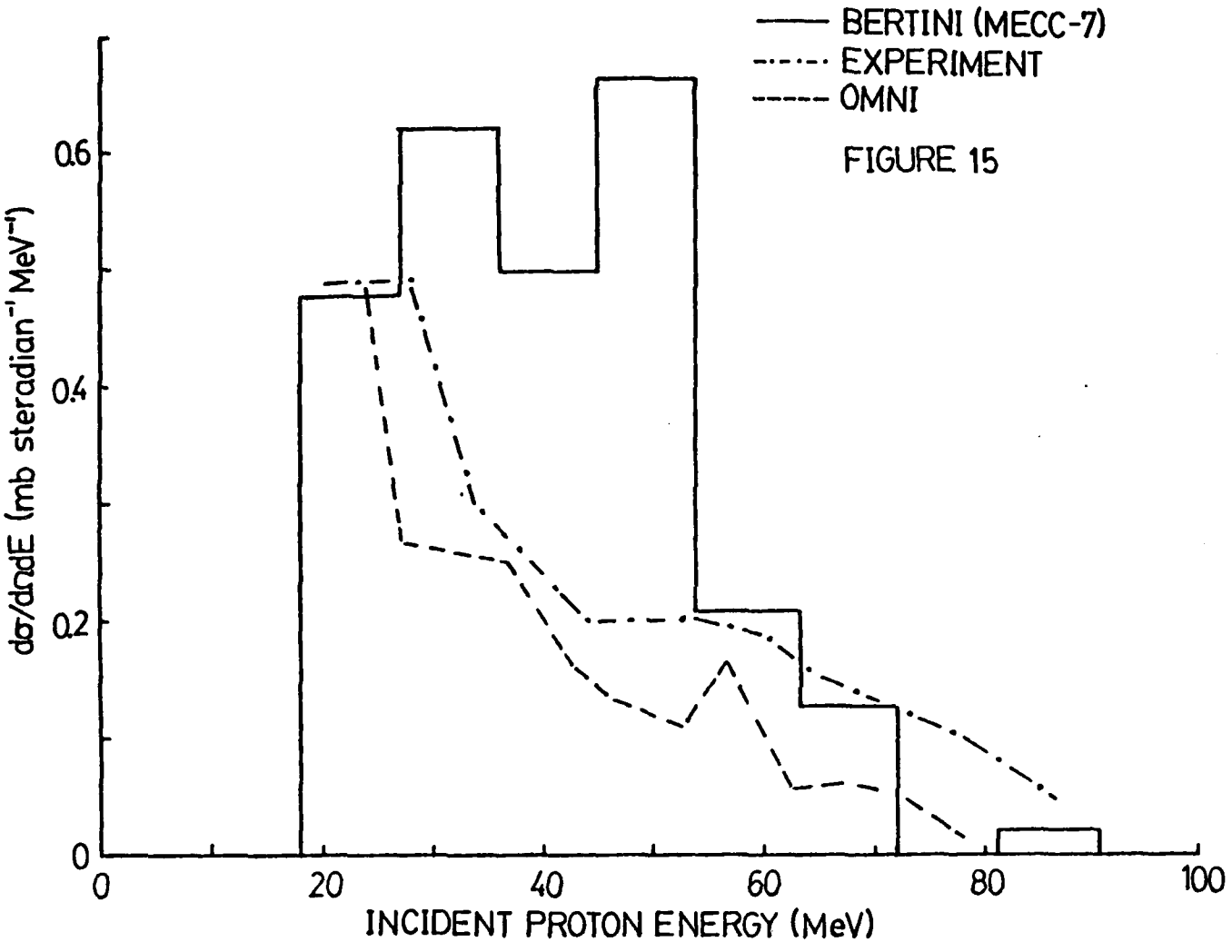
BERTINI (MECC-7)
EXPERIMENT
OMNI
dσ/dΩdE (mb steradian⁻¹ MeV⁻¹)
0
0.2
0.4
0.6
0
20
40
60
80
100
INCIDENT PROTON ENERGY (MeV)

FIGURE 15

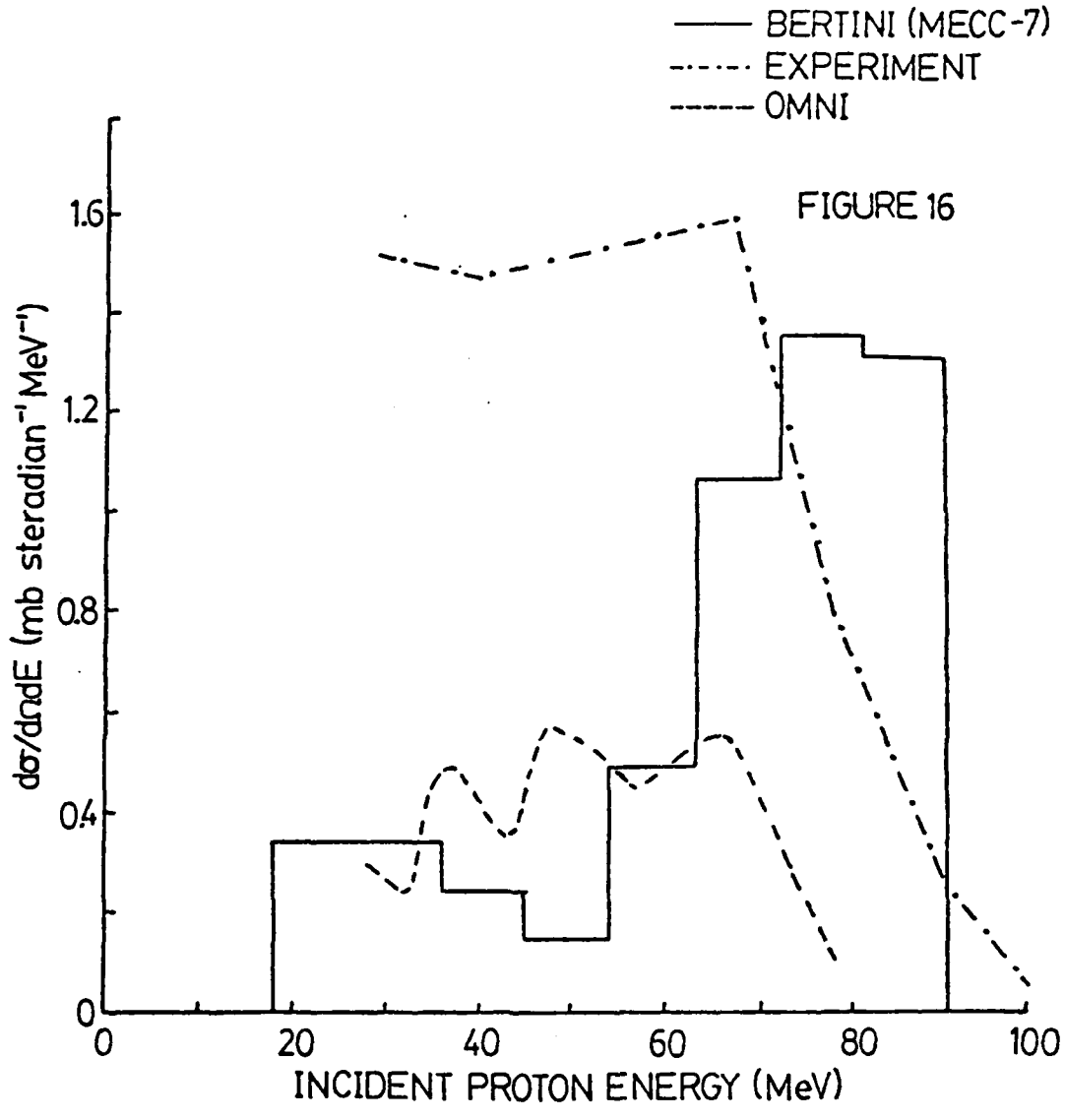
BERTINI (MECC-7)
EXPERIMENT
OMNI
1.6
1.2
0.8
0.4
0
dσ/dΩdE (mb steradian⁻¹ MeV⁻¹)
0
20
40
60
80
100
INCIDENT PROTON ENERGY (MeV)

FIGURE 16

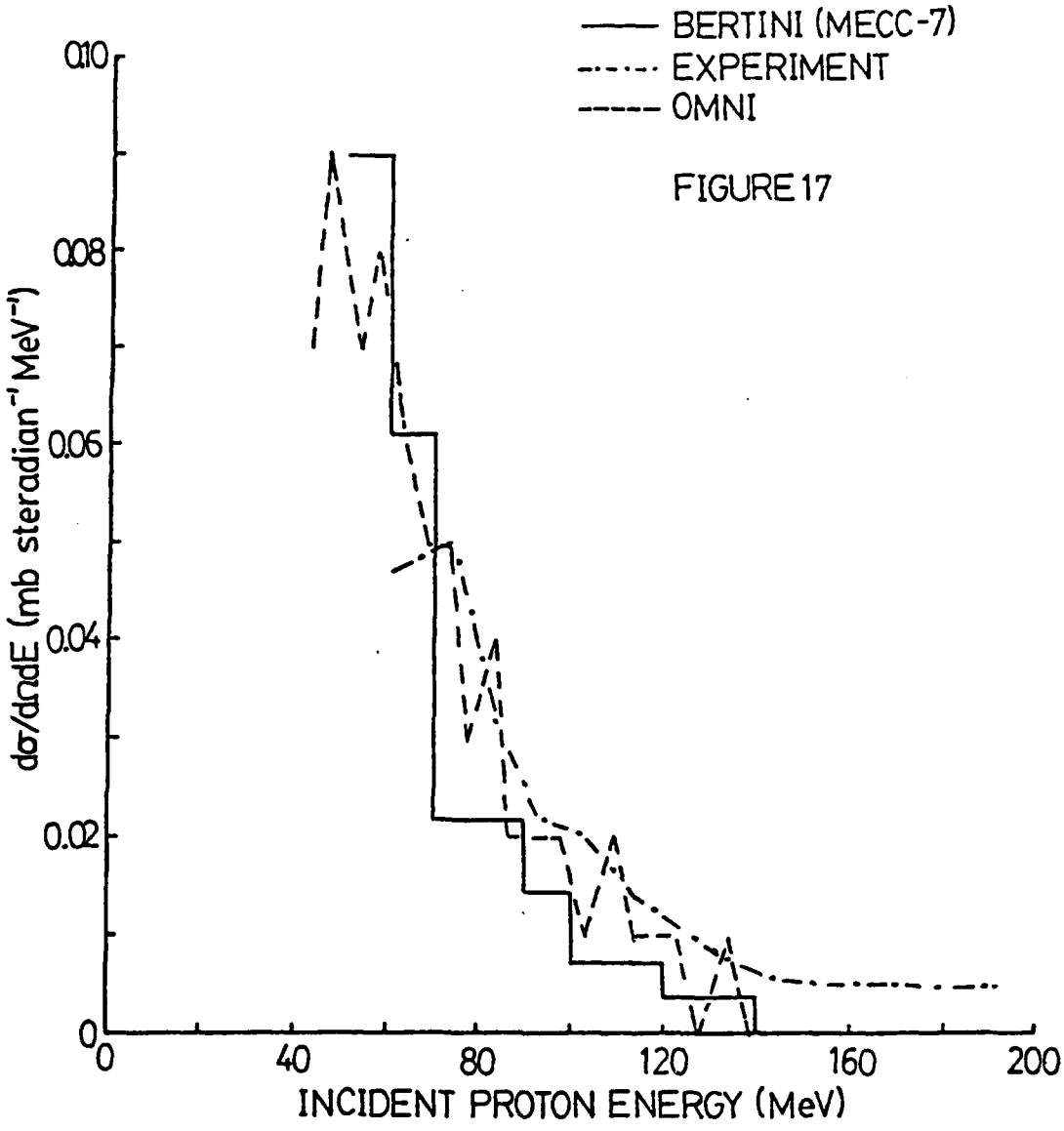
BERTINI (MECC-7)
EXPERIMENT
OMNI
0.10
0.08
0.06
0.04
0.02
0
dσ/dΩdE (mb steradian⁻¹ MeV⁻¹)
0
40
80
120
160
200
INCIDENT PROTON ENERGY (MeV)

FIGURE 17

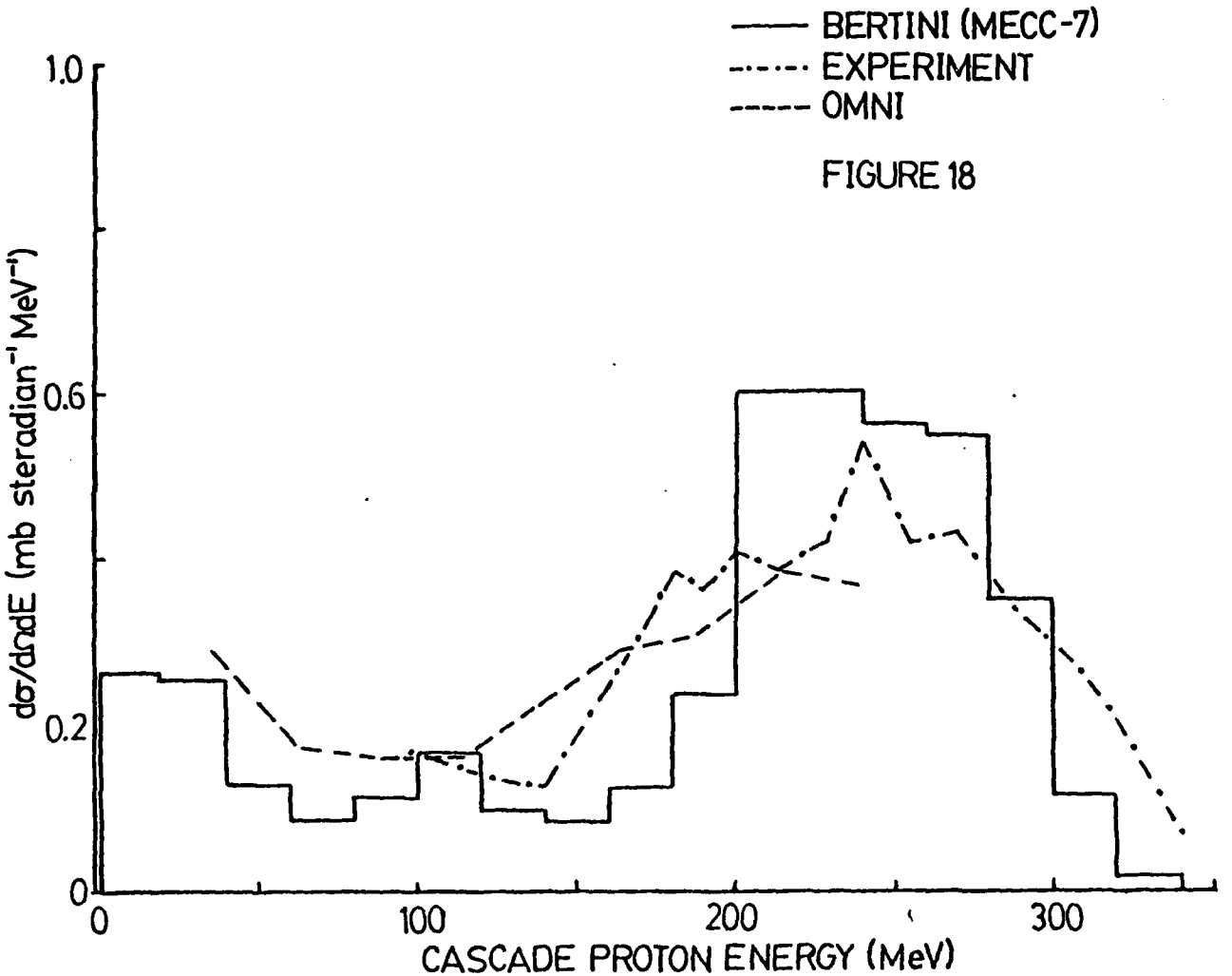
BERTINI (MECC-7)
EXPERIMENT
OMNI
1.0
0.6
0.2
0
dσ/dΩdE (mb steradian⁻¹ MeV⁻¹)
0
100
200
300
CASCADE PROTON ENERGY (MeV)

FIGURE 18

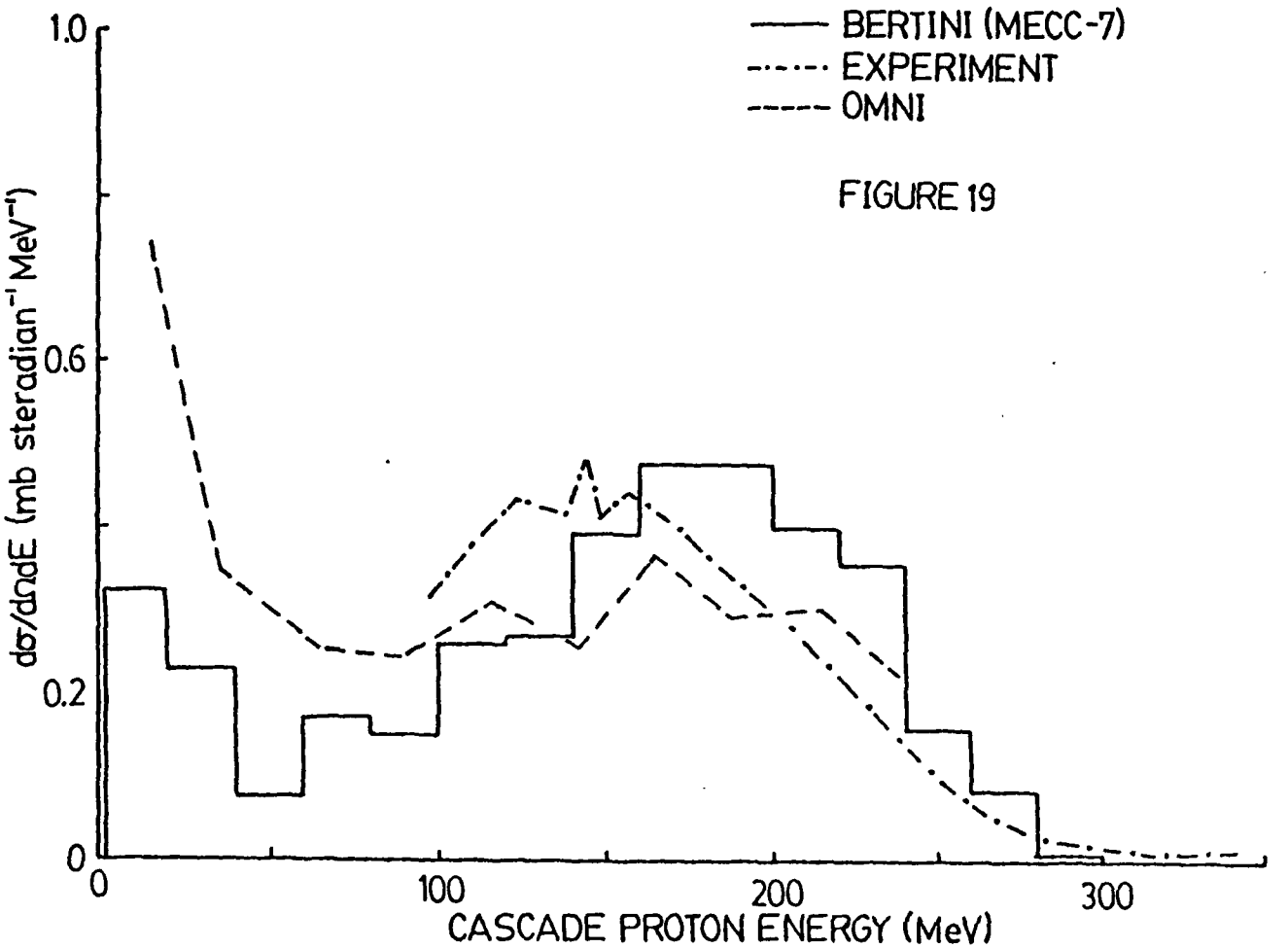
BERTINI (MECC-7)
EXPERIMENT
OMNI
1.0
0.6
0.2
0
dσ/dΩdE (mb steradian⁻¹ MeV⁻¹)
0
100
200
300
CASCADE PROTON ENERGY (MeV)

FIGURE 19

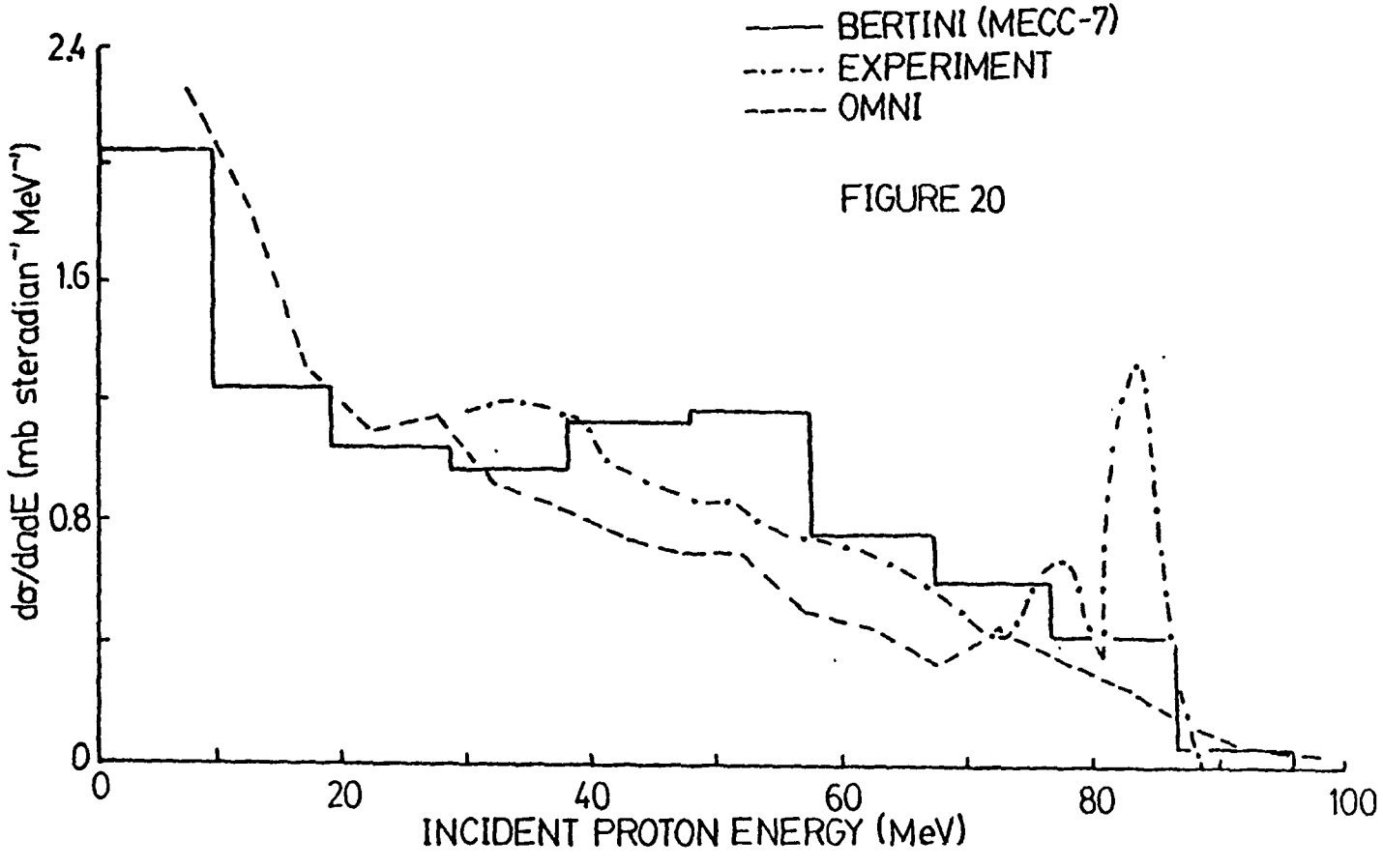
BERTINI (MECC-7)
EXPERIMENT
OMNI
2.4
1.6
0.8
0
dσ/dΩdE (mb steradian⁻¹ MeV⁻¹)
0
20
40
60
80
100
INCIDENT PROTON ENERGY (MeV)

FIGURE 20

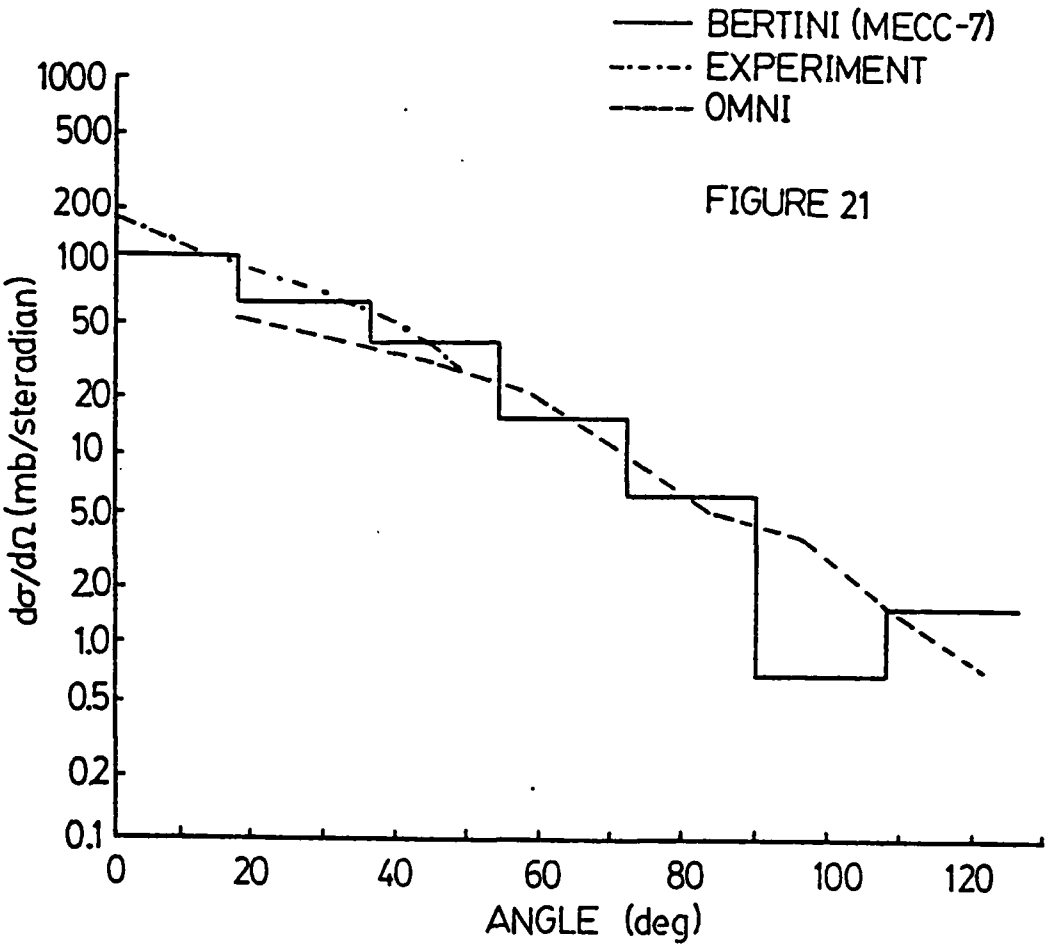
BERTINI (MECC-7)
EXPERIMENT
OMNI
1000
500
200
100
50
20
10
5.0
2.0
1.0
0.5
0.2
0.1
dσ/dΩ (mb/steradian)
0
20
40
60
80
100
120
ANGLE (deg)

FIGURE 21

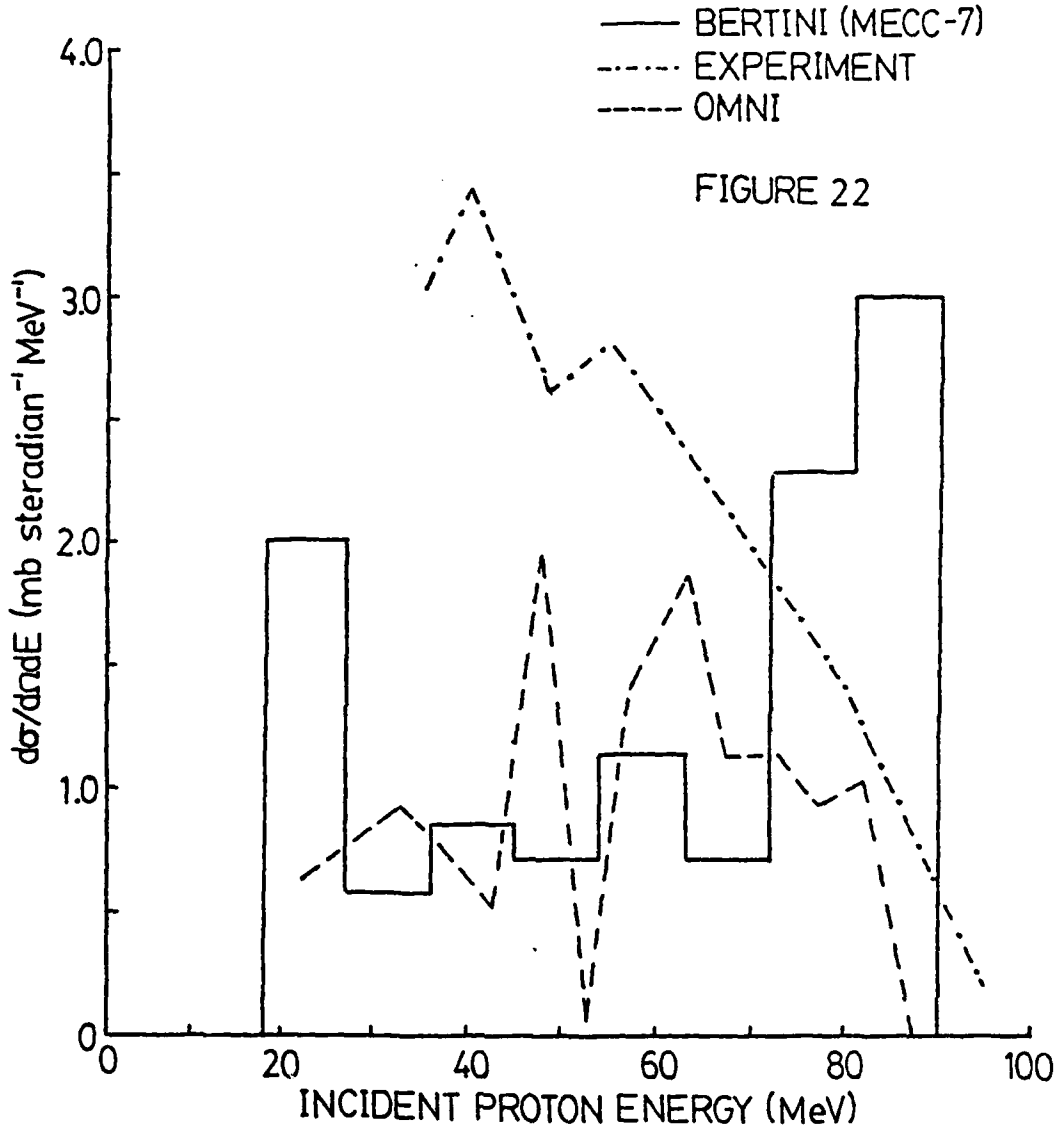
BERTINI (MECC-7)
EXPERIMENT
OMNI
4.0
3.0
2.0
1.0
0
dσ/dΩdE (mb steradian⁻¹ MeV⁻¹)
0
20
40
60
80
100
INCIDENT PROTON ENERGY (MeV)

FIGURE 22

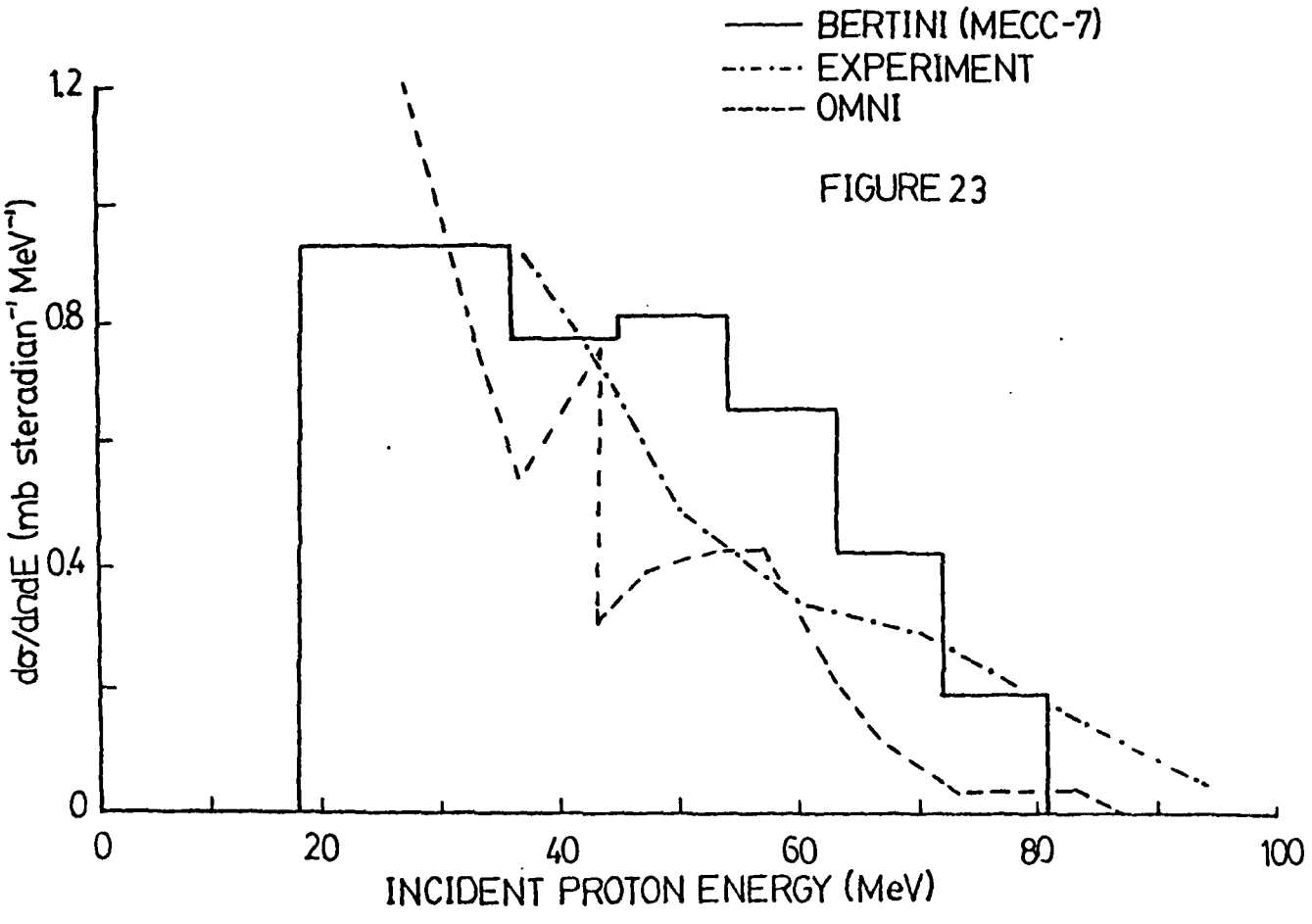
BERTINI (MECC-7)
EXPERIMENT
OMNI
1.2
0.8
0.4
0
dσ/dΩdE (mb steradian⁻¹ MeV⁻¹)
0
20
40
60
80
100
INCIDENT PROTON ENERGY (MeV)

FIGURE 23

A/20 R=1.3 ——
A/8 R=1.3 ·····
BERTINI - - - - -

EVAPORATION NEUTRON SPECTRA

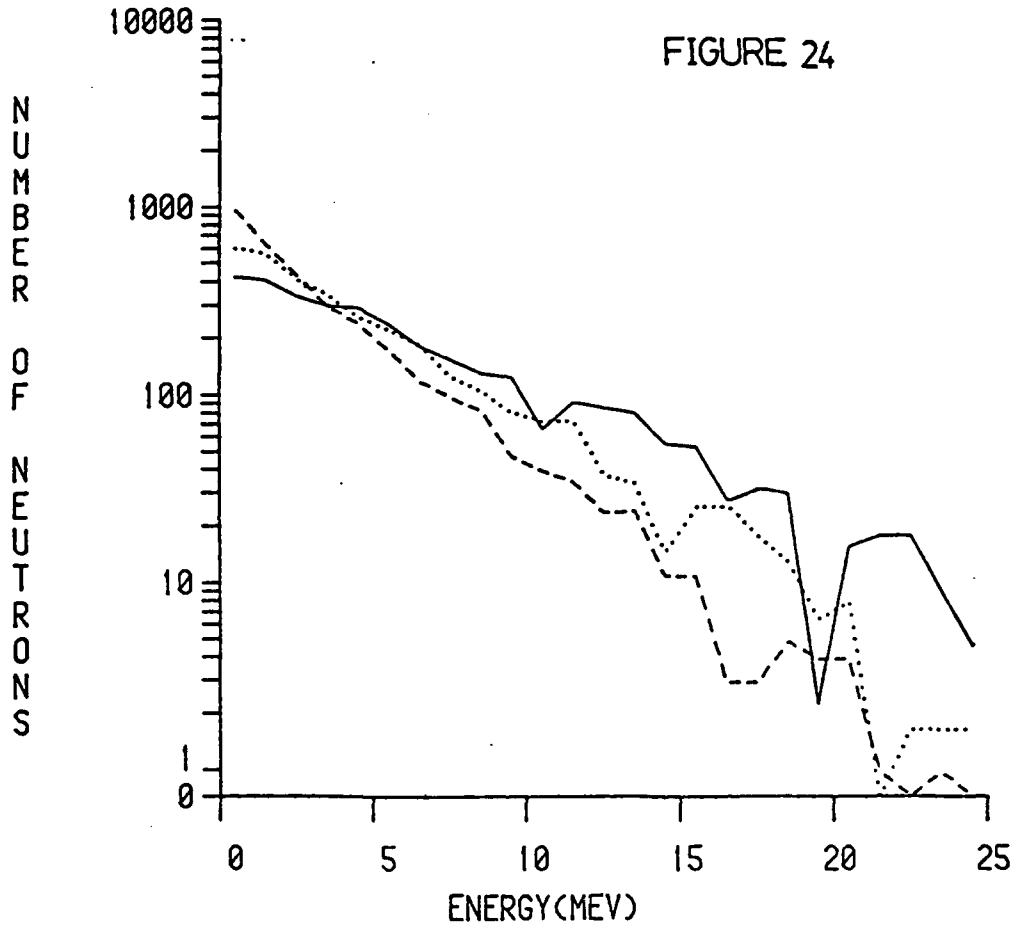

FIGURE 24

A/20 R=1.3 ——
A/8 R=1.3 ·····
BERTINI - - - - -

EVAPORATION PROTON SPECTRA

FIGURE 25

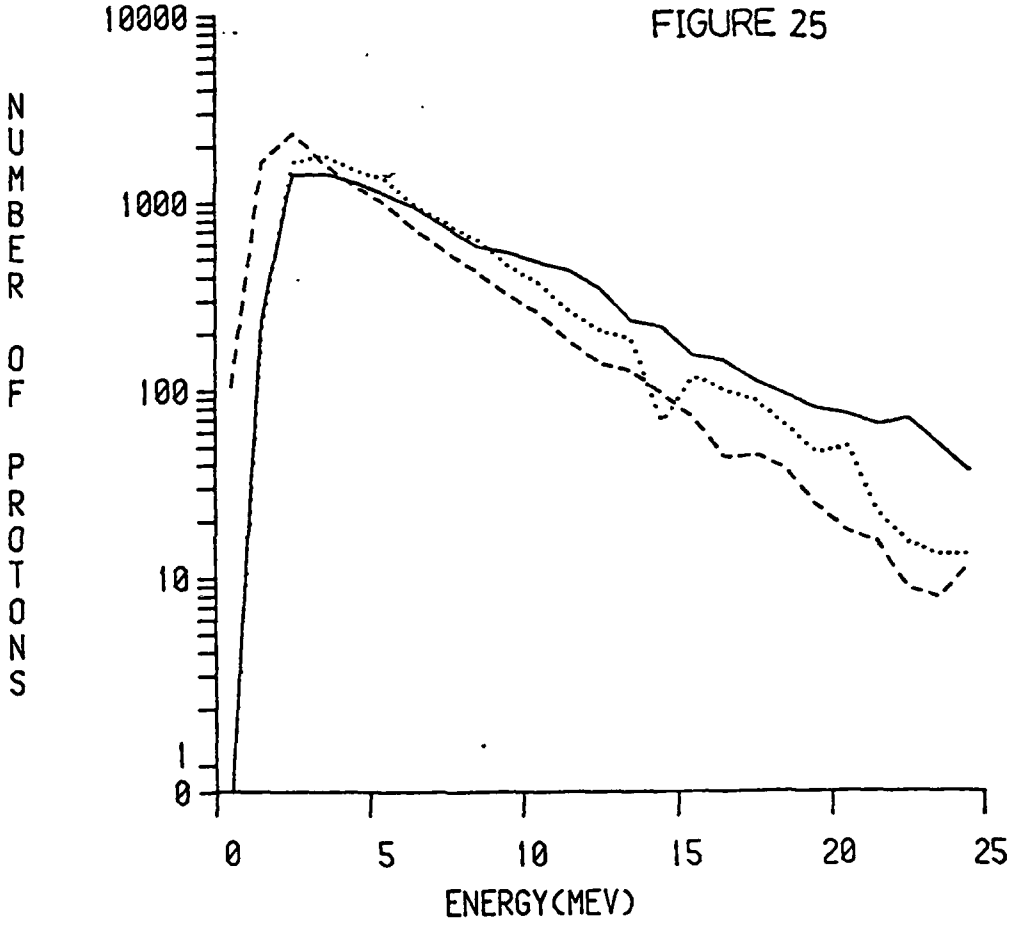

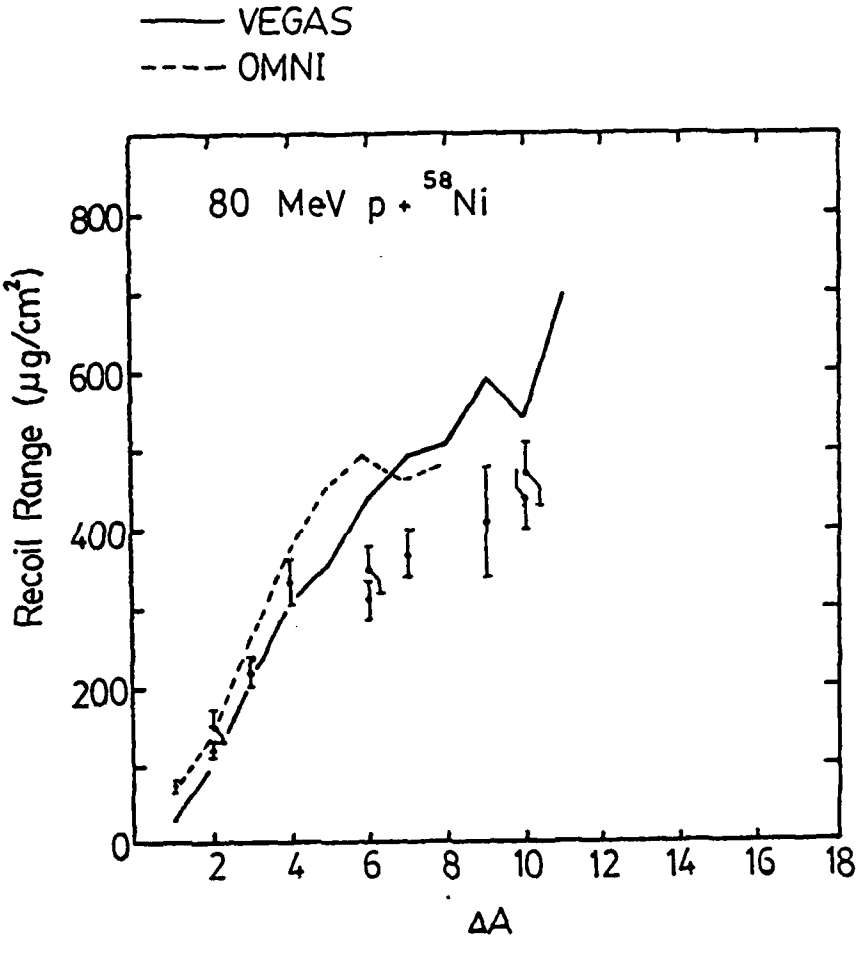
VEGAS
OMNI
80 MeV p + 58Ni
Recoil Range (μg/cm²)
800
600
400
200
0
2
4
6
8
10
12
14
16
18
ΔA

FIGURE 26

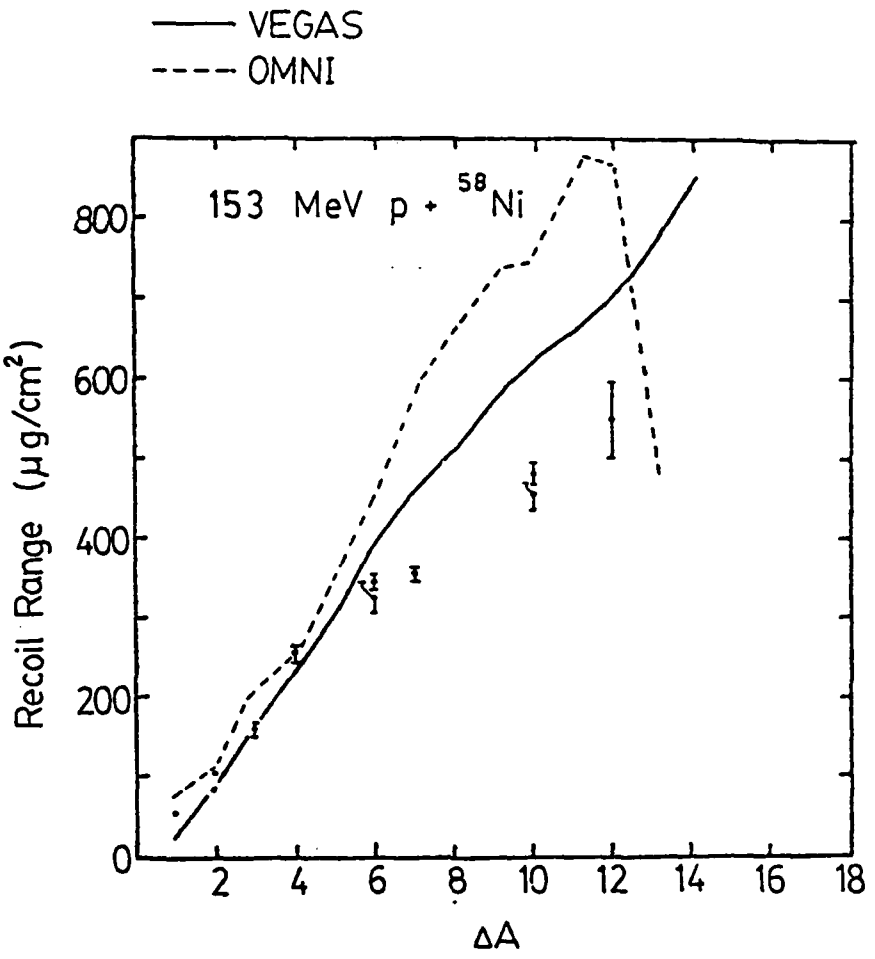
VEGAS
OMNI
153 MeV p + 58Ni
Recoil Range (μg/cm²)
0
200
400
600
800
2
4
6
8
10
12
14
16
18
ΔA

FIGURE 27

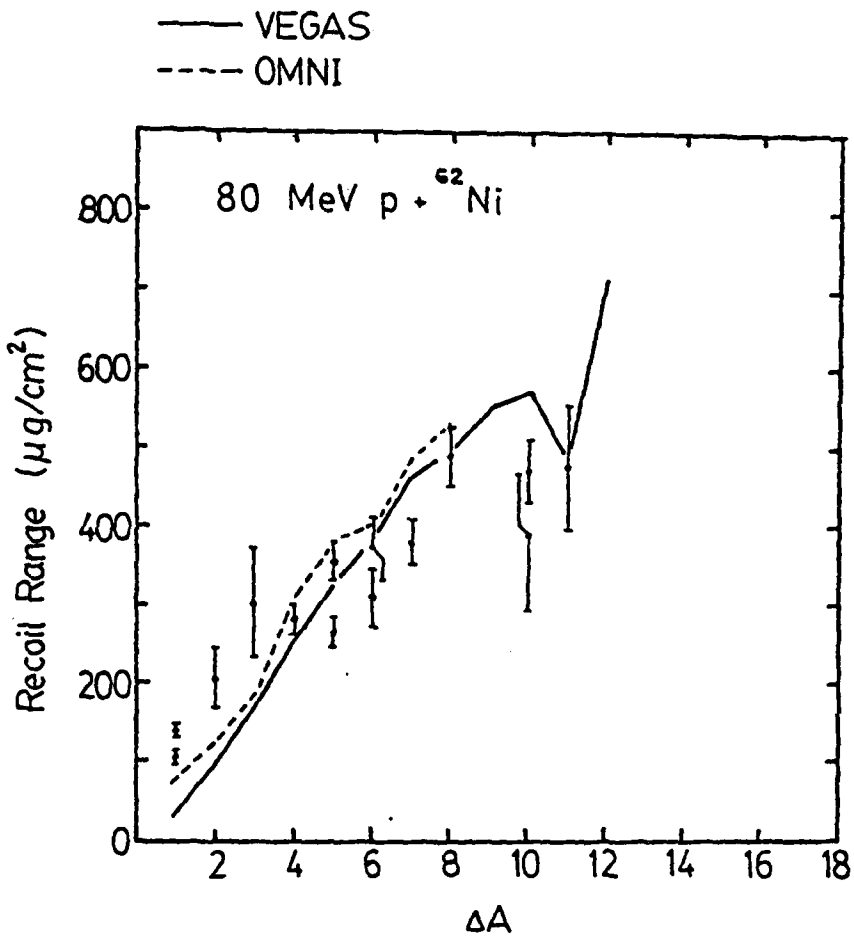
VEGAS
OMNI
80 MeV p + ^{62}Ni
Recoil Range (μg/cm²)
0
200
400
600
800
2
4
6
8
10
12
14
16
18
ΔA

FIGURE 28

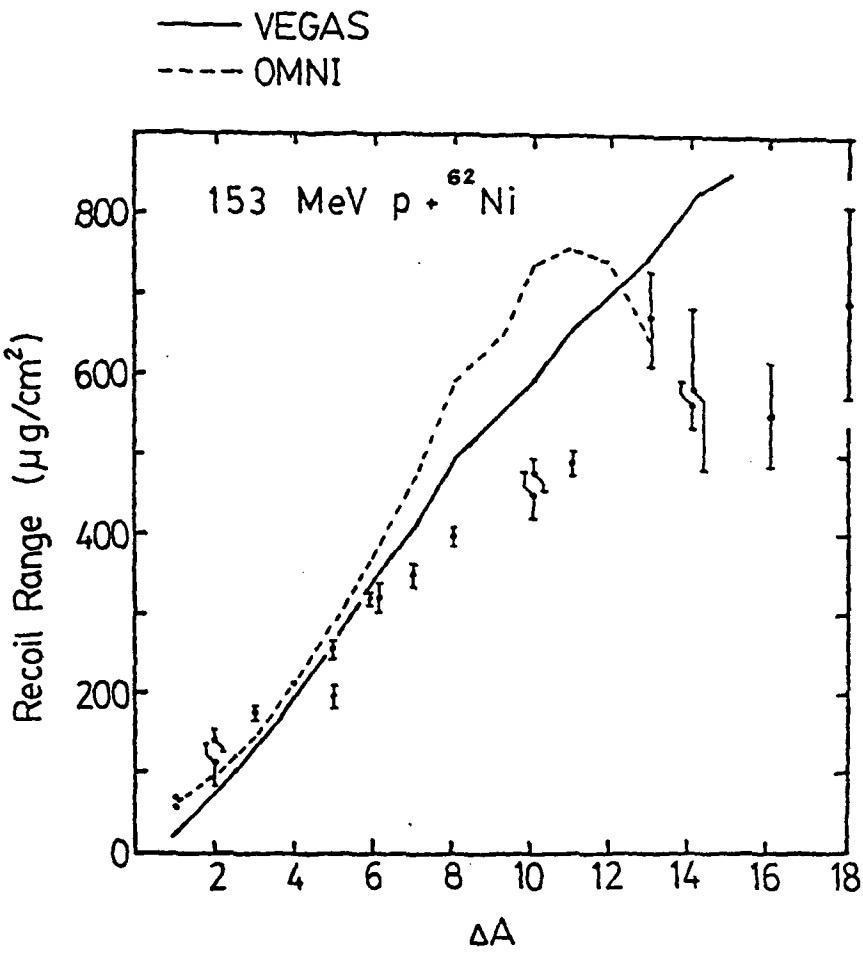
VEGAS
OMNI
153 MeV p + 62Ni
Recoil Range (μg/cm²)
0
200
400
600
800
2
4
6
8
10
12
14
16
18
ΔA

FIGURE 29

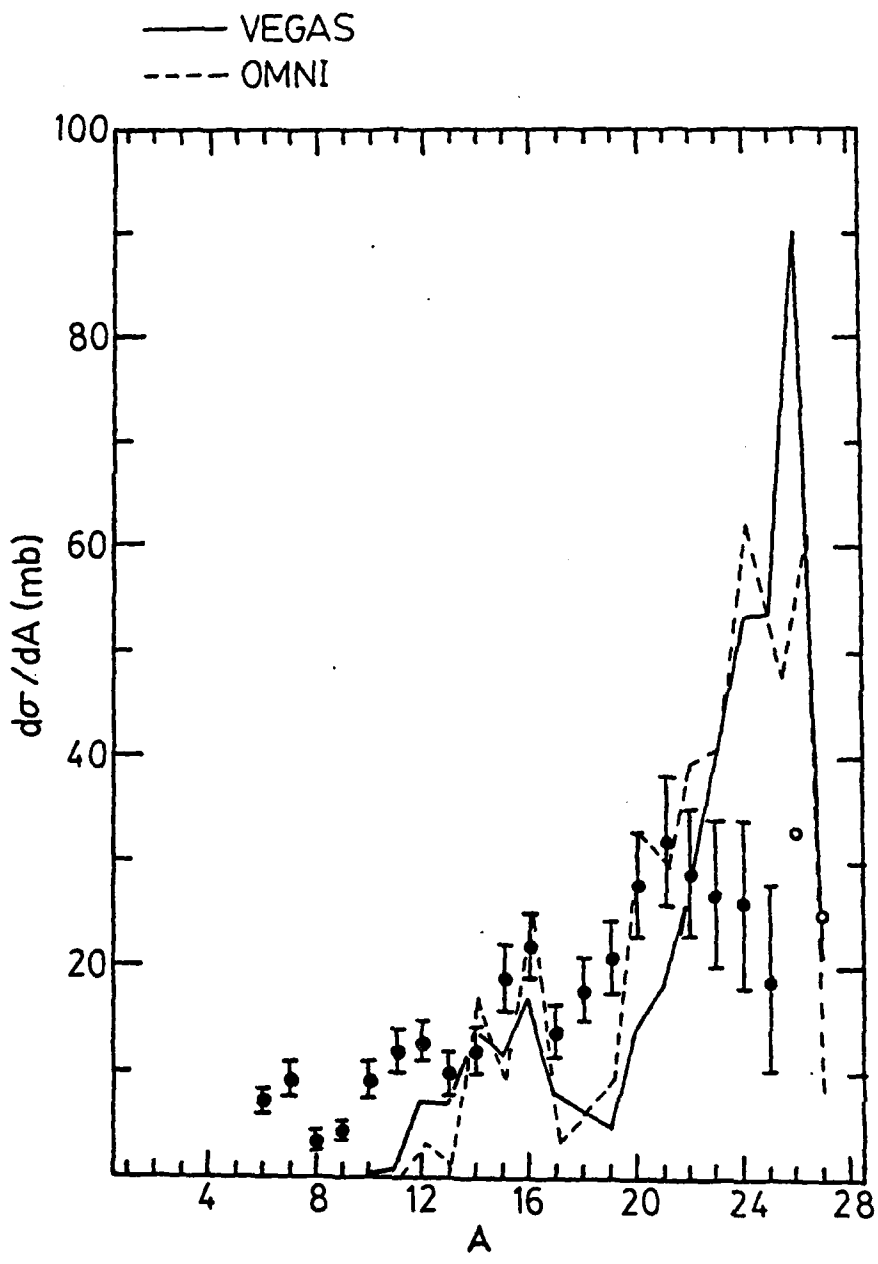

FIGURE 30

V. SILICON DETECTOR COMPARISONS

McNulty et al.[30,41] exposed silicon surface barrier detectors to beams of protons of different energies. Detector thicknesses of 200 um, 97 um, 50 um, 24.1 um, 15 um, 8.7 um, 4.2 um, and 2.5 um were used. The proton beams had energies of 158, 131, 127, 125, 91, 86, 51, 37, 32, 25, and 18 MeV. These experiments, although not part of this work, provide a significant check of the validity of the computer model.

The silicon surface barrier detectors closely approximate the sensitive volumes on a microelectronics chip. On a chip the sensitive volumes are reverse biased p-n junctions. The detector is also a reverse biased p-n junction. Sensitive volume dimensions on a chip are typically a few microns on a side. The surface barrier detector is several microns thick, but has lateral dimensions of several millimeters. Nevertheless, almost all of the incident particles and the particles from the nuclear reactions will leave the detector after traveling a few microns. The chance of any particle traveling exactly in the plane of the detector is exceedingly small. Thus, the detector is a good approximation to the sensitive volume on a chip.

It consists of a wafer of silicon with electrical contacts on each side. The electron-hole pairs generated by the passage of a charged particle are swept up by the electric field across the detector. The amount of charge

is measured by a preamplifier, and the signal is sent through an amplifier to a multichannel analyzer. The detector was calibrated using an Am^{241} alpha source.

The experiments were run at the Harvard Cyclotron. The proton beam emerged from the cyclotron at 158 MeV, and its energy could be reduced by inserting degrader blocks. It was collimated by two defining apertures. Protons reacting in the degraders and collimator walls generate a stream of secondary particles, most of which are removed by an anti-scattering shield. The collimated beam then passes through the detector.

There is a statistical uncertainty in the theoretical computer calculations equal to N, where N is the number of events in an energy bin. There are also uncertainties in the published cross sections. Janni[103] takes these to be 25%. Experimental errors include uncertainty in the exact thicknesses of the detectors, plus some others which will be discussed shortly.

Comparisons of experiment with theory are shown in Fig. 31-49. Theory is shown as a solid line, and the experimental values as a dashed line.

At low proton energies, the beam had to pass through a relatively large amount of degrader. This introduced considerable spread in the energy of the beam. At 18 MeV the FWHM of the energy is 17 MeV, at 32 MeV it is 14 MeV, at 51 MeV it is 10 MeV, and at 131 MeV it is 4 MeV. The 97 um data are shown in Figures 31-33. The fits are quite good.

The 50 um data are shown in Fig. 34-36. The fits here are also quite good. For all of the 24.1 um theoretical runs the statistics were quite poor. For these runs a discriminator setting caused no data to be read below a certain energy.

The 15 um thick detector is also in good agreement with the program at 86 MeV. The 8.7 um thick detector is in good agreement with the program at 86, 125, and 158 MeV.

The 4.2 and 2.5 um data, shown in Figures 44-49, are in good agreement with the program. These are from detectors with thicknesses in the size range of current LSI technology devices. A possible influence on the data is multiple scattering. In the computer simulation, the paths of the particles are straight lines. A real particle is constantly undergoing small deflections caused by the Coulomb fields of the atoms in the medium. Occasionally, in the computer simulation, a particle deposits a large amount of energy by traveling a long distance in the plane of the detector. A real particle would be likely to be scattered out of the detector before traveling a large distance. This could result in an overestimation of the deposited energy for thin detectors at high incident proton energy. From the 125 and 158 MeV results for the 2.5 and 4.2 um thick detectors, this would appear not to be a very large effect.

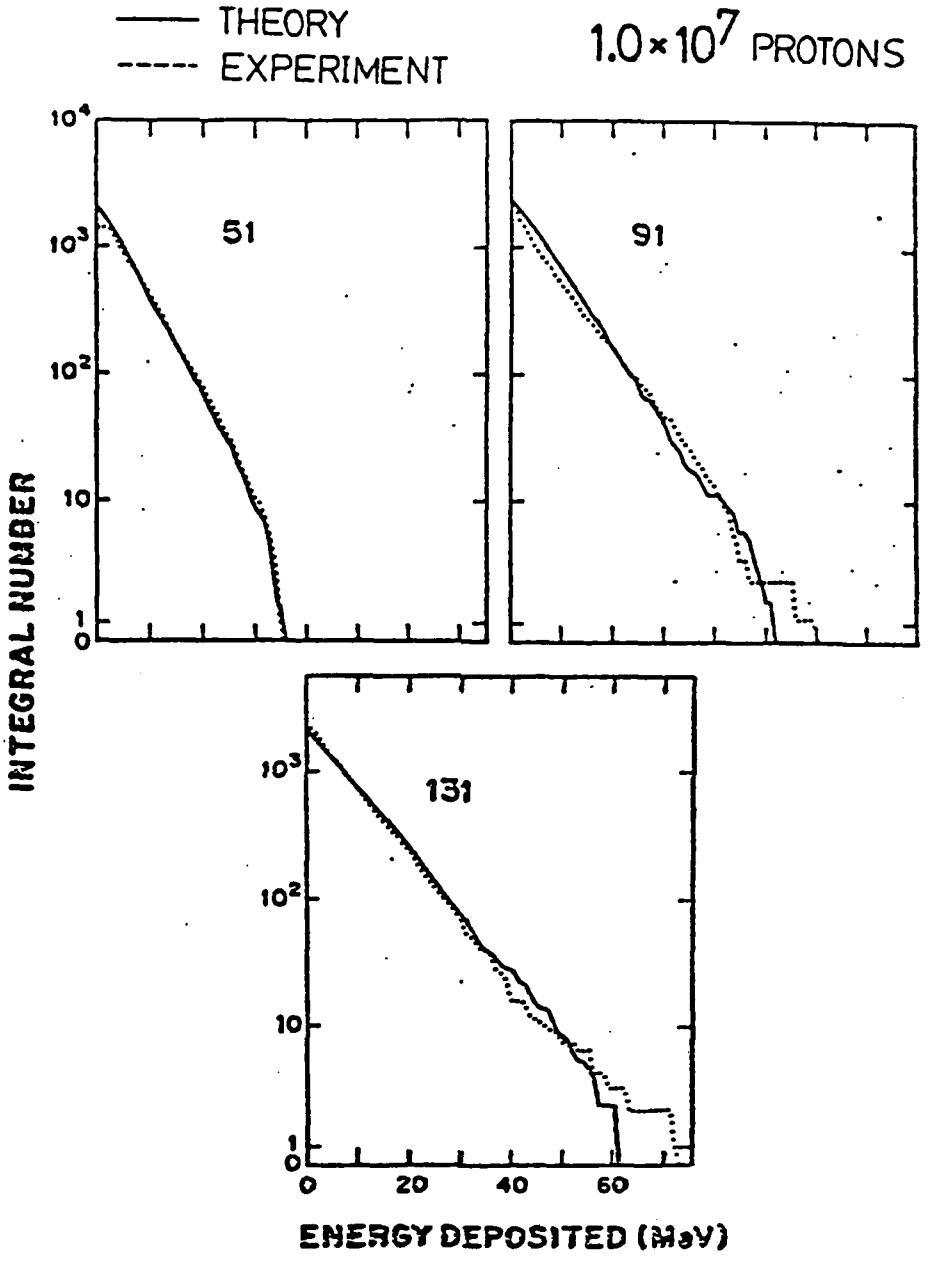
THEORY
EXPERIMENT
1.0×10^7 PROTONS
INTEGRAL NUMBER
10^4
10^3
10^2
10
1
0
51
91
131
0
20
40
60
ENERGY DEPOSITED (MeV)

FIGURE 31

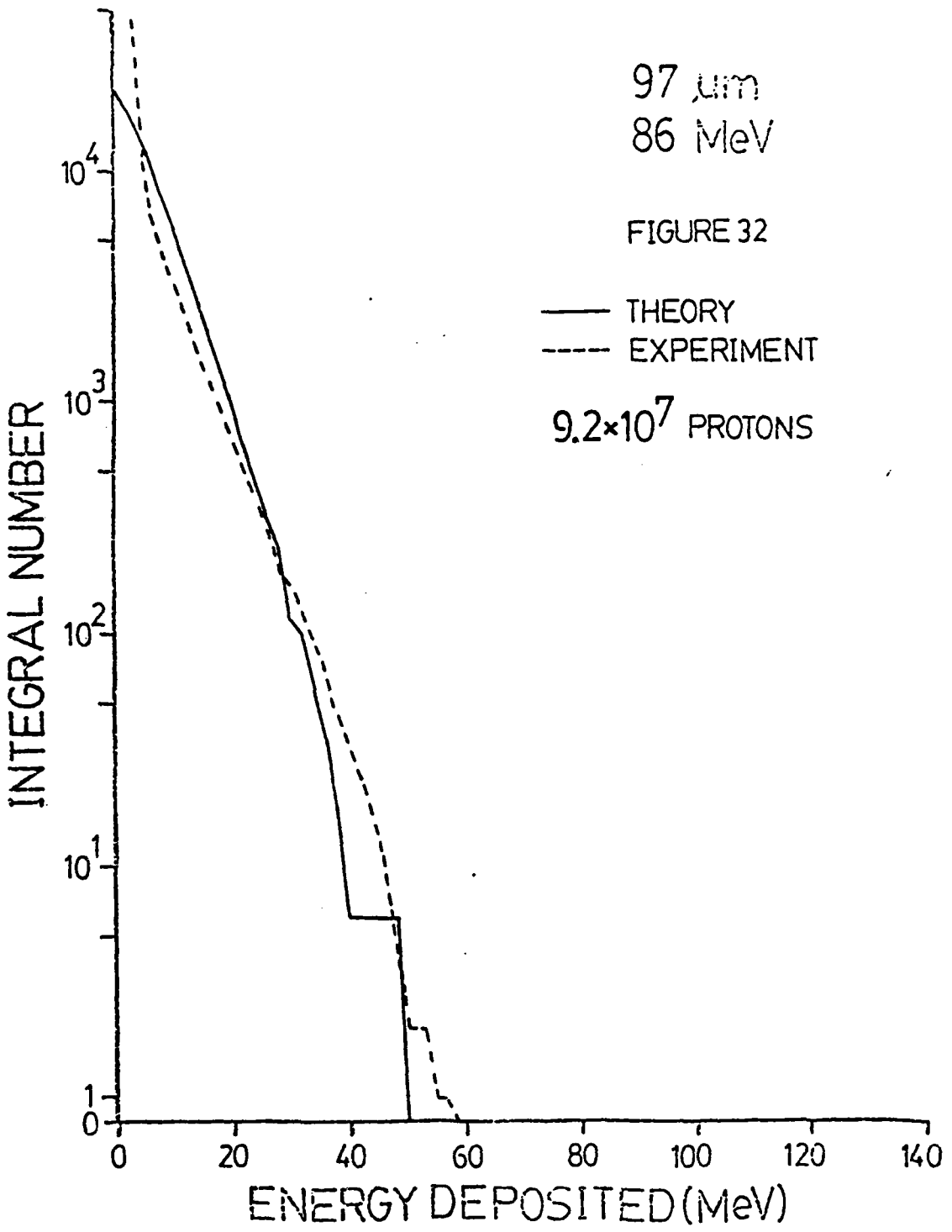
97 μm
86 MeV
FIGURE 32
THEORY
EXPERIMENT
9.2×10^7 PROTONS
INTEGRAL NUMBER
10^4
10^3
10^2
10^1
1
0
0
20
40
60
80
100
120
140
ENERGY DEPOSITED (MeV)

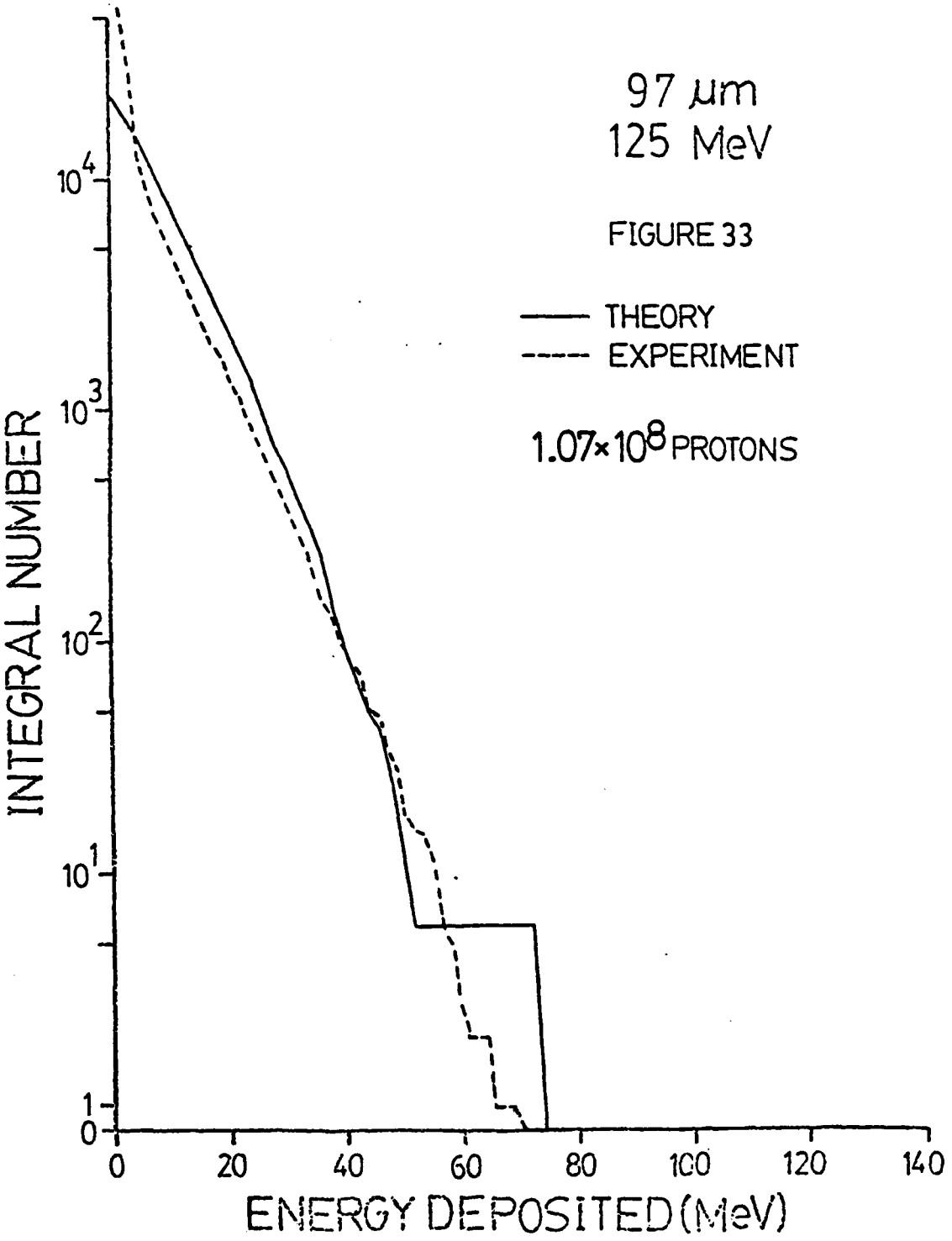
97 μm
125 MeV
FIGURE 33
THEORY
EXPERIMENT
1.07×10^8 PROTONS
INTEGRAL NUMBER
10^4
10^3
10^2
10^1
1
0
0
20
40
60
80
100
120
140
ENERGY DEPOSITED (MeV)

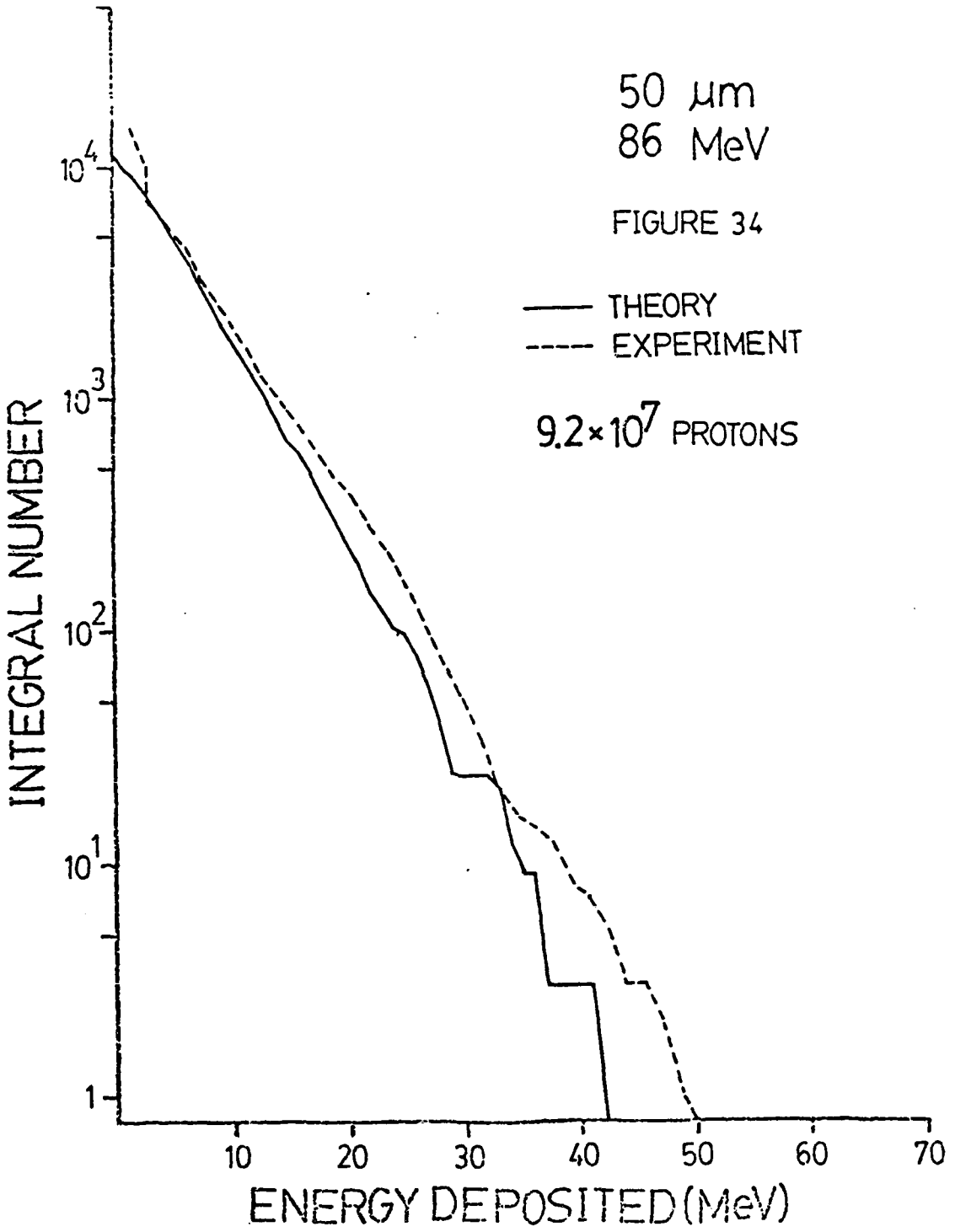
50 μm
86 MeV
FIGURE 34
THEORY
EXPERIMENT
9.2×10^7 PROTONS
INTEGRAL NUMBER
10^4
10^3
10^2
10^1
1
10
20
30
40
50
60
70
ENERGY DEPOSITED (MeV)

AD-A136 957 MICRODOSIMETRIC MEASUREMENTS ON NUCLEAR REACTIONS(U) 2/2
CLARKSON COLL OF TECHNOLOGY POTSDAM N Y DEPT OF PHYSICS
P J MCNULTY 1983 SBI-AD-E001 638 N00014-81-K-2011

UNCLASSIFIED F/G 20/8 NL

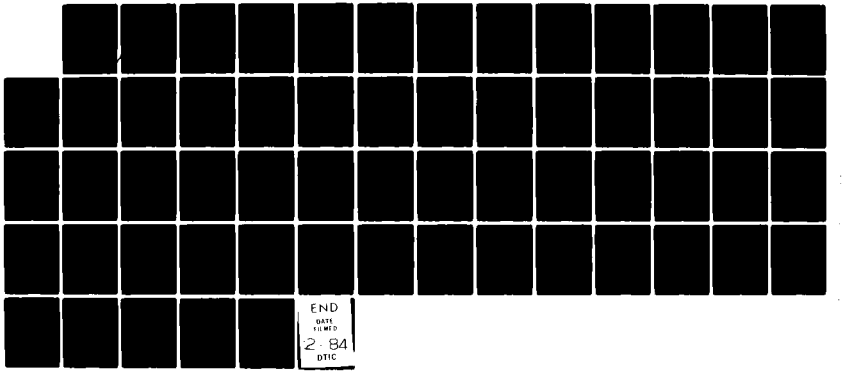

END
DATE FILMED
2-84
DTIC

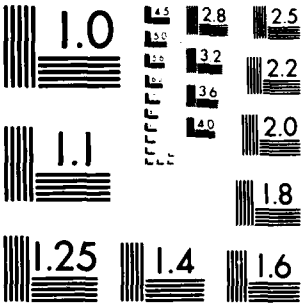

MICROCOPY RESOLUTION TEST CHART
NATIONAL BUREAU OF STANDARDS 1963-A

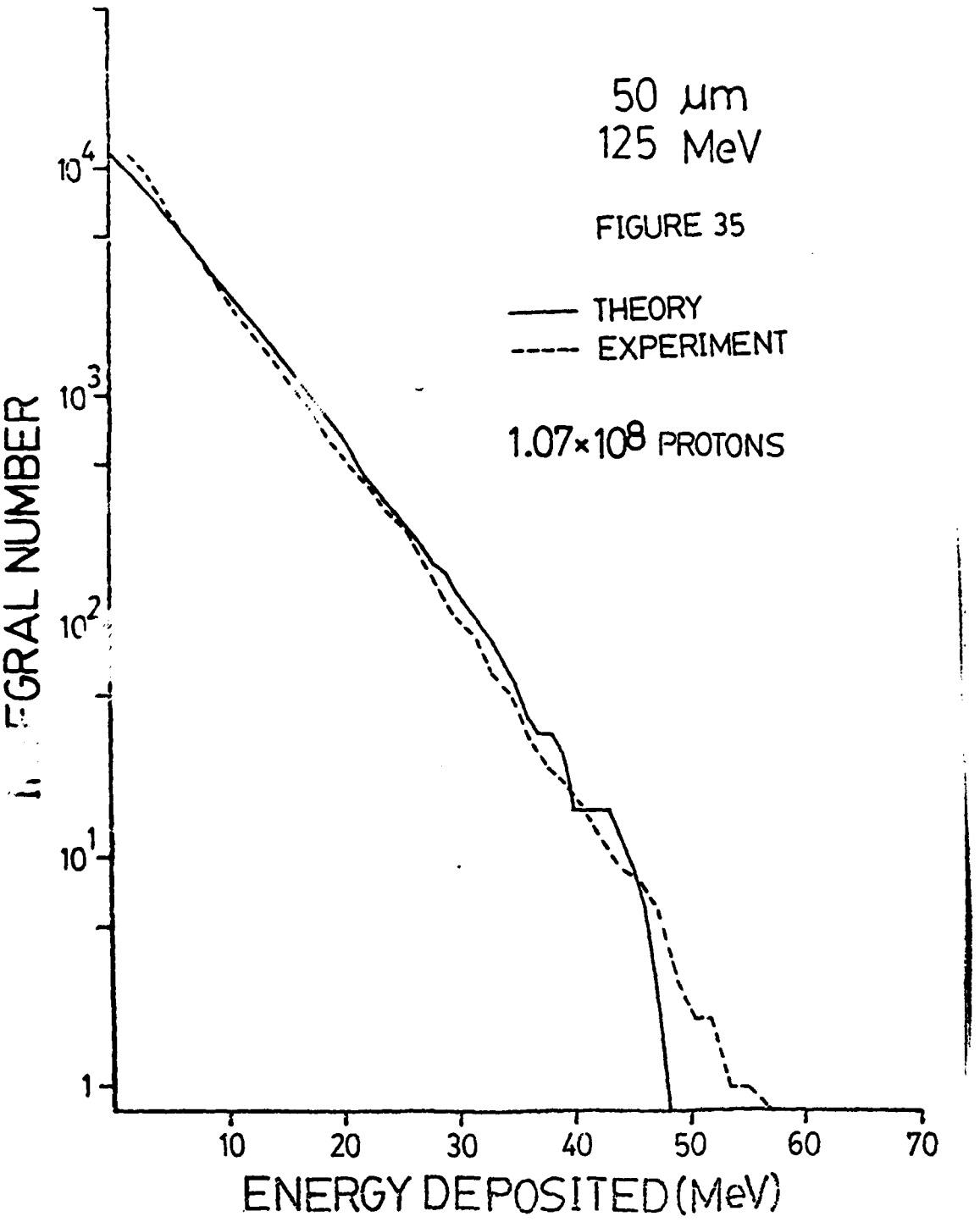
50 μm
125 MeV
FIGURE 35
THEORY
EXPERIMENT
1.07×10^8 PROTONS
INTEGRAL NUMBER
10^4
10^3
10^2
10^1
1
10
20
30
40
50
60
70
ENERGY DEPOSITED (MeV)

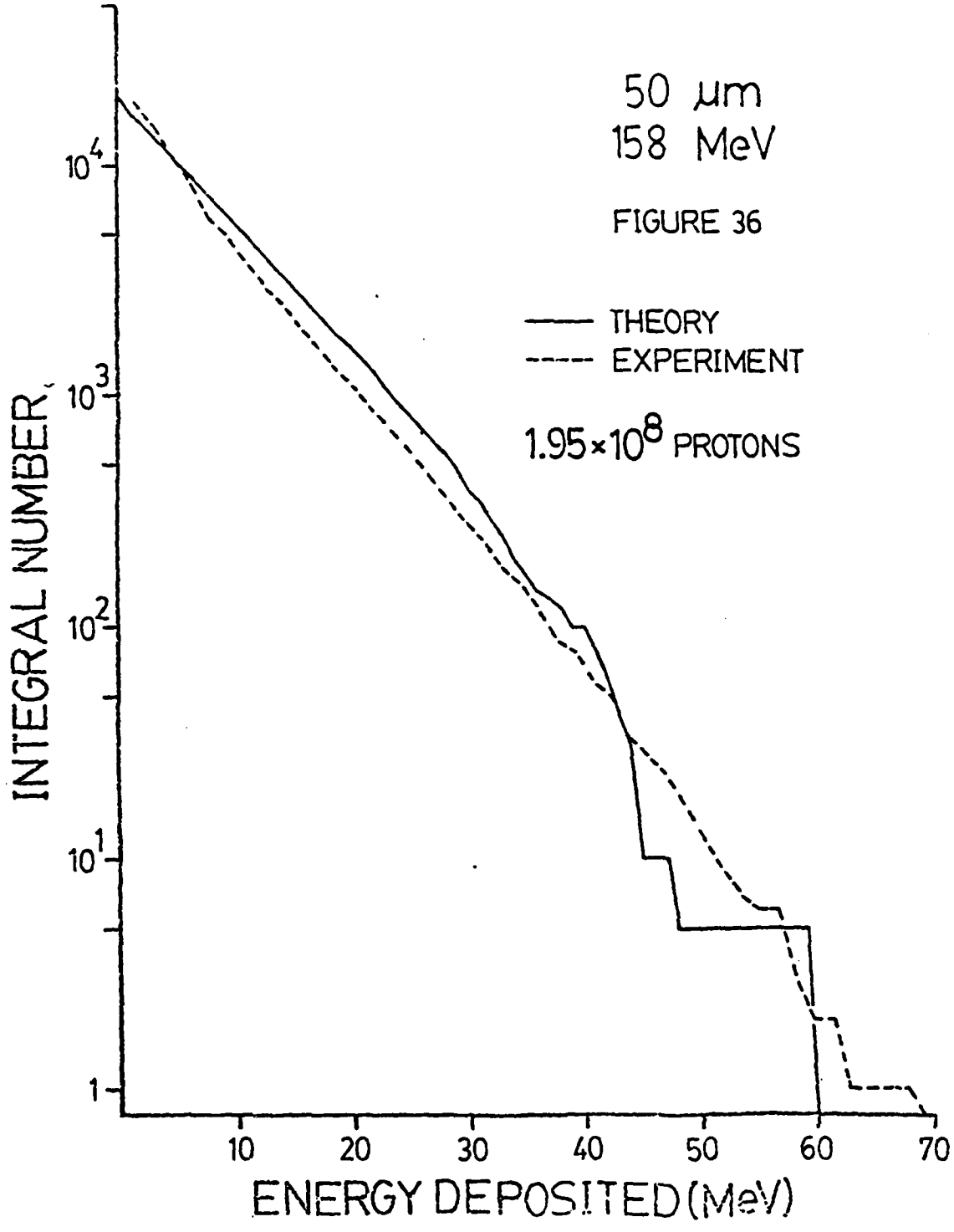
50 μm
158 MeV
FIGURE 36
THEORY
EXPERIMENT
1.95×10^8 PROTONS
INTEGRAL NUMBER
10^4
10^3
10^2
10^1
1
10
20
30
40
50
60
70
ENERGY DEPOSITED (MeV)

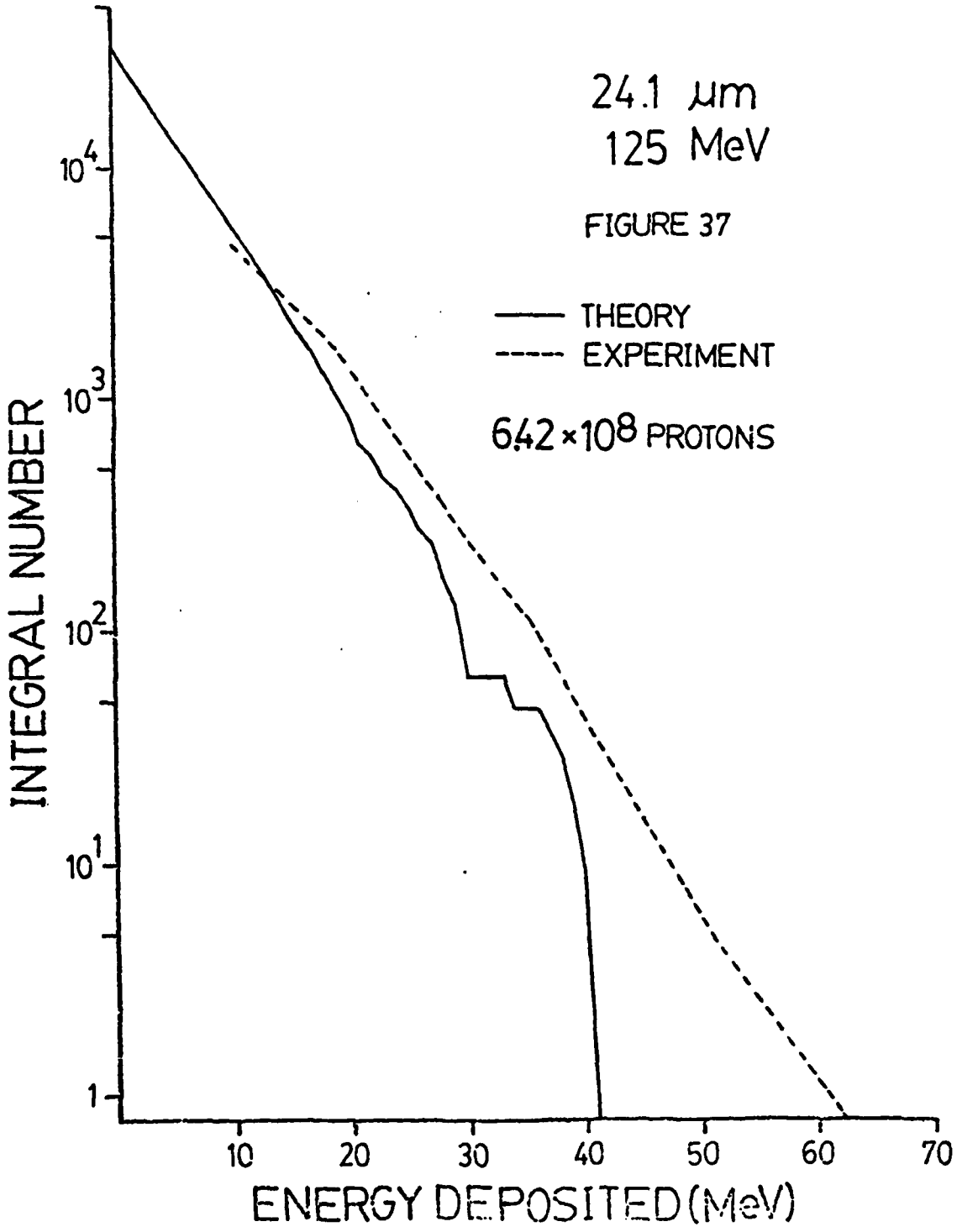
24.1 μm
125 MeV
FIGURE 37
THEORY
EXPERIMENT
6.42×10^8 PROTONS
INTEGRAL NUMBER
10^4
10^3
10^2
10^1
1
10
20
30
40
50
60
70
ENERGY DEPOSITED (MeV)

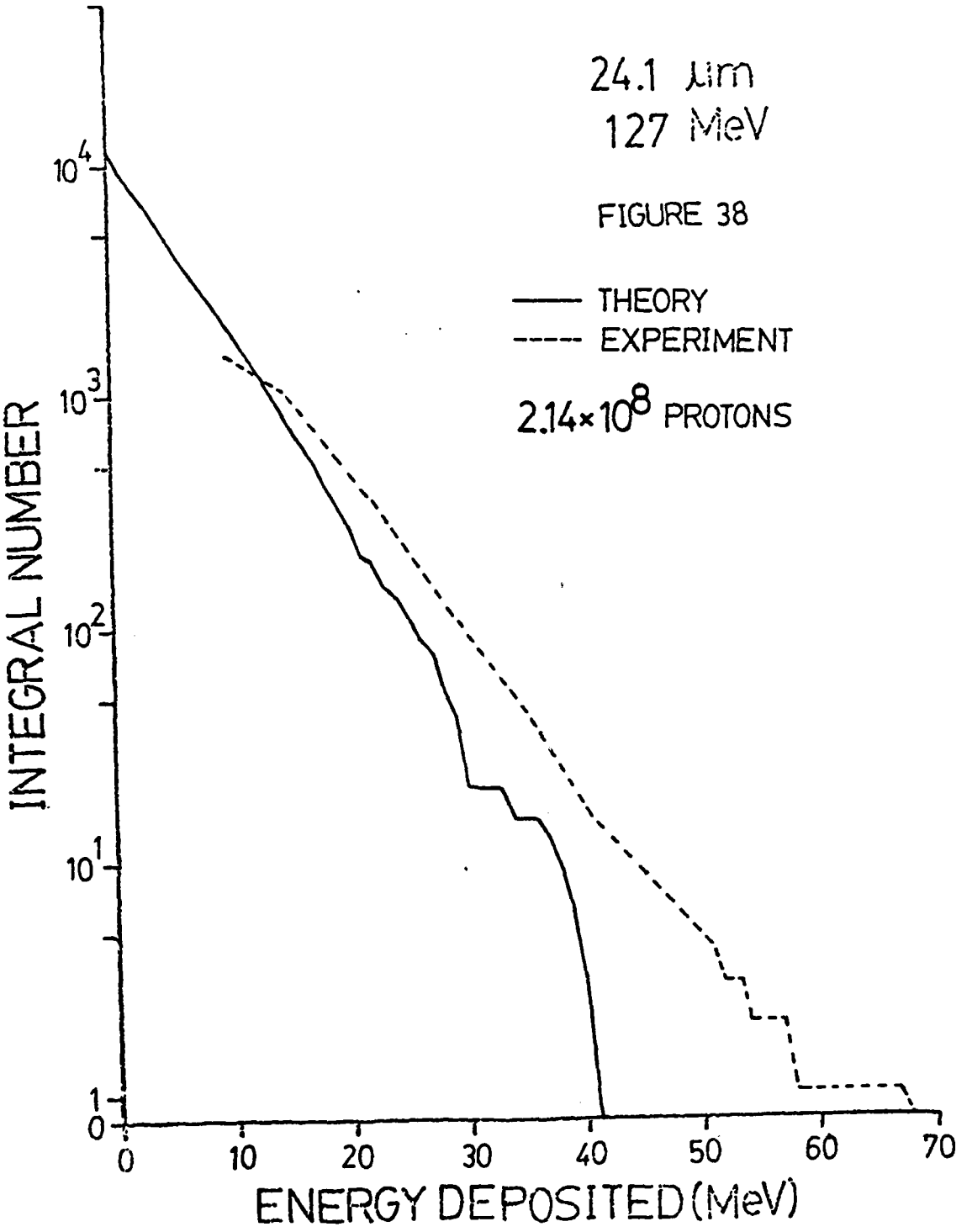
24.1 μm
127 MeV
FIGURE 38
THEORY
EXPERIMENT
2.14×10^8 PROTONS
INTEGRAL NUMBER
10^4
10^3
10^2
10^1
1
0
0
10
20
30
40
50
60
70
ENERGY DEPOSITED (MeV)

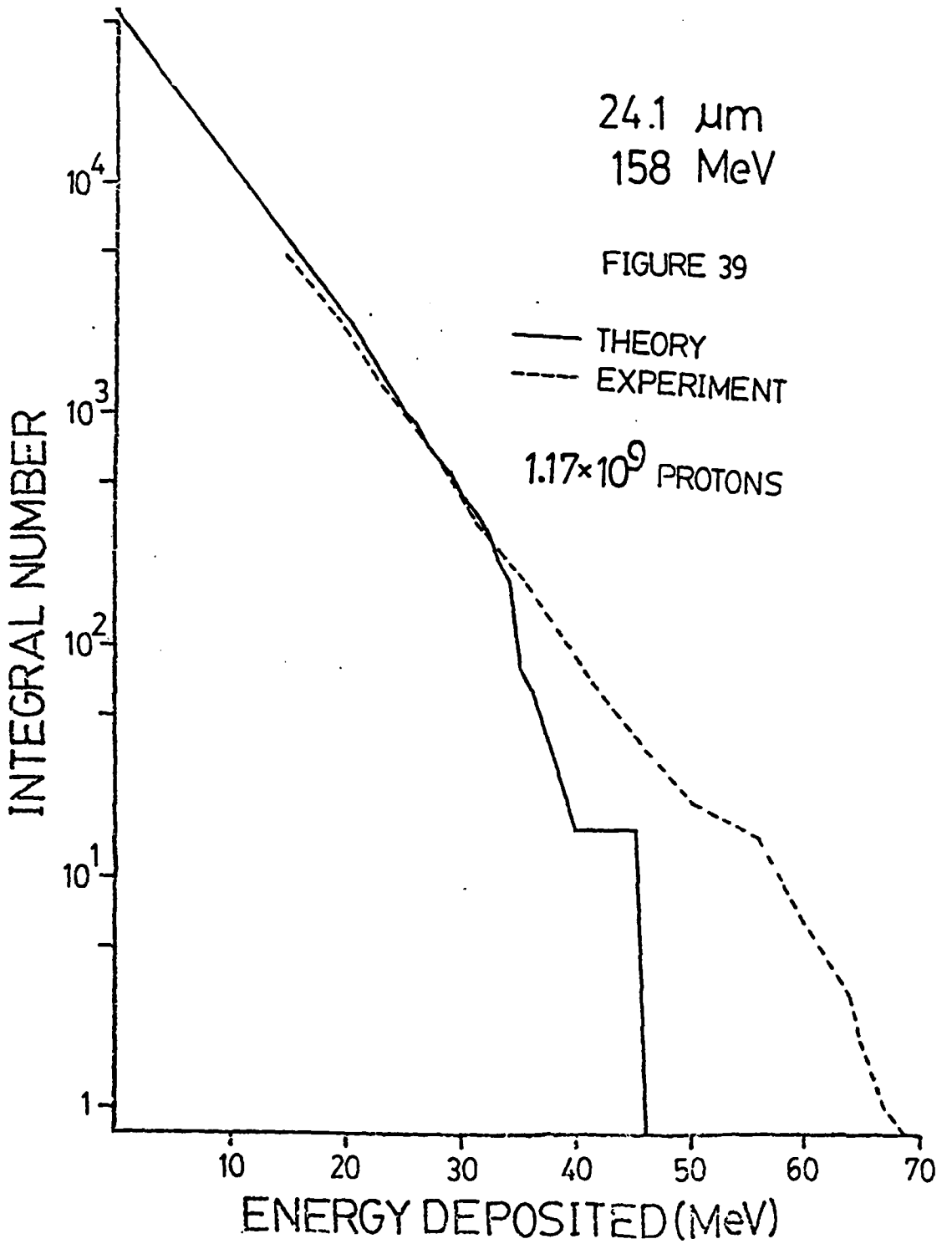
24.1 μm
158 MeV
FIGURE 39
THEORY
EXPERIMENT
1.17×10^9 PROTONS
INTEGRAL NUMBER
10^4
10^3
10^2
10^1
1
10
20
30
40
50
60
70
ENERGY DEPOSITED (MeV)

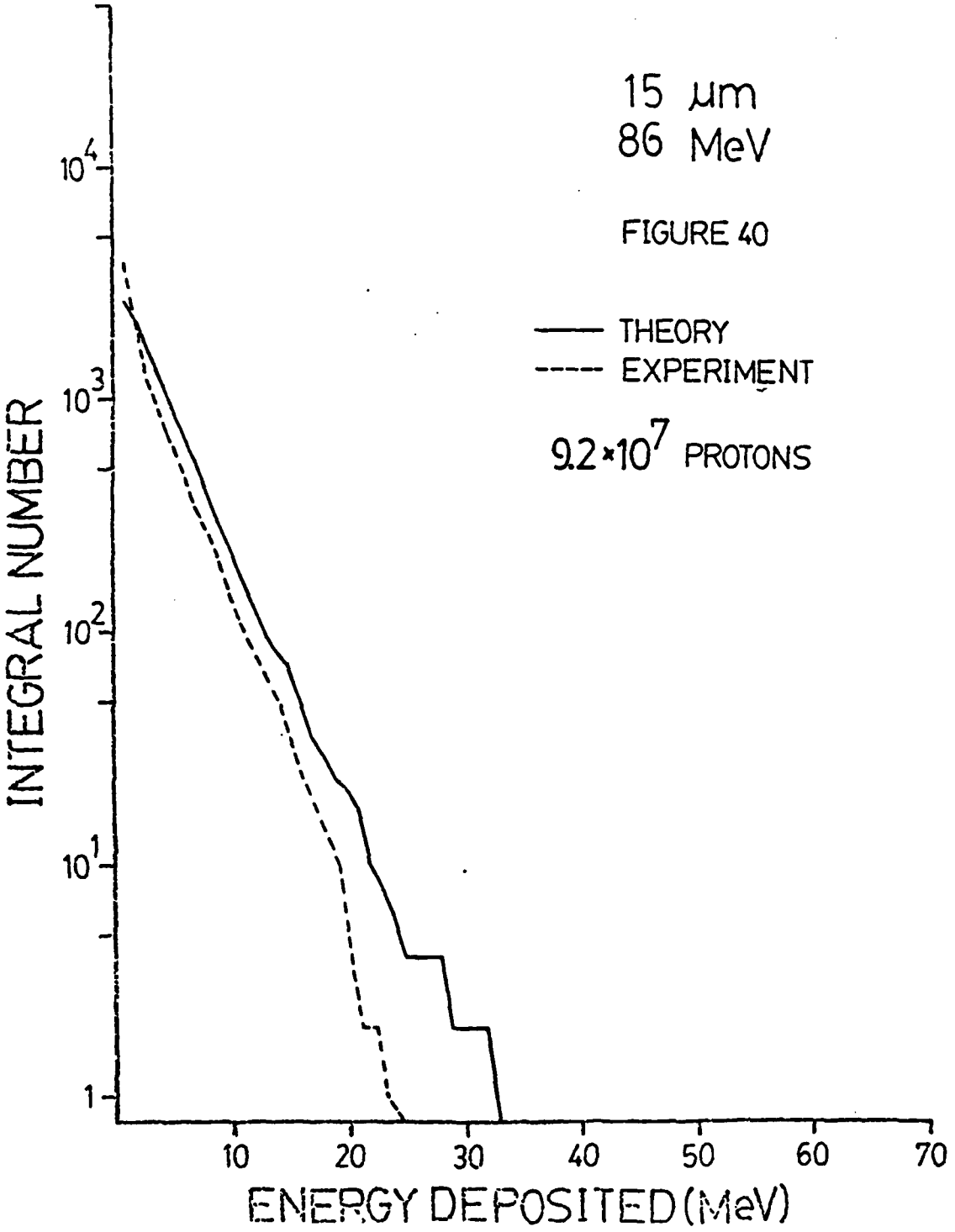
15 μm
86 MeV
FIGURE 40
THEORY
EXPERIMENT
9.2×10^7 PROTONS
INTEGRAL NUMBER
10^4
10^3
10^2
10^1
1
10
20
30
40
50
60
70
ENERGY DEPOSITED (MeV)

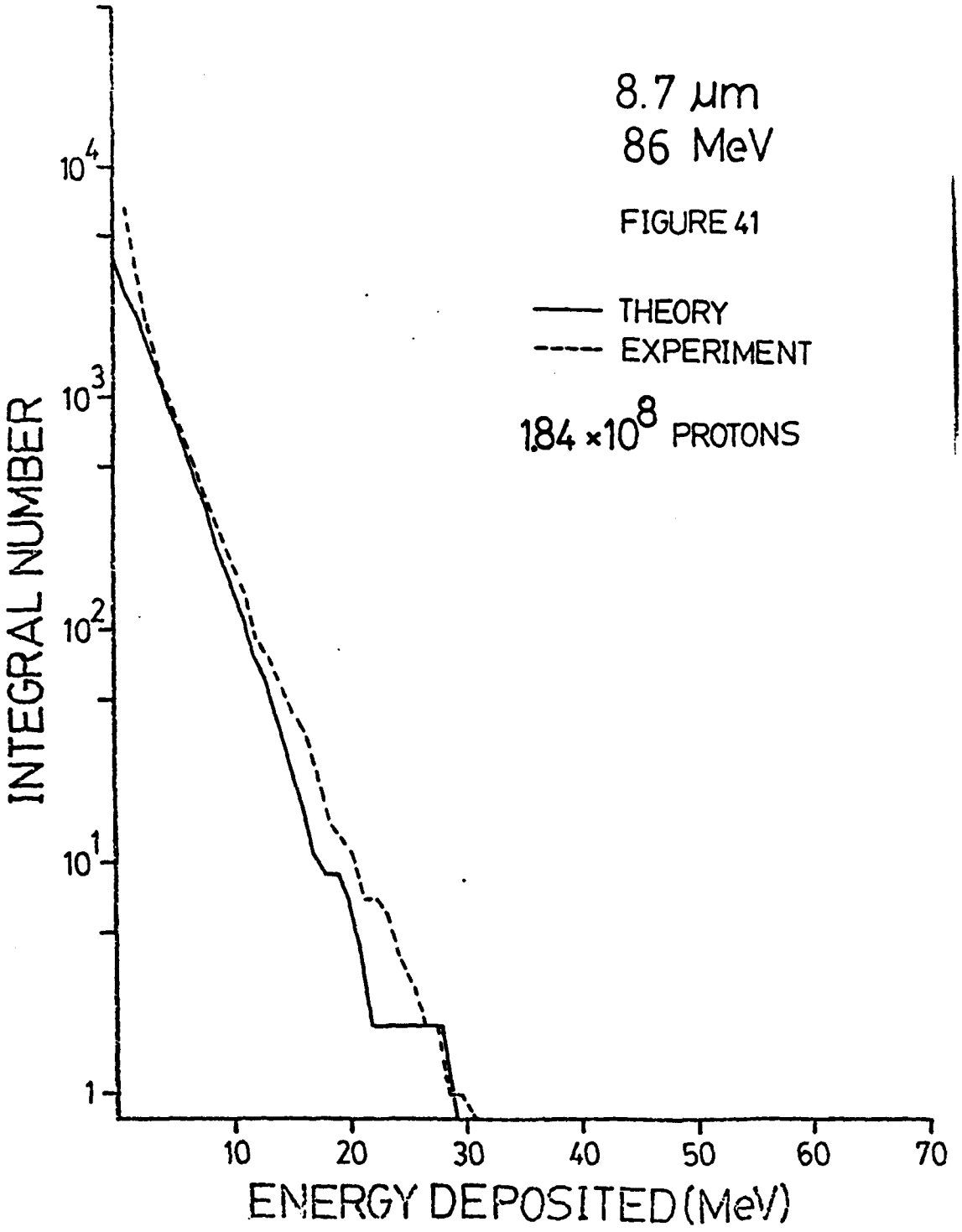
8.7 μm
86 MeV
FIGURE 41
THEORY
EXPERIMENT
1.84 ×10^8 PROTONS
INTEGRAL NUMBER
10^4
10^3
10^2
10^1
1
10
20
30
40
50
60
70
ENERGY DEPOSITED (MeV)

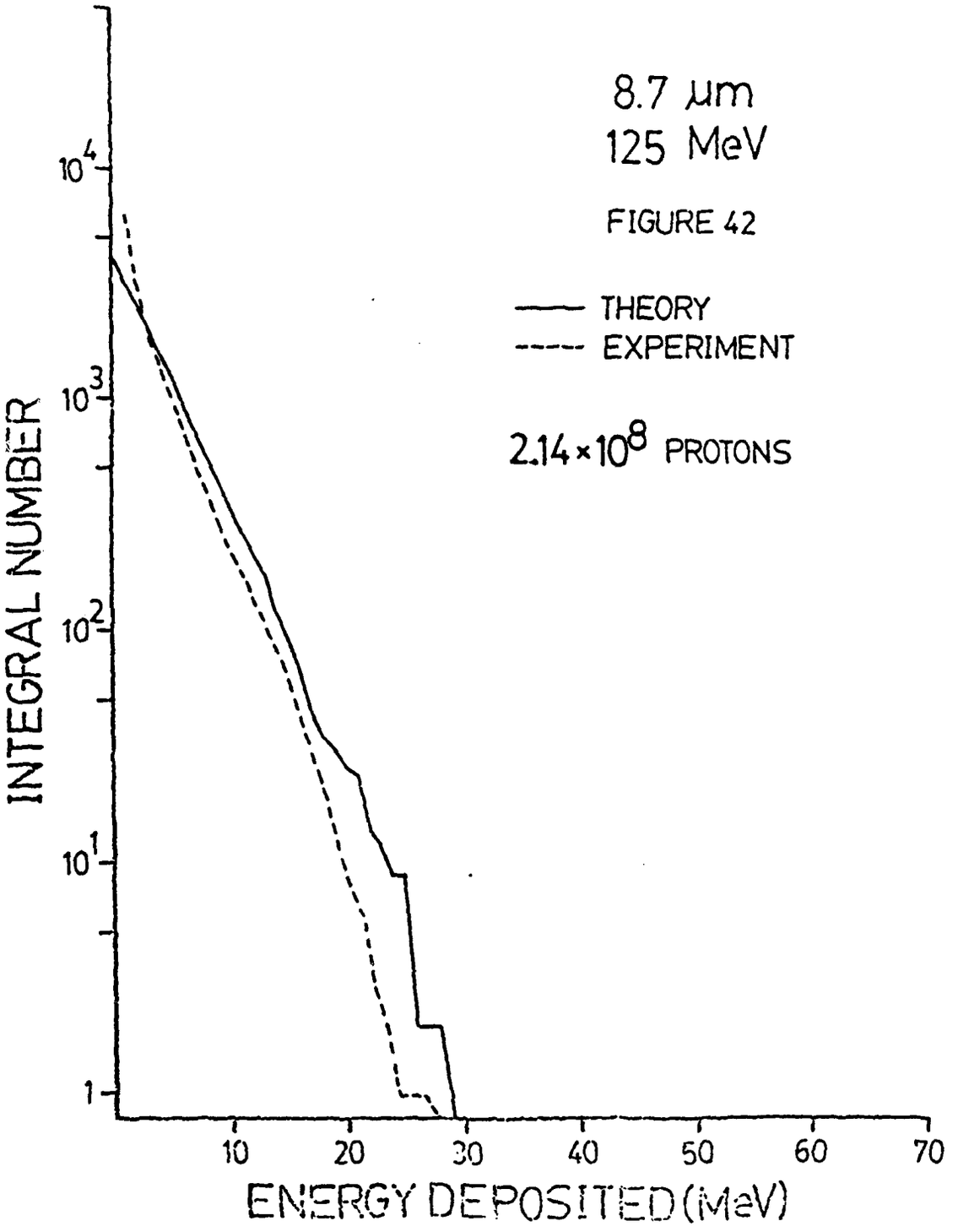
8.7 μm
125 MeV
FIGURE 42
THEORY
EXPERIMENT
2.14×10^8 PROTONS
INTEGRAL NUMBER
10^4
10^3
10^2
10^1
1
10
20
30
40
50
60
70
ENERGY DEPOSITED (MeV)

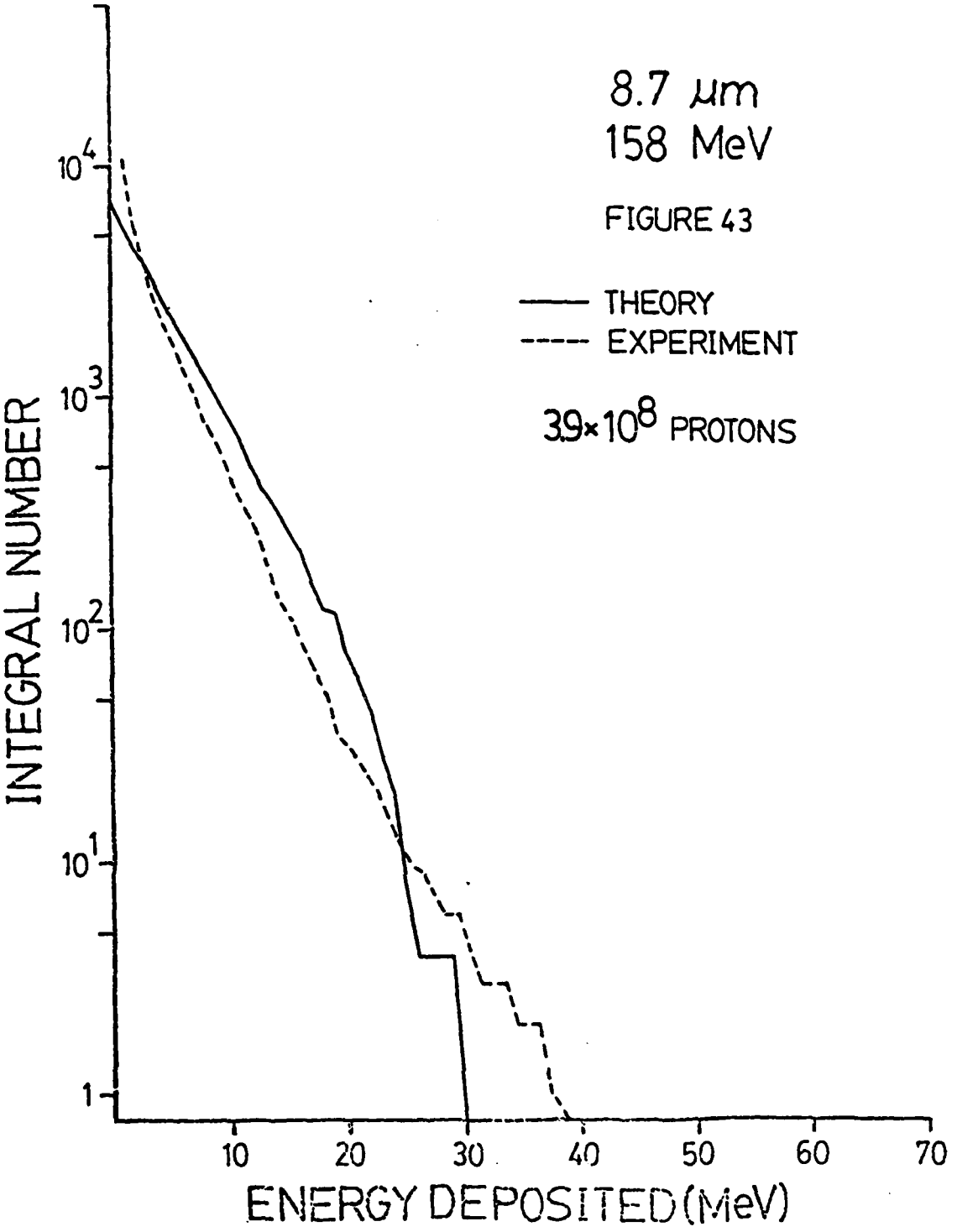
8.7 μm
158 MeV
FIGURE 43
THEORY
EXPERIMENT
3.9×10^8 PROTONS
INTEGRAL NUMBER
10^4
10^3
10^2
10^1
1
10
20
30
40
50
60
70
ENERGY DEPOSITED (MeV)

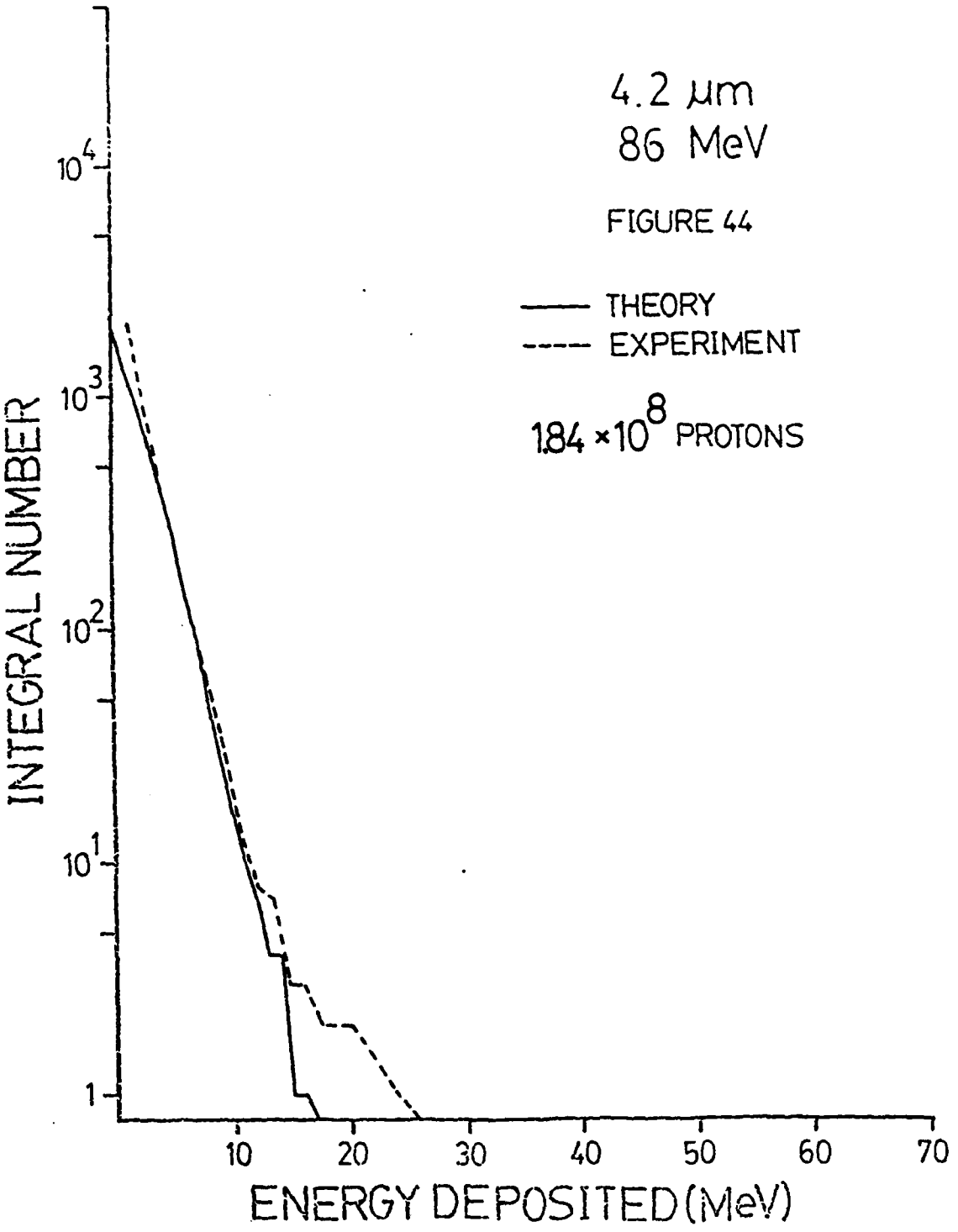
4.2 μm
86 MeV
FIGURE 44
THEORY
EXPERIMENT
1.84 ×10^8 PROTONS
INTEGRAL NUMBER
10^4
10^3
10^2
10^1
1
10
20
30
40
50
60
70
ENERGY DEPOSITED (MeV)

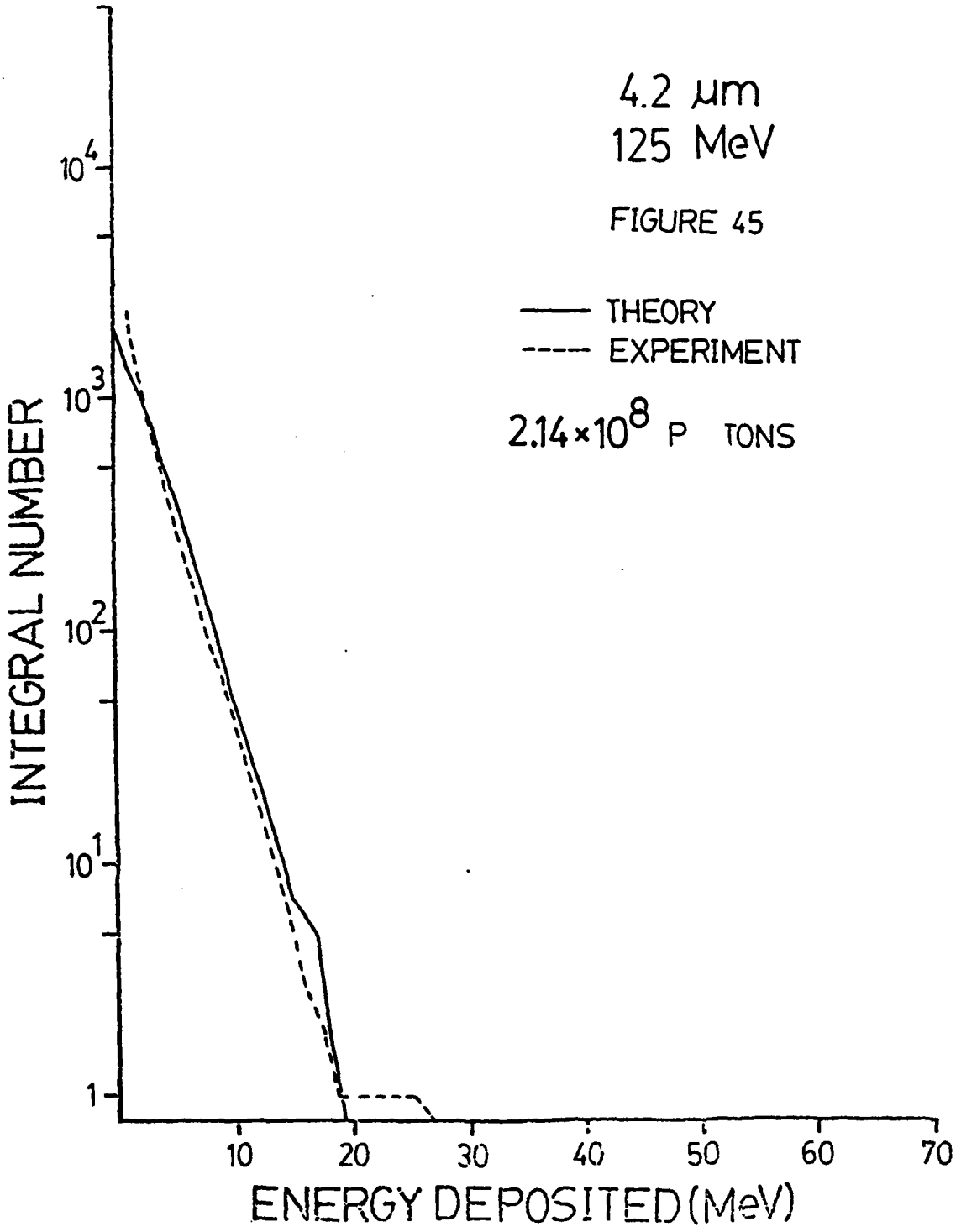
4.2 μm
125 MeV
FIGURE 45
THEORY
EXPERIMENT
2.14×10^8 P TONS
INTEGRAL NUMBER
10^4
10^3
10^2
10^1
1
10
20
30
40
50
60
70
ENERGY DEPOSITED (MeV)

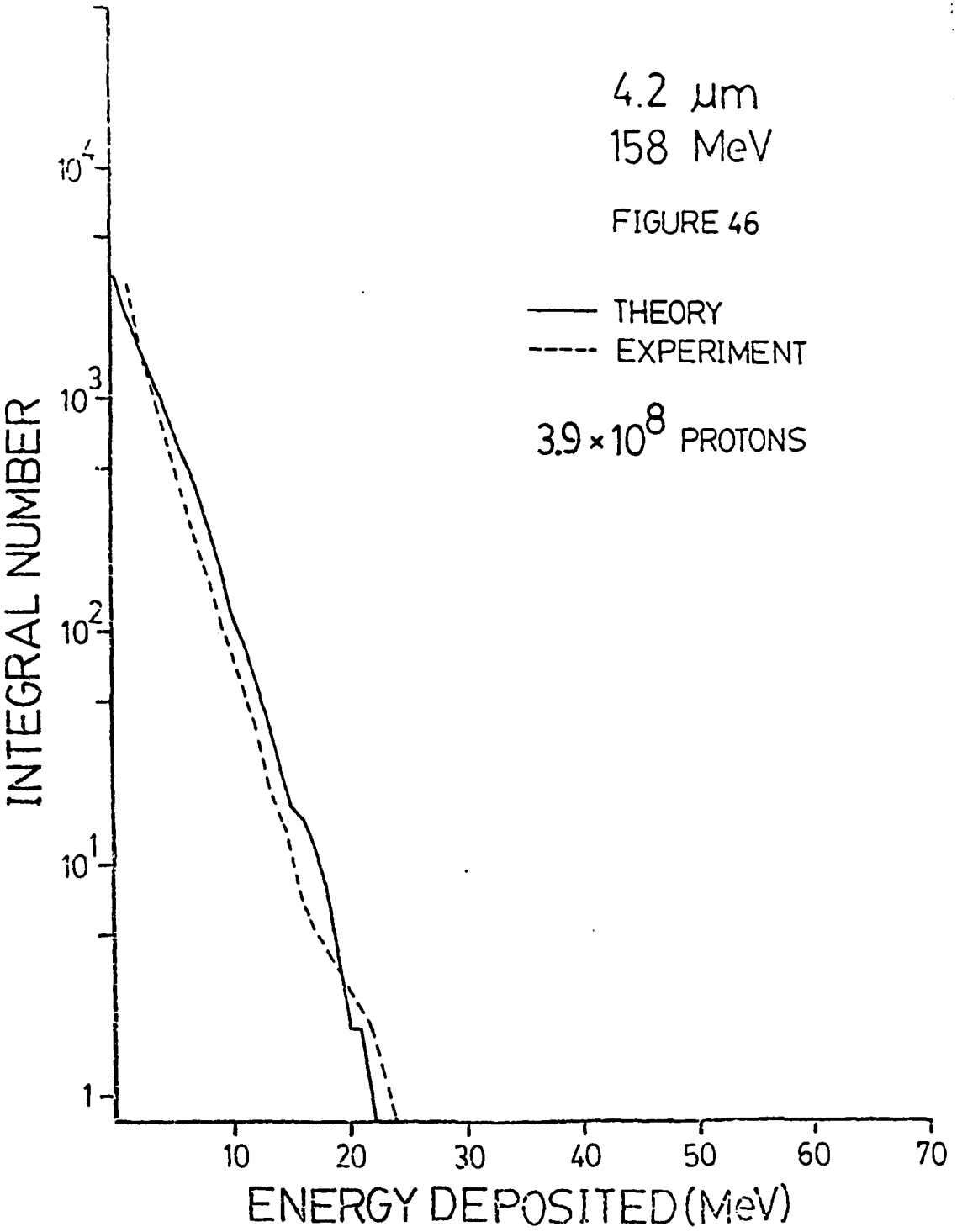
4.2 μm
158 MeV
FIGURE 46
THEORY
EXPERIMENT
3.9 × 10^8 PROTONS
INTEGRAL NUMBER
10^4
10^3
10^2
10^1
1
10
20
30
40
50
60
70
ENERGY DEPOSITED (MeV)

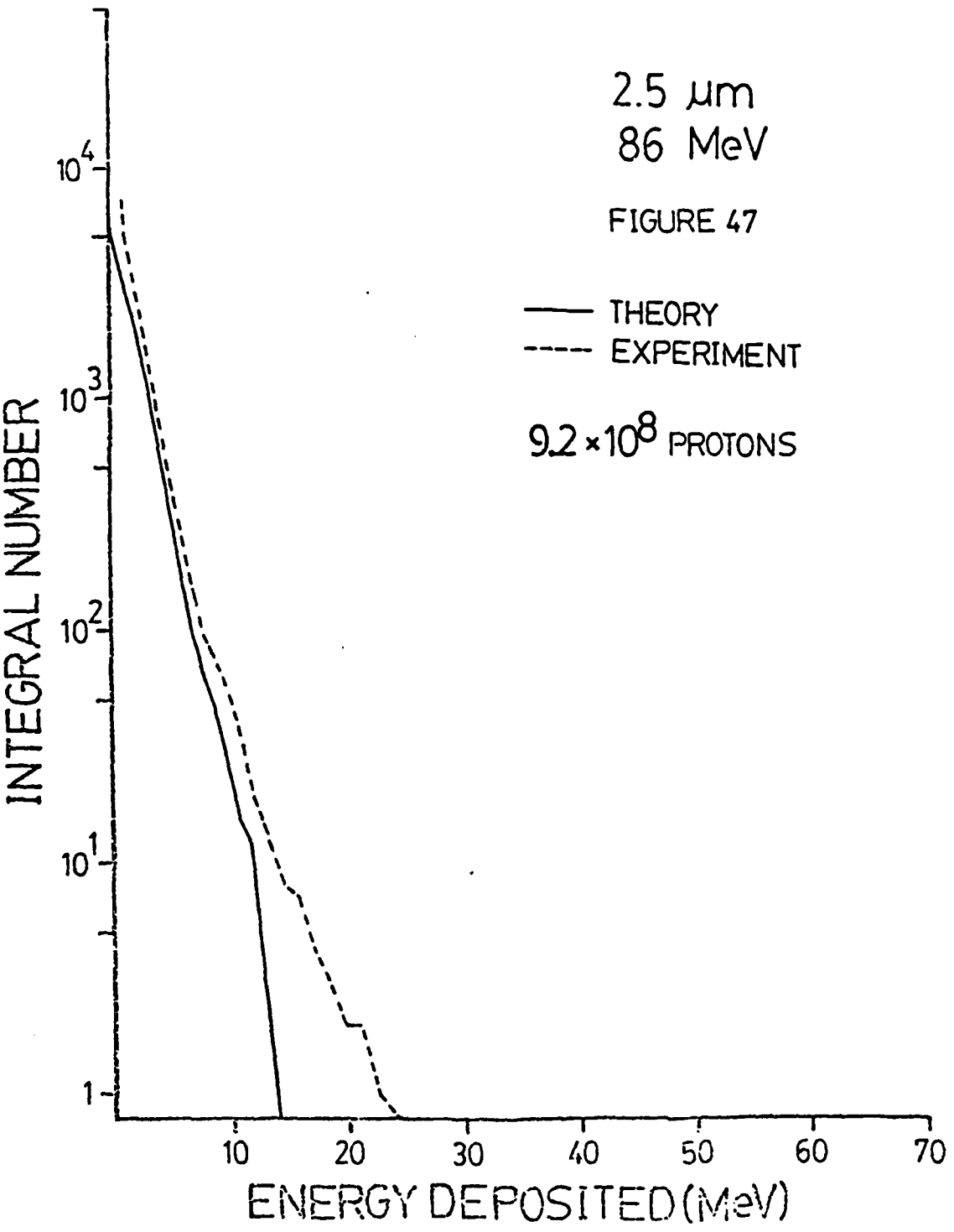
2.5 μm
86 MeV
FIGURE 47
THEORY
EXPERIMENT
9.2 × 10^8 PROTONS
INTEGRAL NUMBER
10^4
10^3
10^2
10^1
1
10
20
30
40
50
60
70
ENERGY DEPOSITED (MeV)

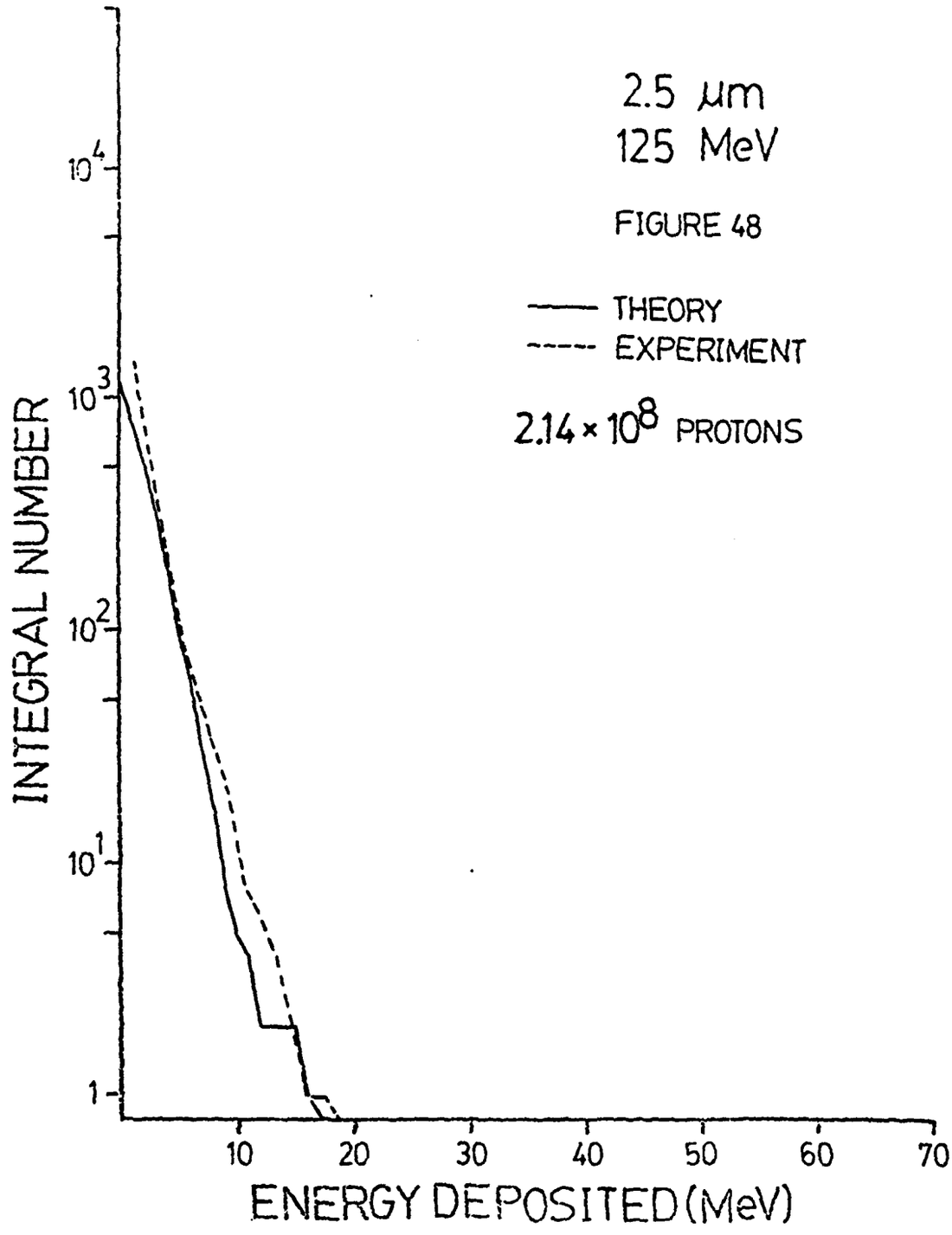
2.5 μm
125 MeV
FIGURE 48
THEORY
EXPERIMENT
2.14 × 10^8 PROTONS
INTEGRAL NUMBER
10^4
10^3
10^2
10^1
1
10
20
30
40
50
60
70
ENERGY DEPOSITED (MeV)

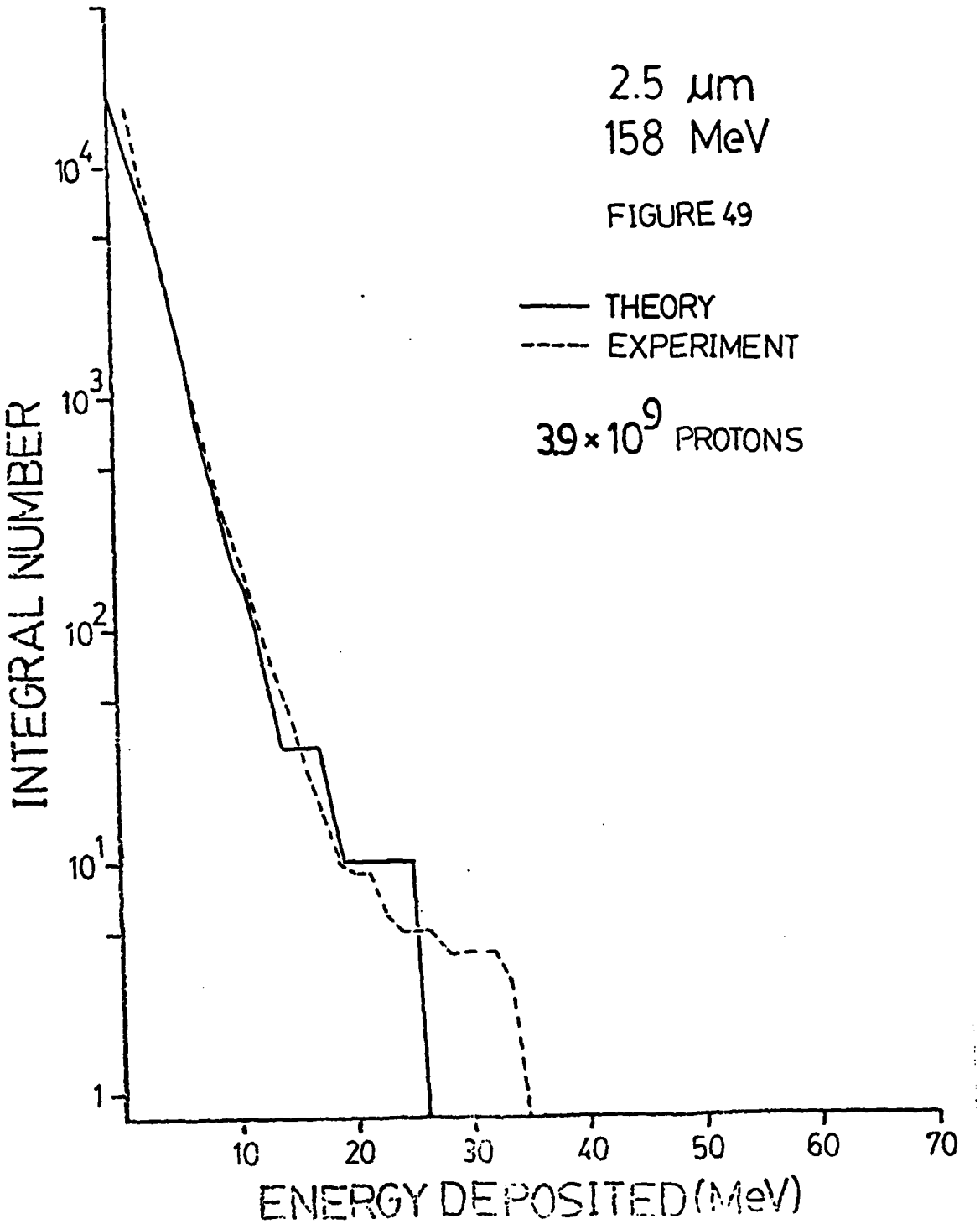
2.5 μm
158 MeV
FIGURE 49
THEORY
EXPERIMENT
3.9 × 10^9 PROTONS
INTEGRAL NUMBER
10^4
10^3
10^2
10^1
1
10
20
30
40
50
60
70
ENERGY DEPOSITED (MeV)

VI. ADDITIONAL PREDICTIONS

Figures 50-63 show the predicted energy deposition spectra for incident protons of 250 and 350 MeV on the detectors. This is beyond the energy available at the Harvard Cyclotron. These curves give an indication of the amount of energy which could be deposited in microelectronics devices of dimensions similar to the detector thicknesses.

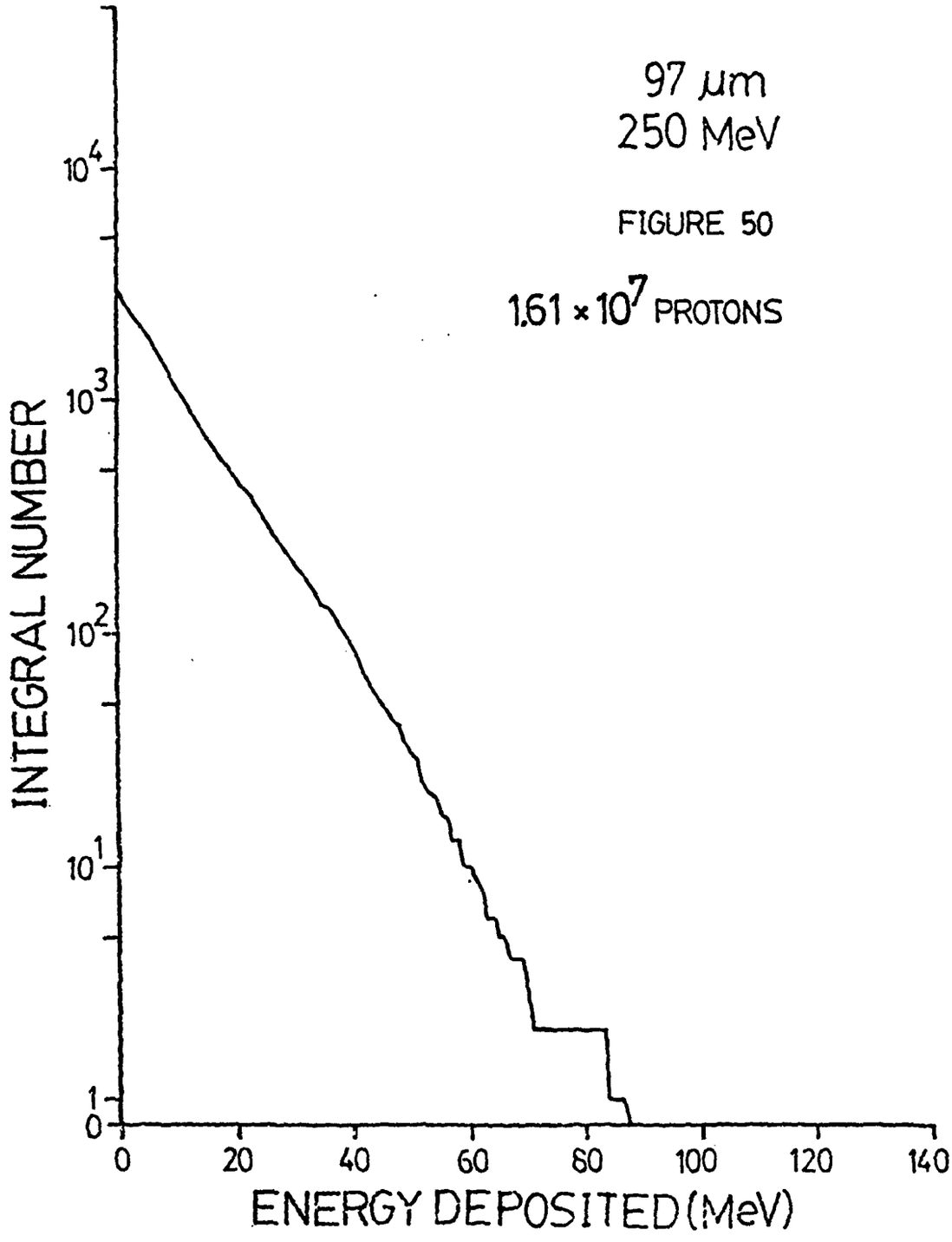
97 μm
250 MeV
FIGURE 50
1.61 × 10^7 PROTONS
INTEGRAL NUMBER
10^4
10^3
10^2
10^1
1
0
0
20
40
60
80
100
120
140
ENERGY DEPOSITED (MeV)

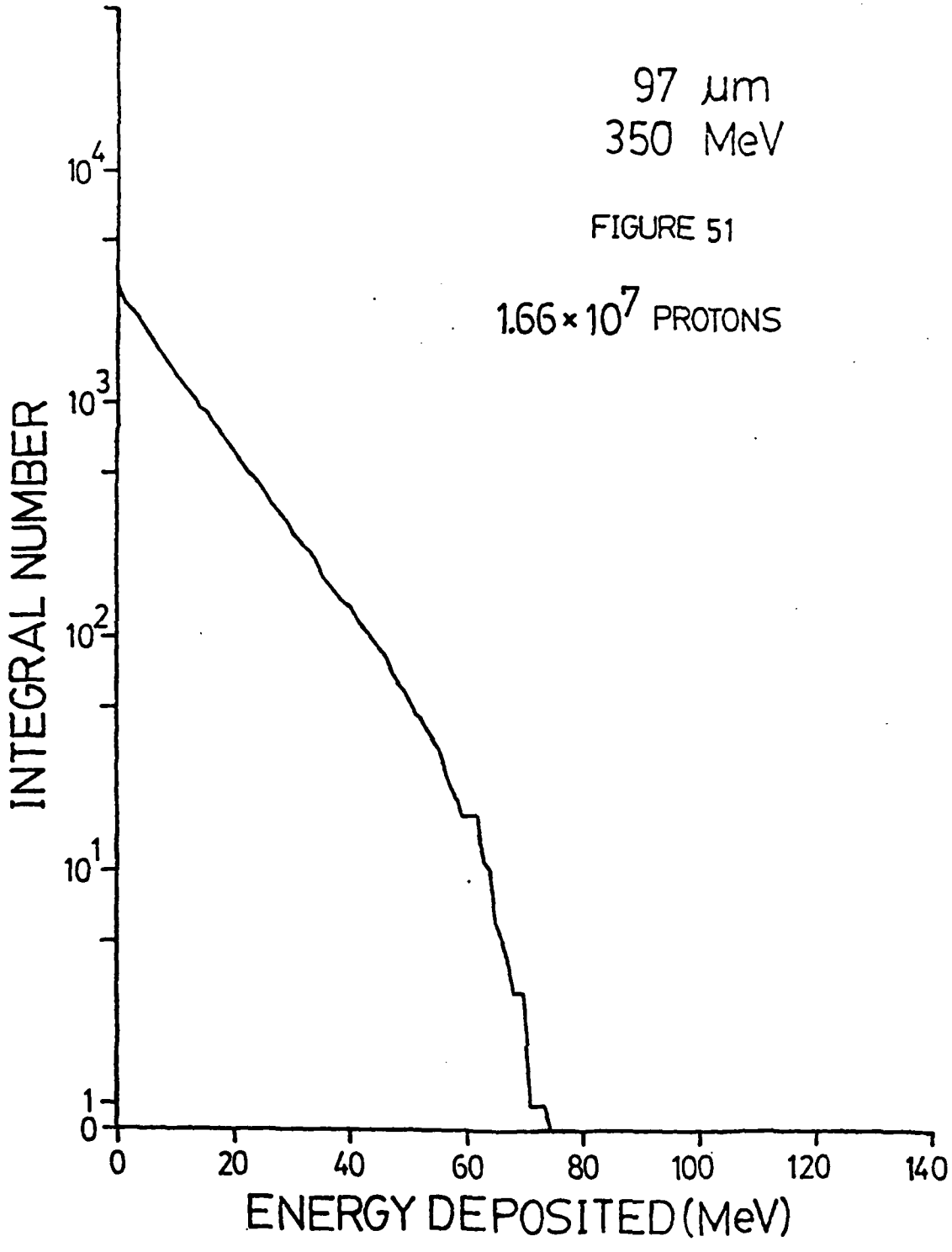
97 μm
350 MeV
1.66 × 10^7 PROTONS
INTEGRAL NUMBER
10^4
10^3
10^2
10^1
1
0
0
20
40
60
80
100
120
140
ENERGY DEPOSITED (MeV)

FIGURE 51

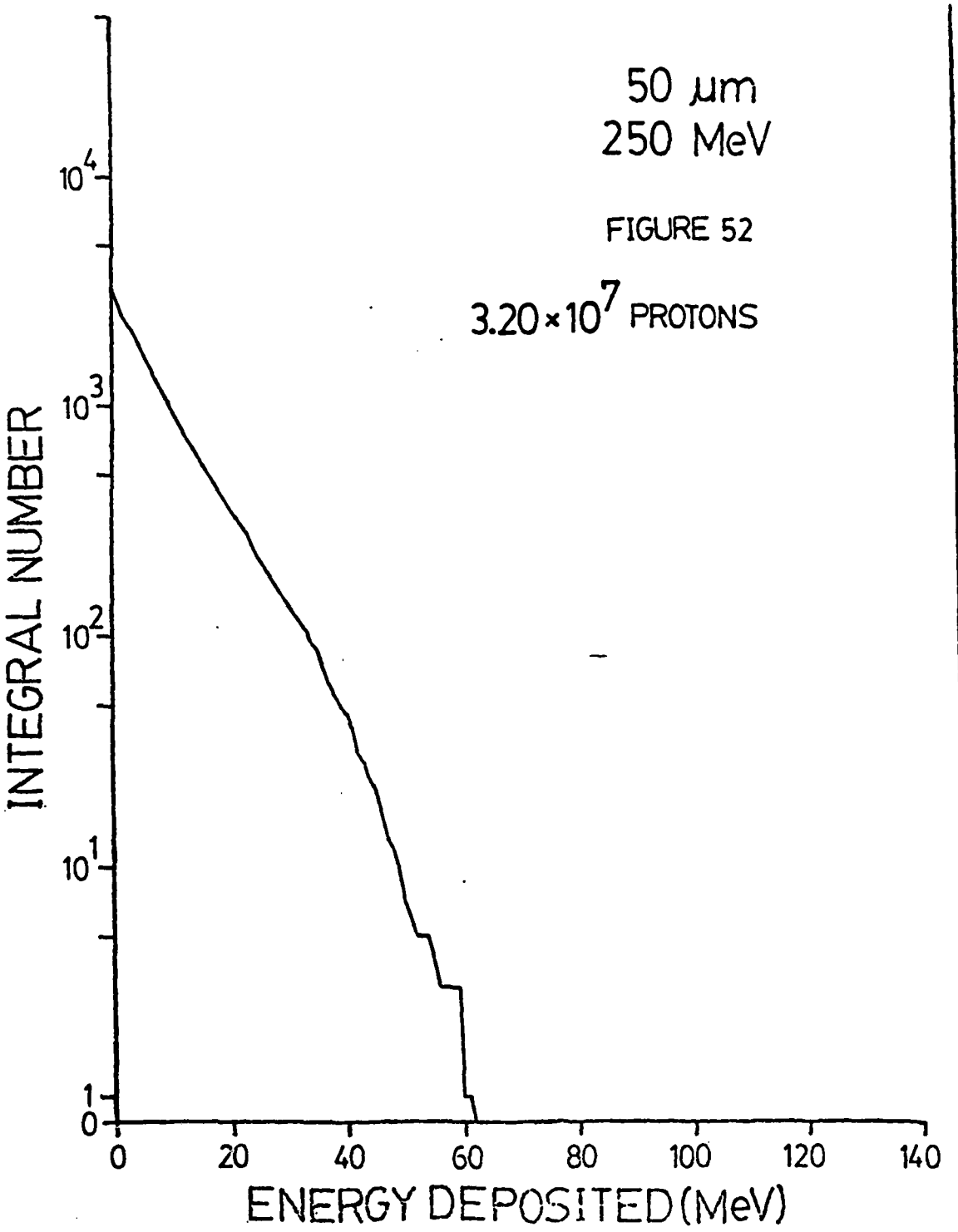
50 μm
250 MeV
FIGURE 52
3.20×10^7 PROTONS
INTEGRAL NUMBER
10^4
10^3
10^2
10^1
1
0
0
20
40
60
80
100
120
140
ENERGY DEPOSITED (MeV)

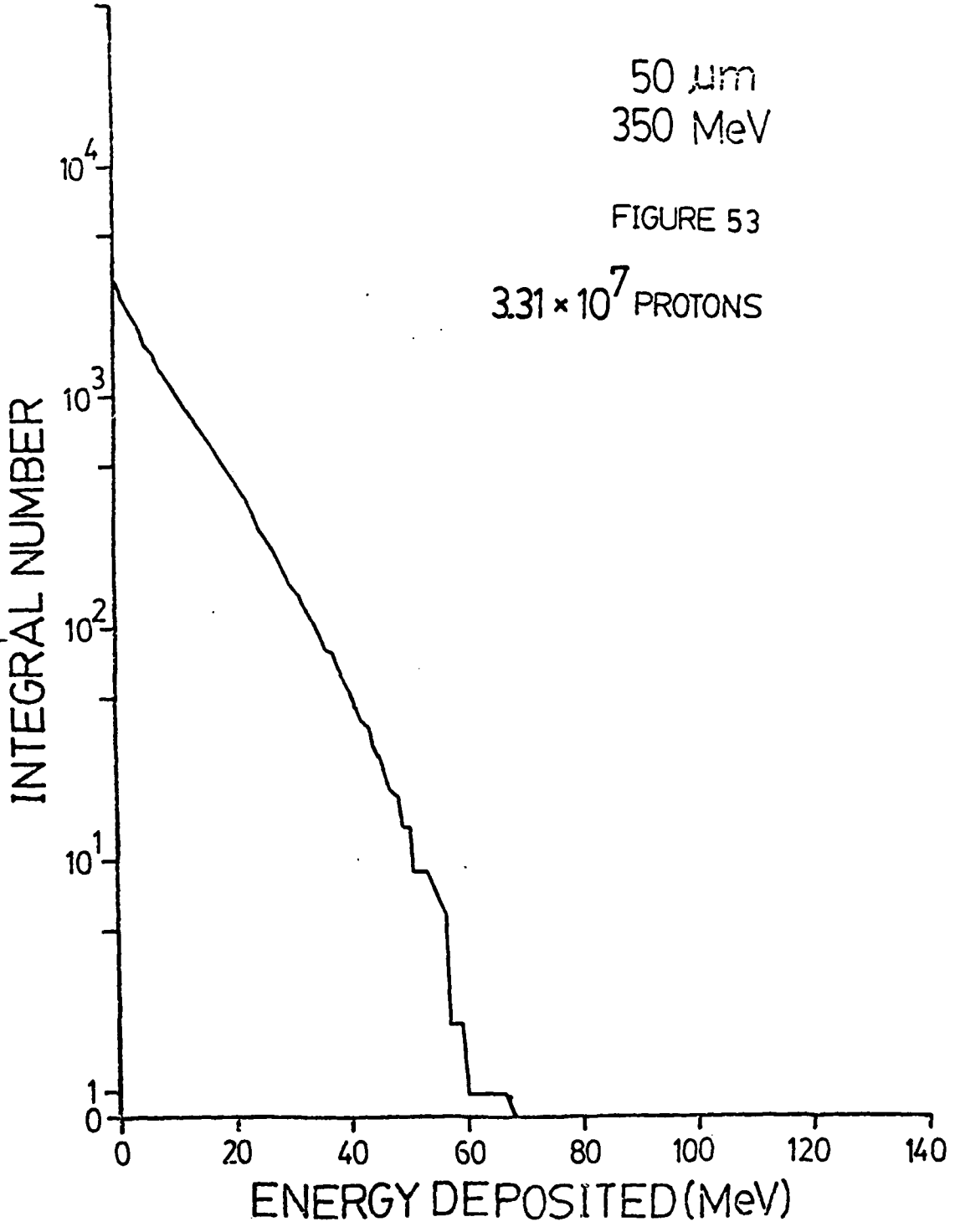
50 μm
350 MeV
FIGURE 53
3.31 × 10^7 PROTONS
INTEGRAL NUMBER
10^4
10^3
10^2
10^1
1
0
0
20
40
60
80
100
120
140
ENERGY DEPOSITED (MeV)

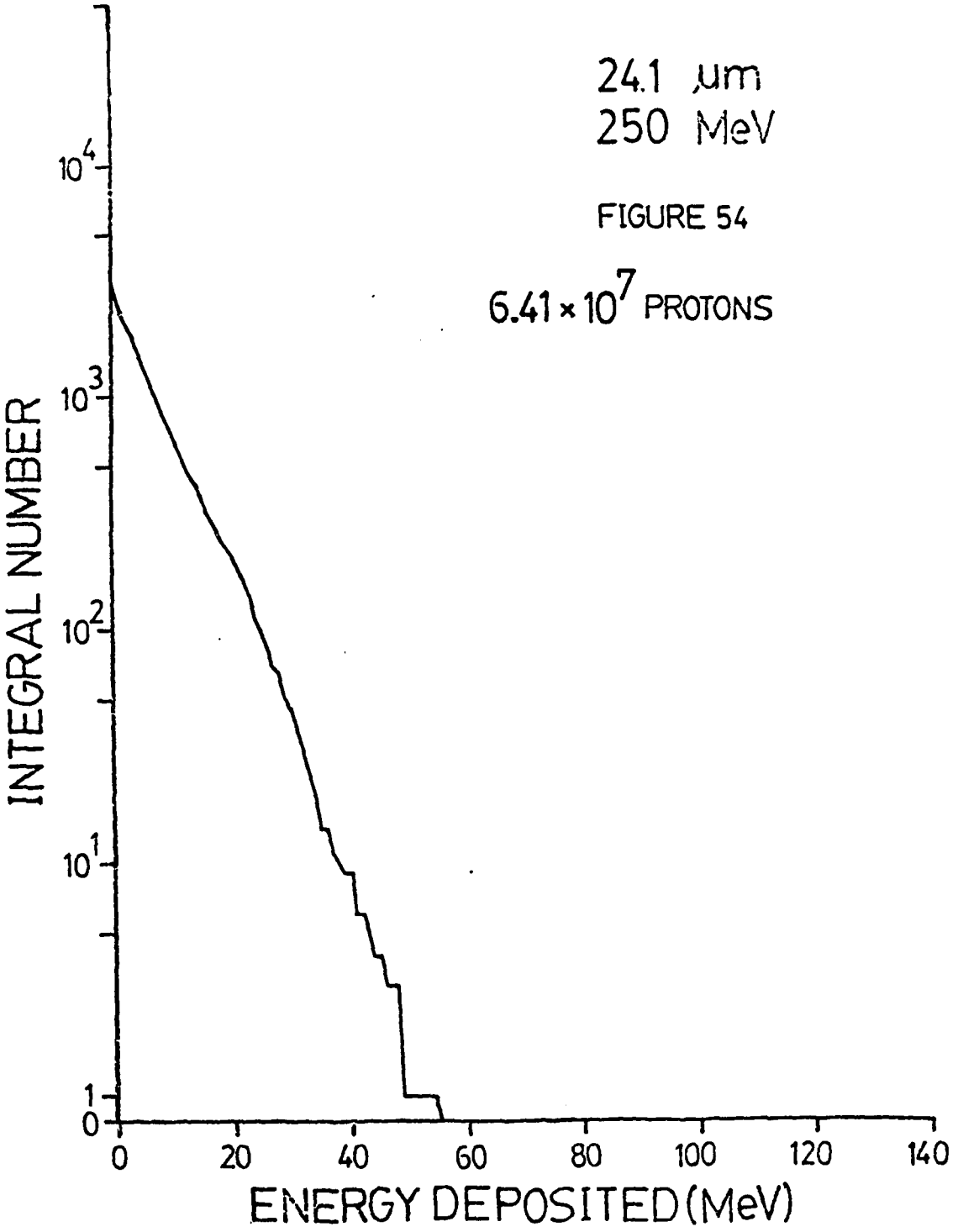
24.1 μm
250 MeV
FIGURE 54
6.41 × 10^7 PROTONS
INTEGRAL NUMBER
10^4
10^3
10^2
10^1
1
0
0
20
40
60
80
100
120
140
ENERGY DEPOSITED (MeV)

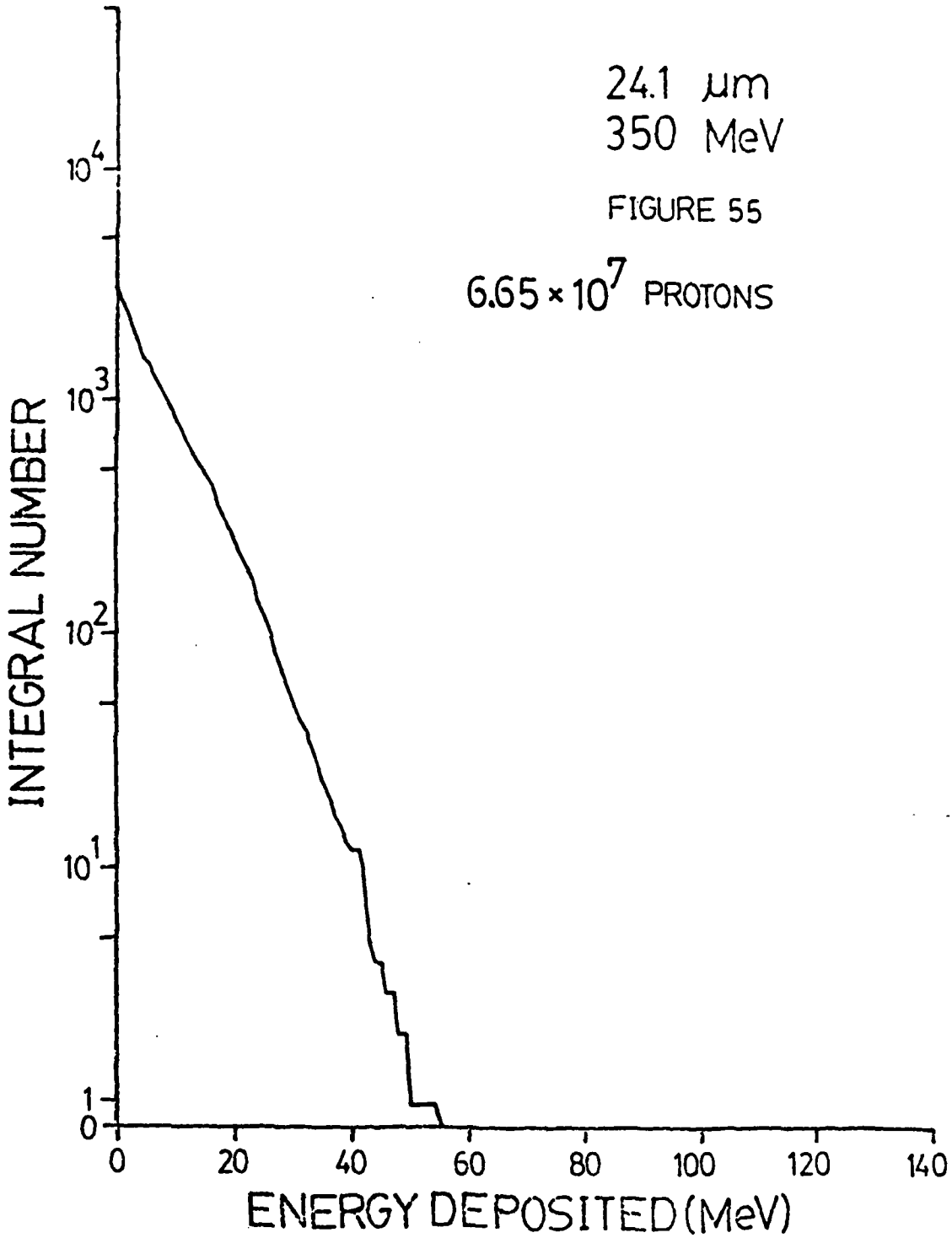
24.1 μm
350 MeV
6.65 × 10^7 PROTONS
INTEGRAL NUMBER
10^4
10^3
10^2
10^1
1
0
0
20
40
60
80
100
120
140
ENERGY DEPOSITED (MeV)

FIGURE 55

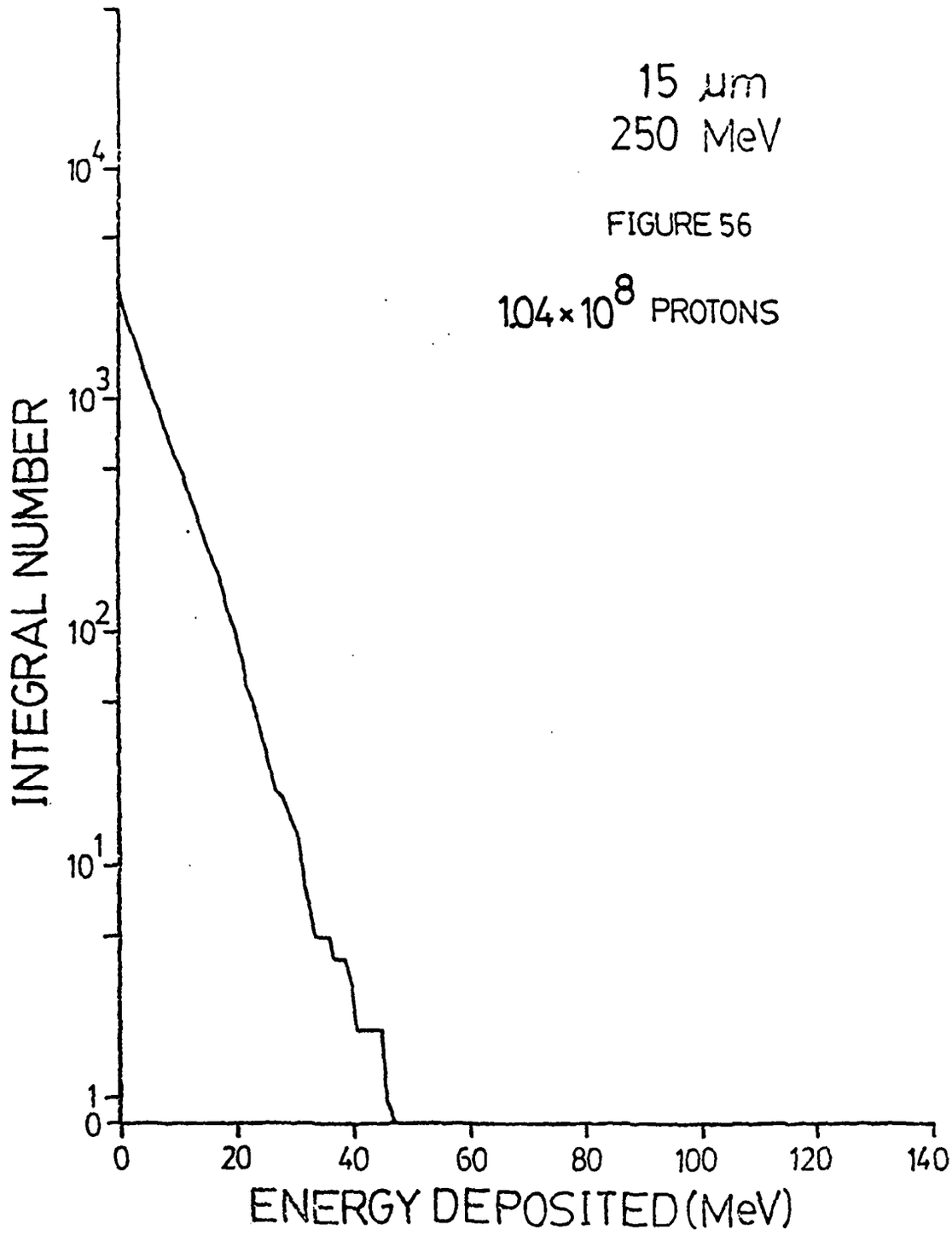
15 μm
250 MeV
FIGURE 56
1.04 × 10^8 PROTONS
INTEGRAL NUMBER
10^4
10^3
10^2
10^1
1
0
0
20
40
60
80
100
120
140
ENERGY DEPOSITED (MeV)

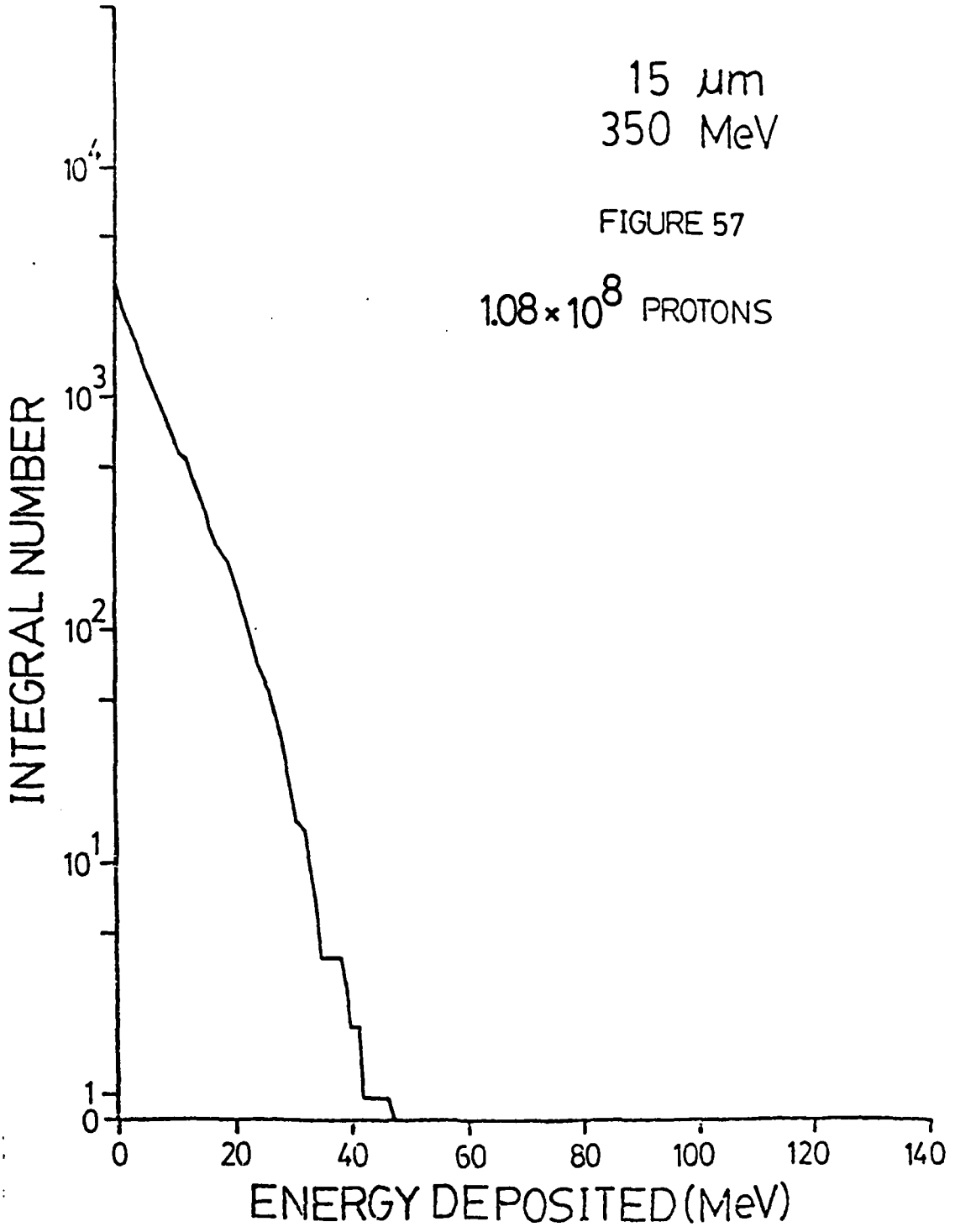
15 μm
350 MeV
FIGURE 57
1.08 × 10^8 PROTONS
INTEGRAL NUMBER
10^4
10^3
10^2
10^1
1
0
0
20
40
60
80
100
120
140
ENERGY DEPOSITED (MeV)

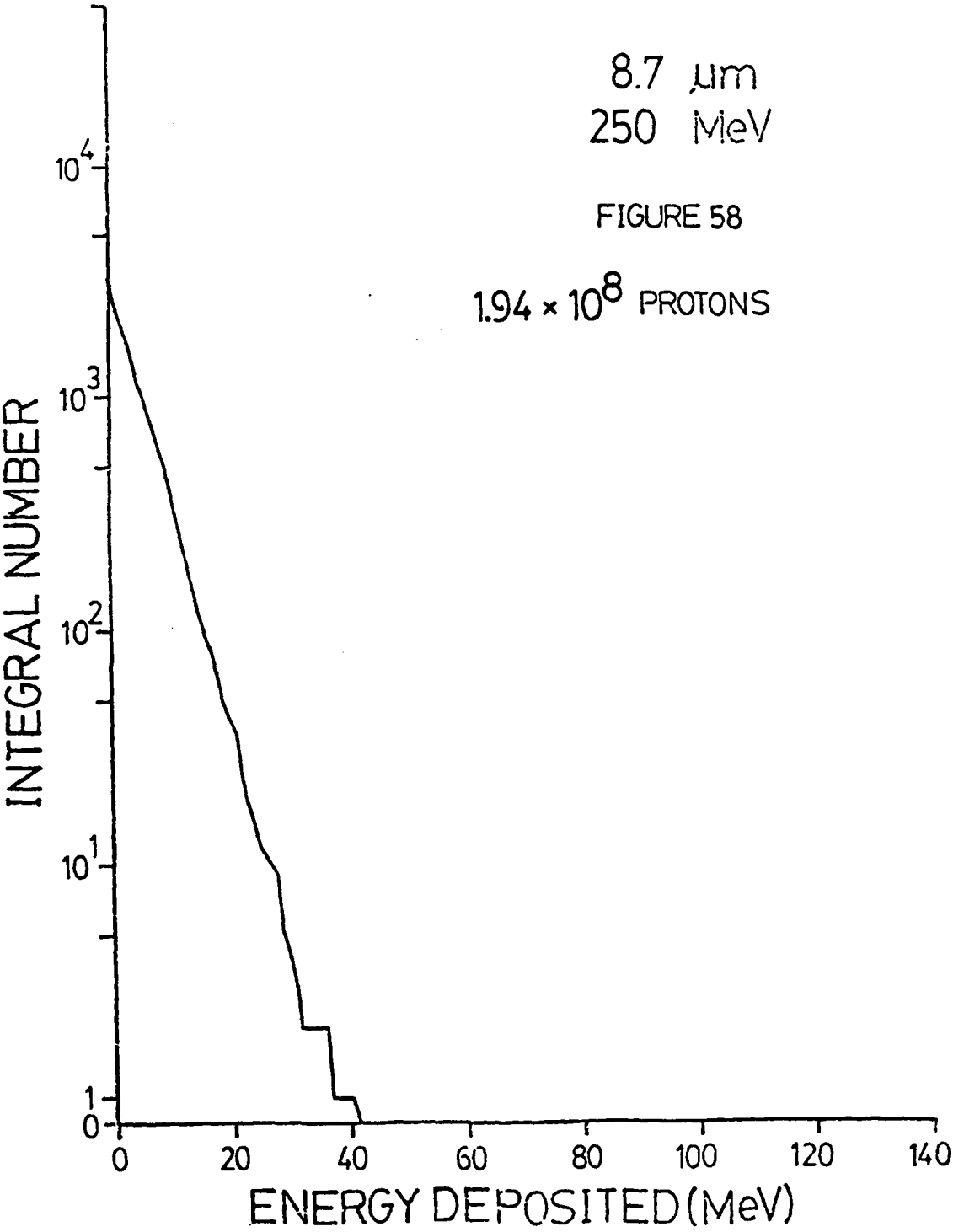

FIGURE 58

1.94×10^8 PROTONS

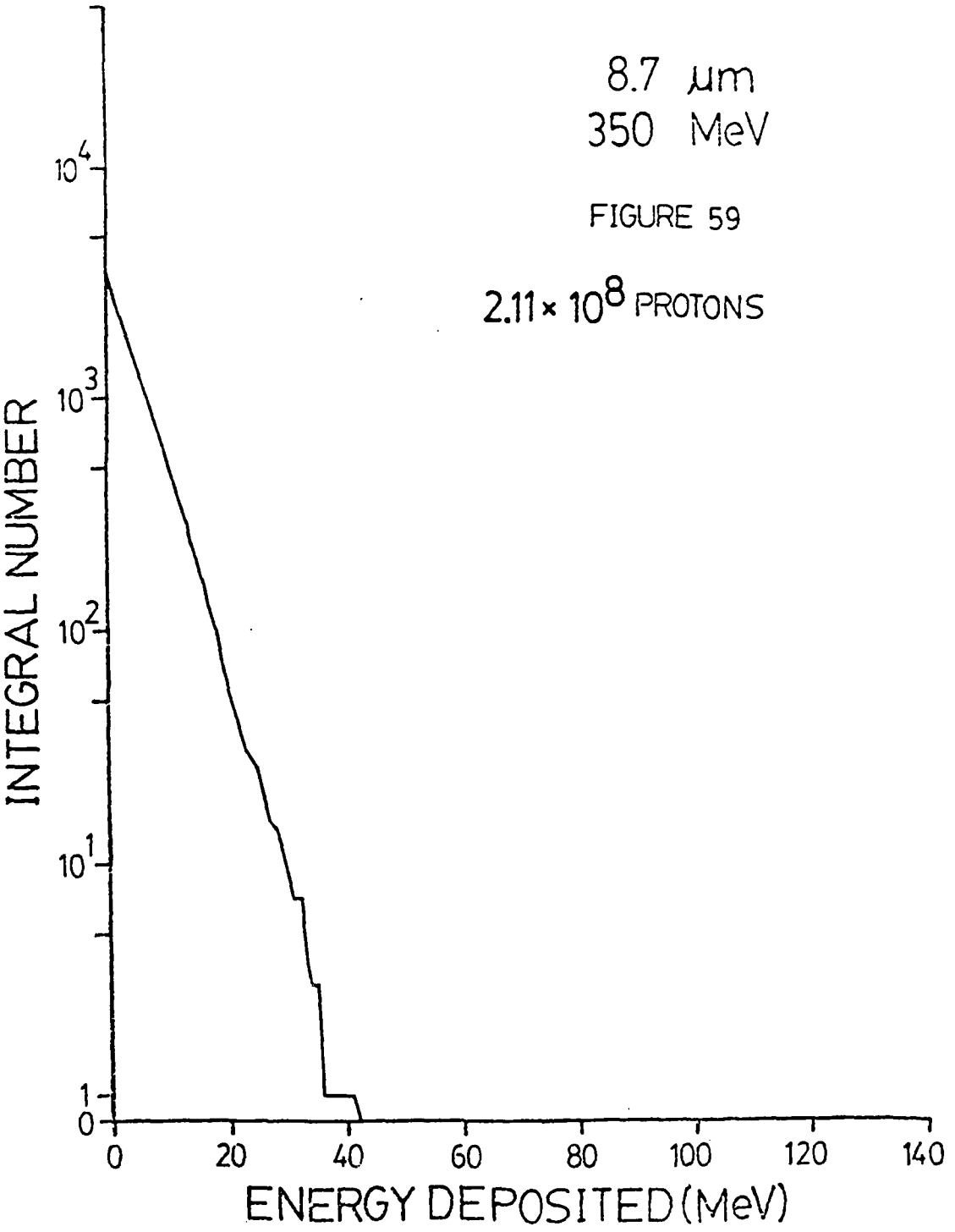

FIGURE 59

2.11×10^8 PROTONS

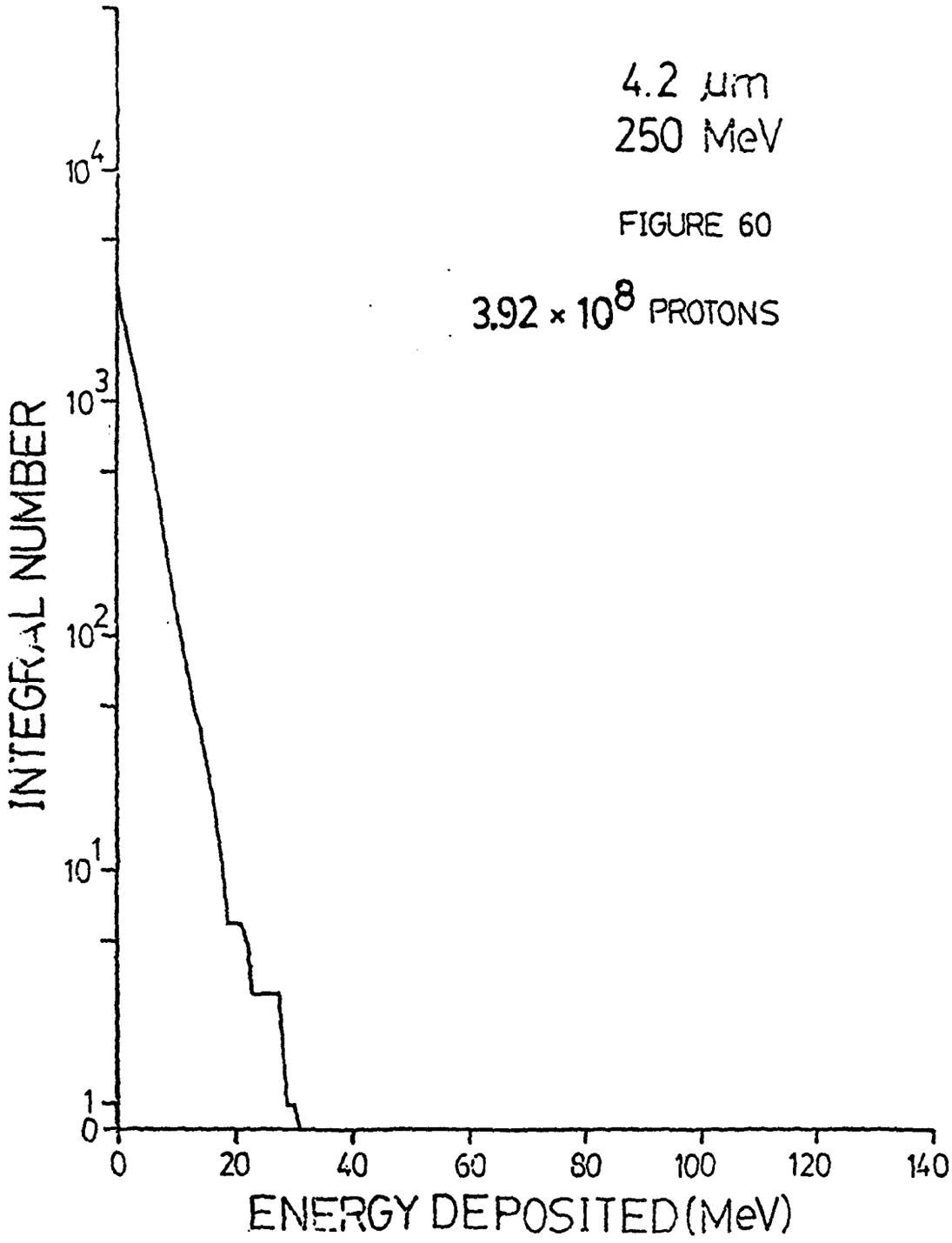
4.2 μm
250 MeV
FIGURE 60
3.92 × 10^8 PROTONS
INTEGRAL NUMBER
10^4
10^3
10^2
10^1
1
0
0
20
40
60
80
100
120
140
ENERGY DEPOSITED (MeV)

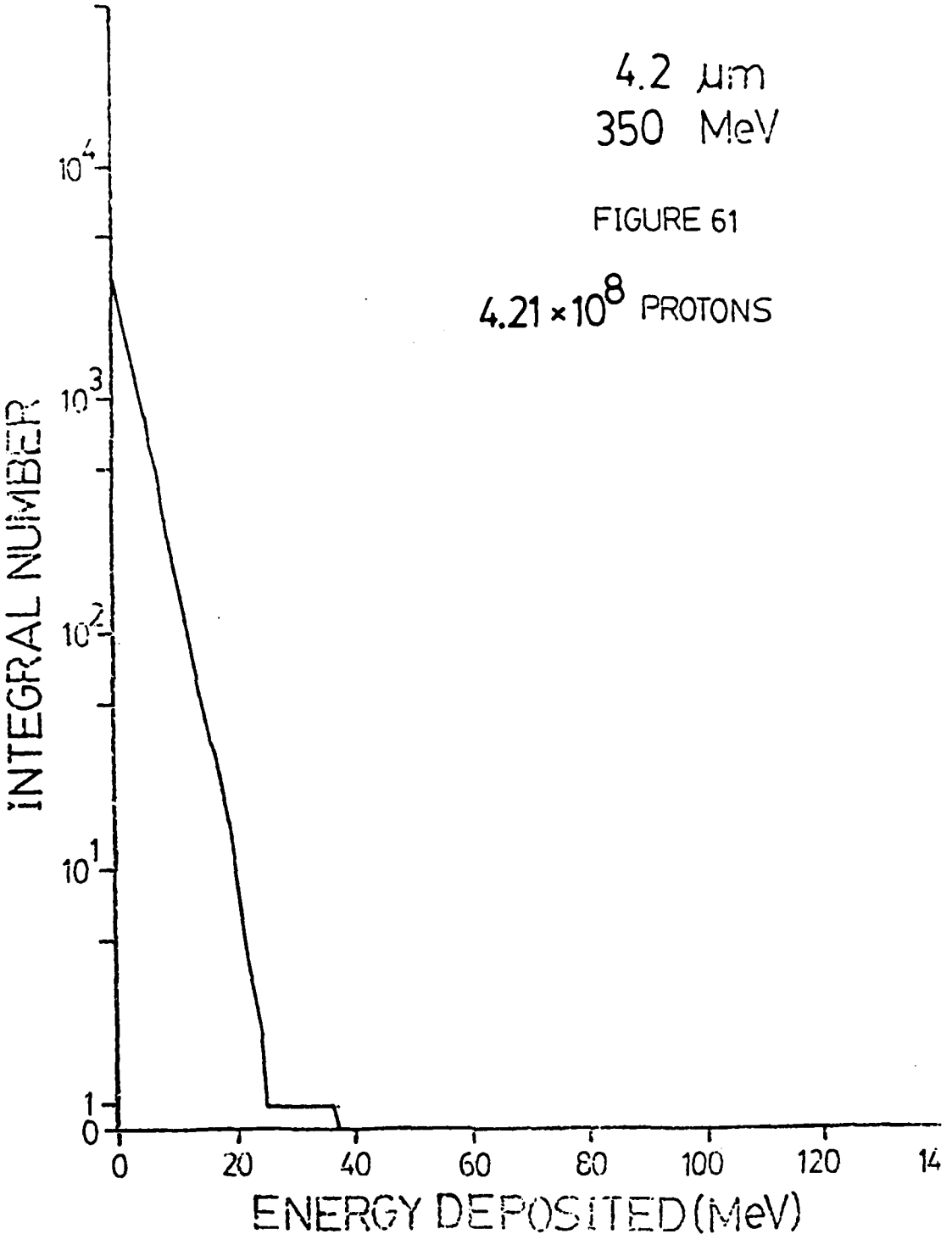

FIGURE 61

4.21×10^8 PROTONS

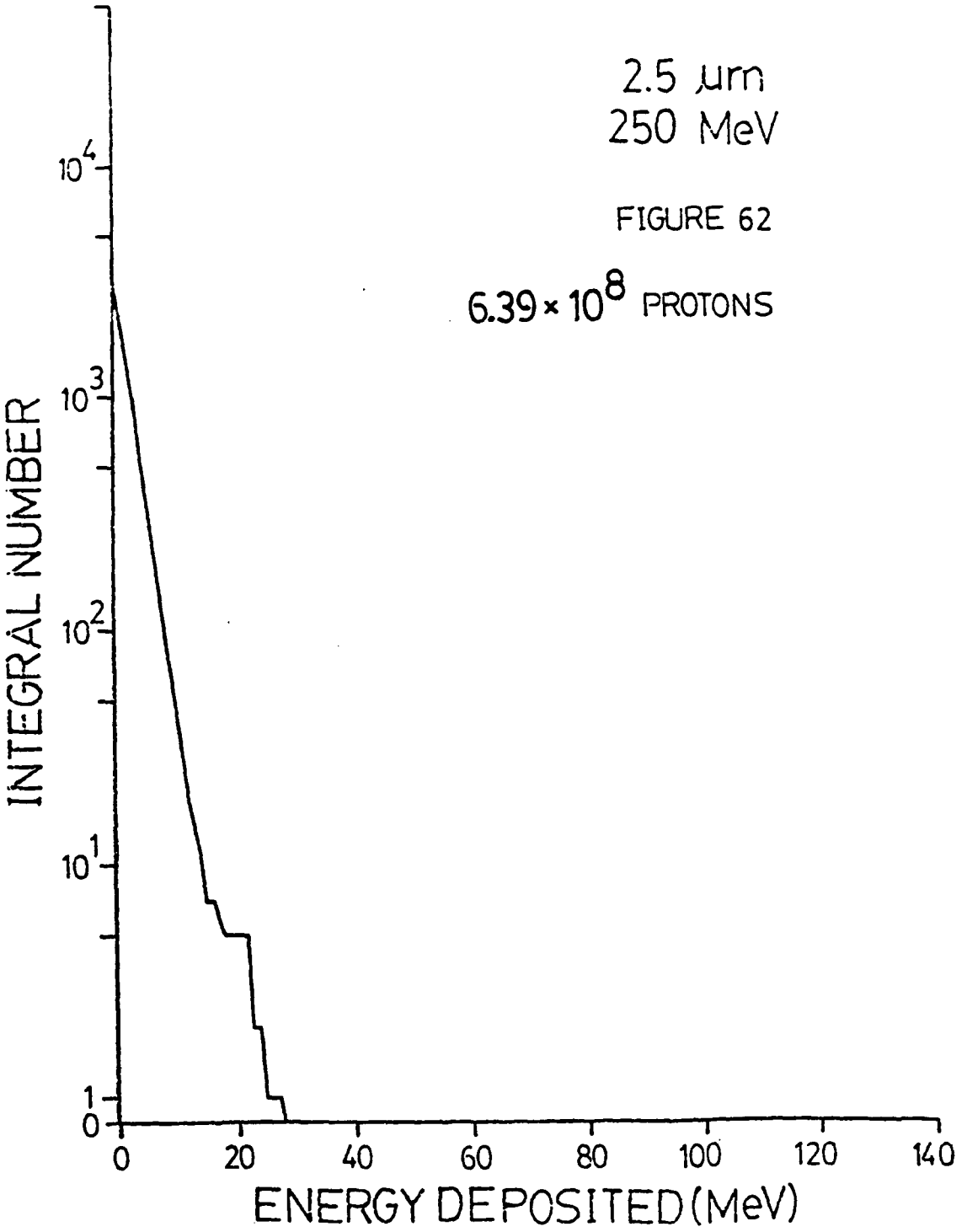
2.5 μm
250 MeV
FIGURE 62
6.39 × 10^8 PROTONS
INTEGRAL NUMBER
10^4
10^3
10^2
10^1
1
0
0
20
40
60
80
100
120
140
ENERGY DEPOSITED (MeV)

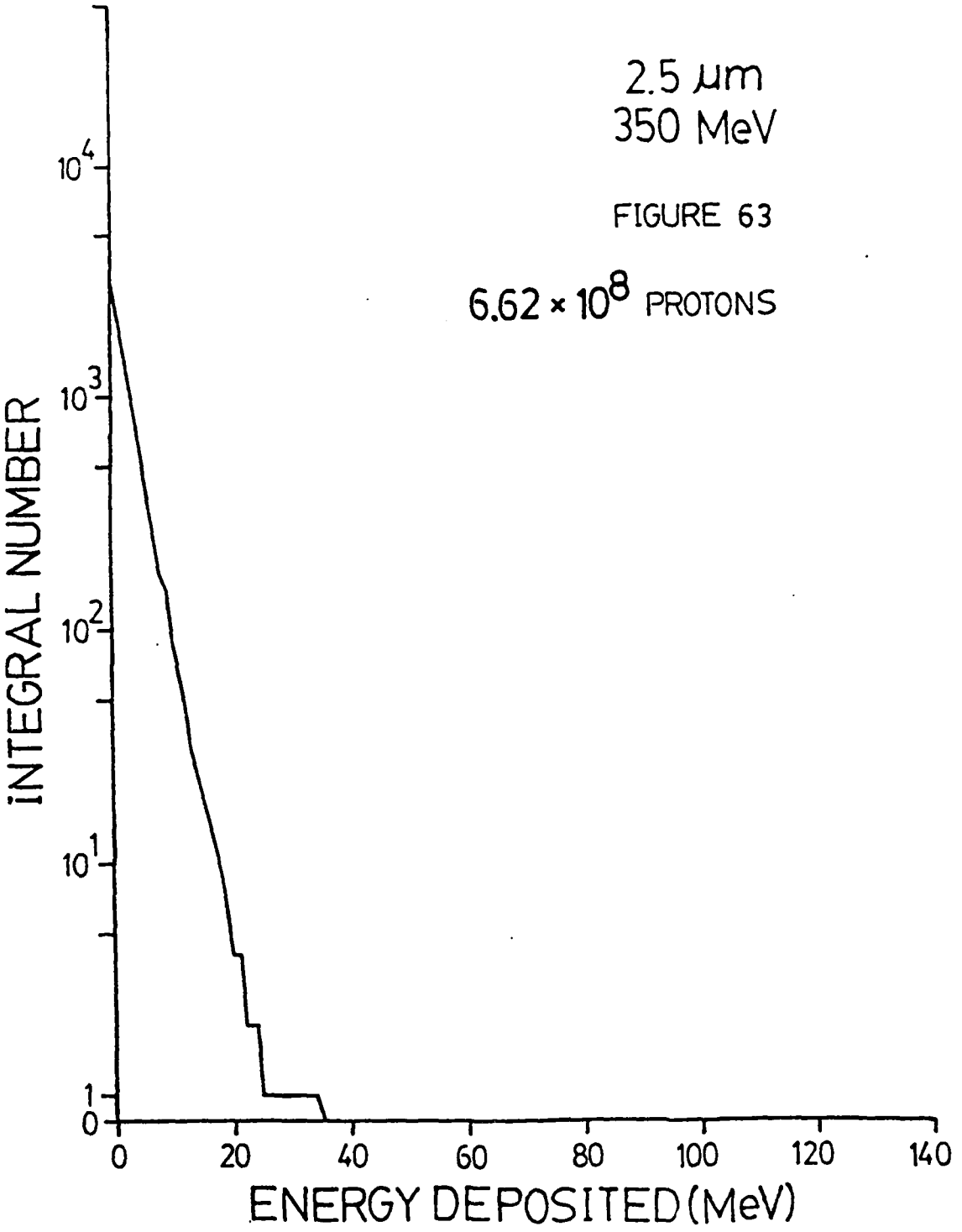
2.5 μm
350 MeV
FIGURE 63
6.62 × 10^8 PROTONS
INTEGRAL NUMBER
10^4
10^3
10^2
10^1
1
0
0
20
40
60
80
100
120
140
ENERGY DEPOSITED (MeV)

Figures 64-68 show the energy spectrum of the recoiling nuclei resulting from the interaction of 25, 27, 86, 125, and 158 MeV protons with a 2.5 um thick silicon detector. These nuclei can be the dominant means of energy deposition in thin detectors. Calculations showed that for a 20 um x 20 um x 4.2 um silicon device, roughly 85% of the energy deposited by nuclear interactions would come from the residual nucleus.

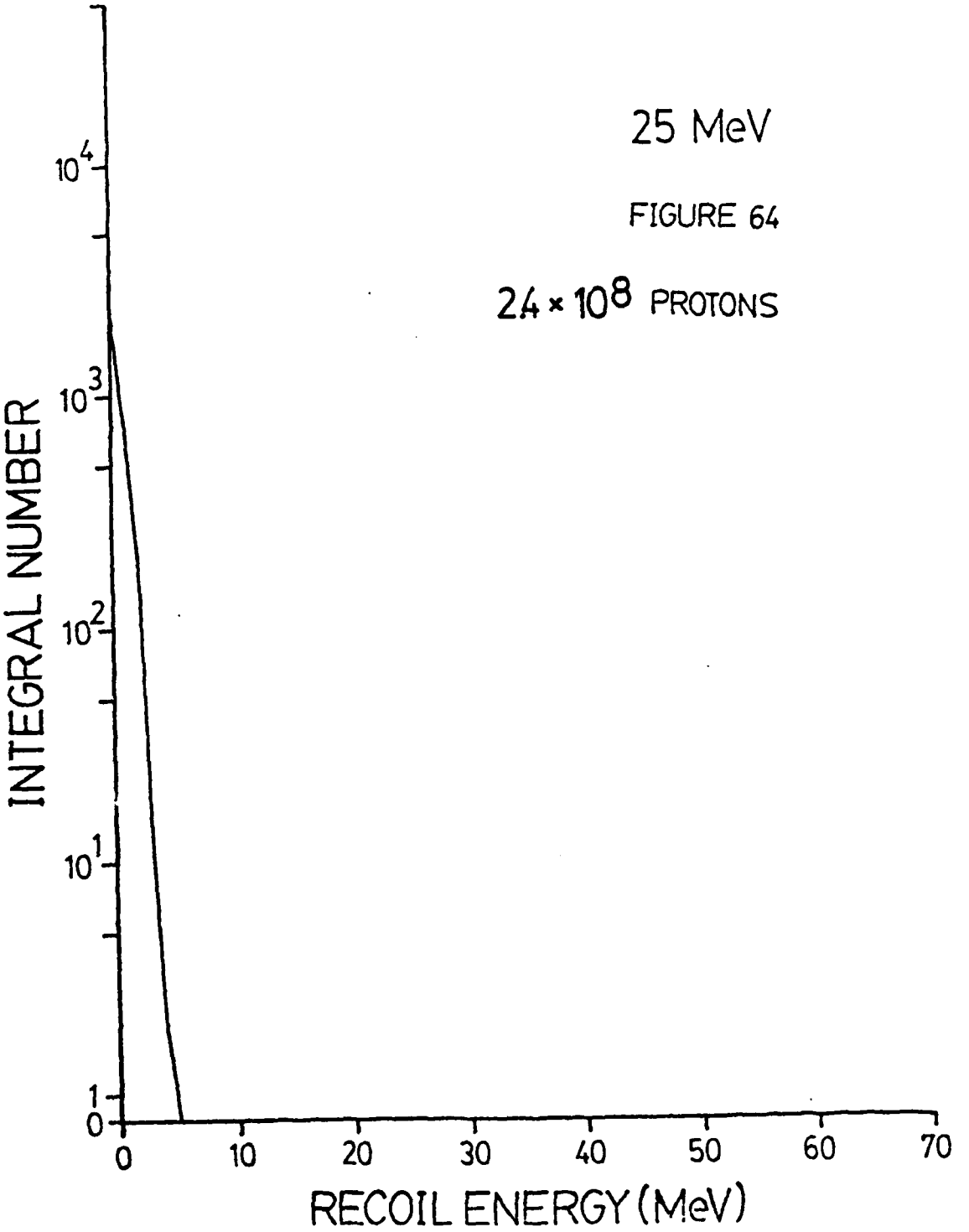
25 MeV
FIGURE 64
24 × 10^8 PROTONS
INTEGRAL NUMBER
10^4
10^3
10^2
10^1
1
0
0
10
20
30
40
50
60
70
RECOIL ENERGY (MeV)

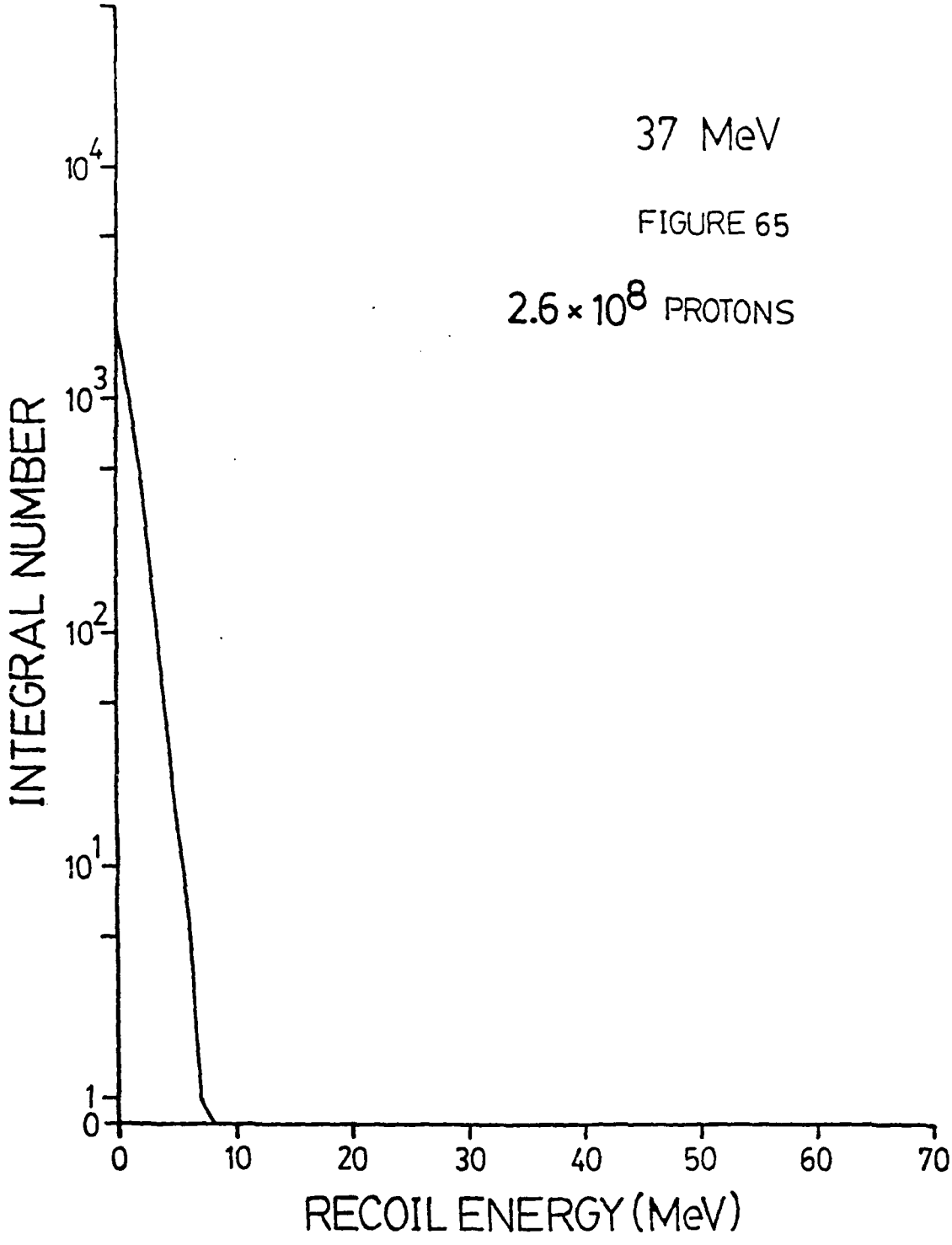
37 MeV
FIGURE 65
2.6 × 10^8 PROTONS
INTEGRAL NUMBER
10^4
10^3
10^2
10^1
1
0
0
10
20
30
40
50
60
70
RECOIL ENERGY (MeV)

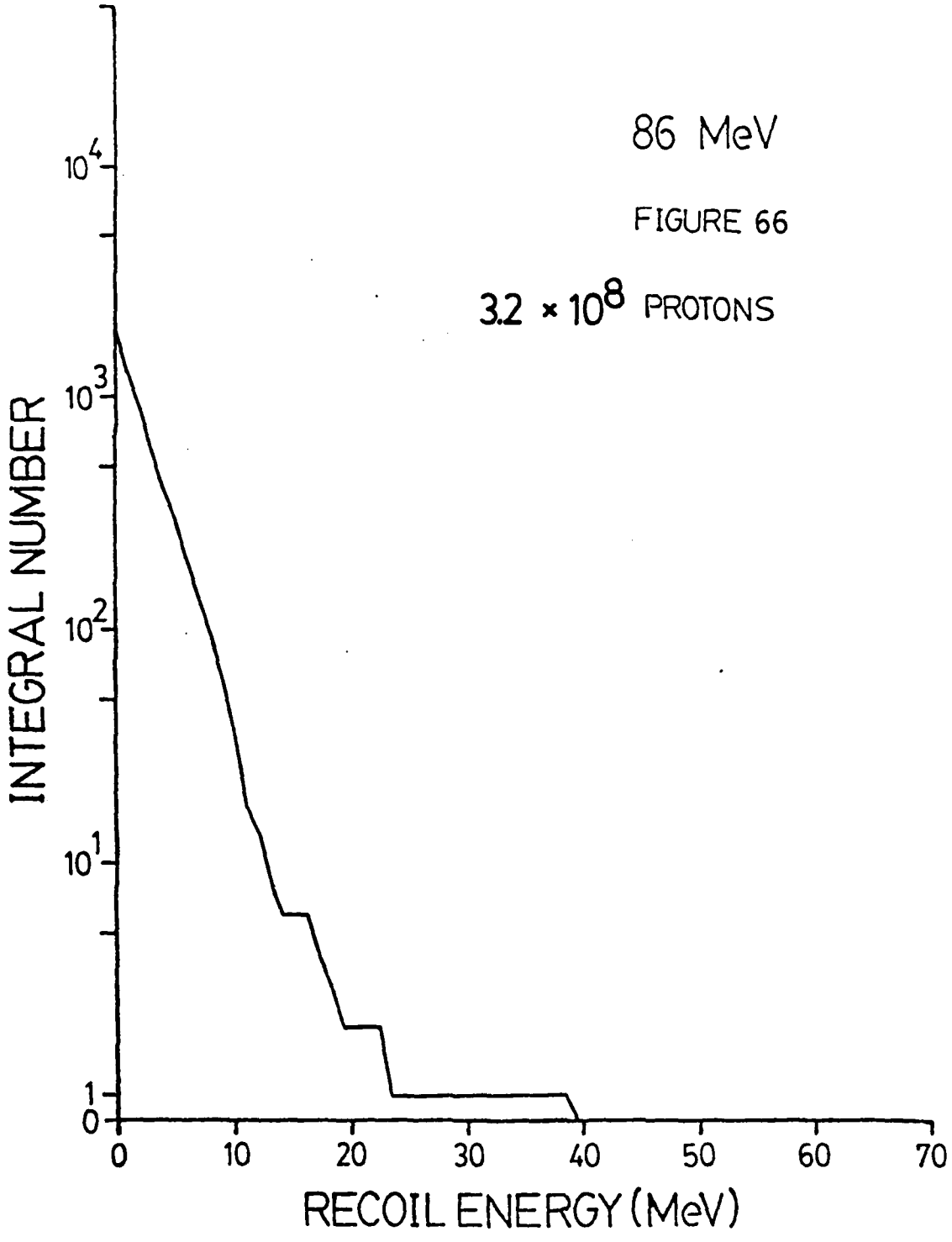
86 MeV
FIGURE 66
3.2 × 10^8 PROTONS
INTEGRAL NUMBER
10^4
10^3
10^2
10^1
1
0
0
10
20
30
40
50
60
70
RECOIL ENERGY (MeV)

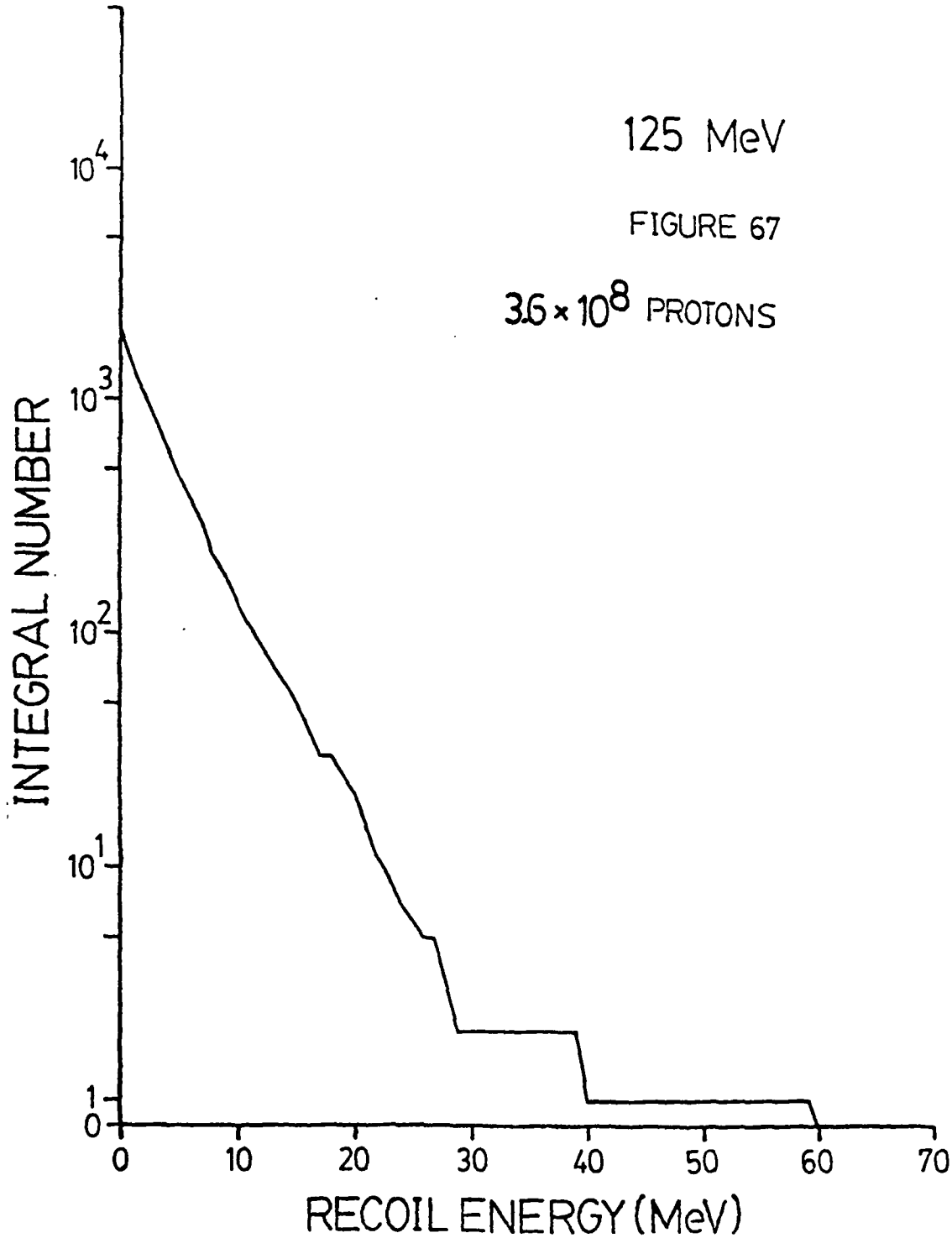
125 MeV
FIGURE 67
3.6 × 10^8 PROTONS
INTEGRAL NUMBER
10^4
10^3
10^2
10^1
1
0
0
10
20
30
40
50
60
70
RECOIL ENERGY (MeV)

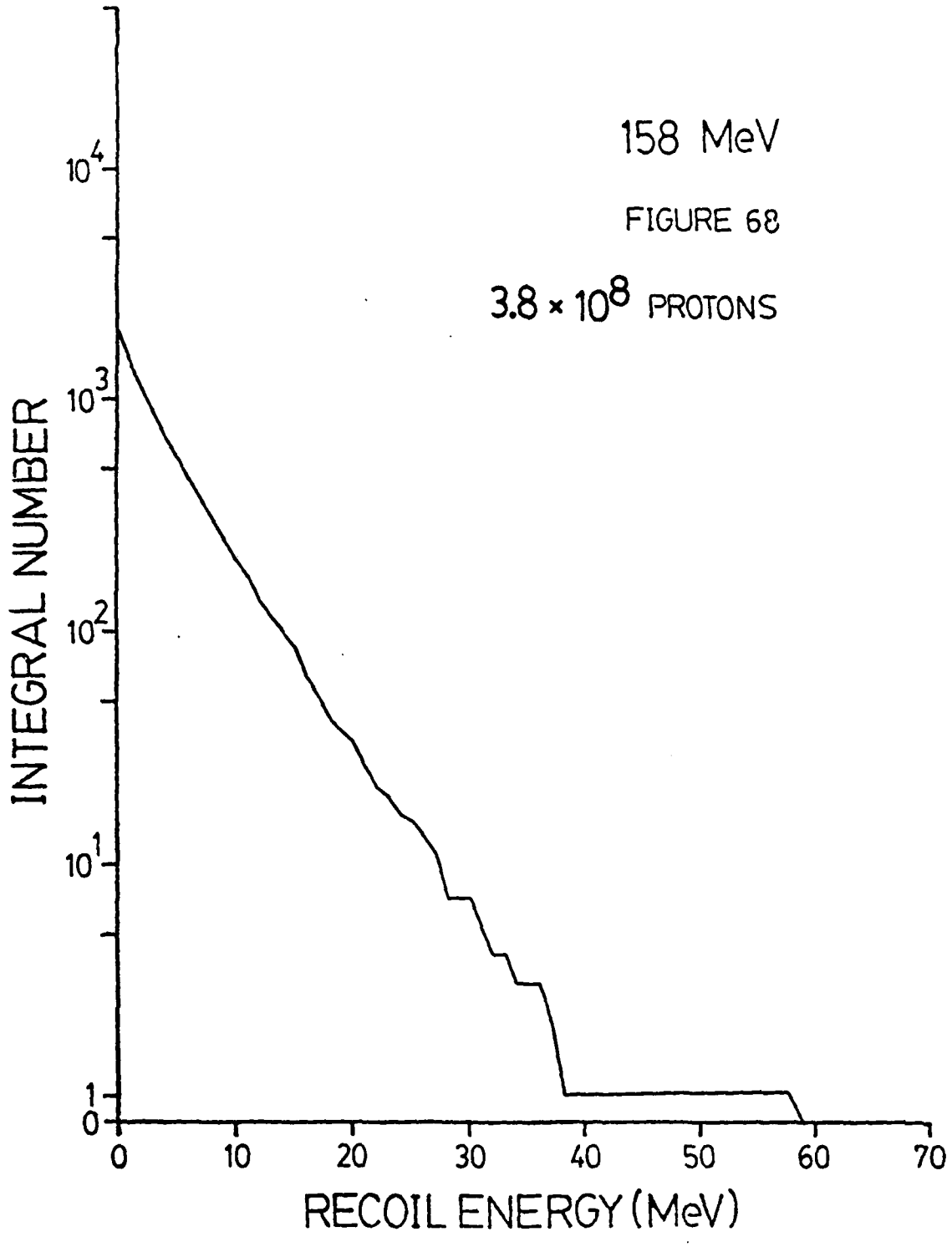
158 MeV
FIGURE 68
3.8 × 10^8 PROTONS
INTEGRAL NUMBER
10^4
10^3
10^2
10^1
1
0
0
10
20
30
40
50
60
70
RECOIL ENERGY (MeV)

Figures 69-75 show distributions of the total energy of the residual recoiling nuclei divided by their total range in silicon. These provide a rough estimate of the amount of energy deposited by these particles in a given thickness of silicon. A 30 um thick silicon detector was the target.

FIGURE 69

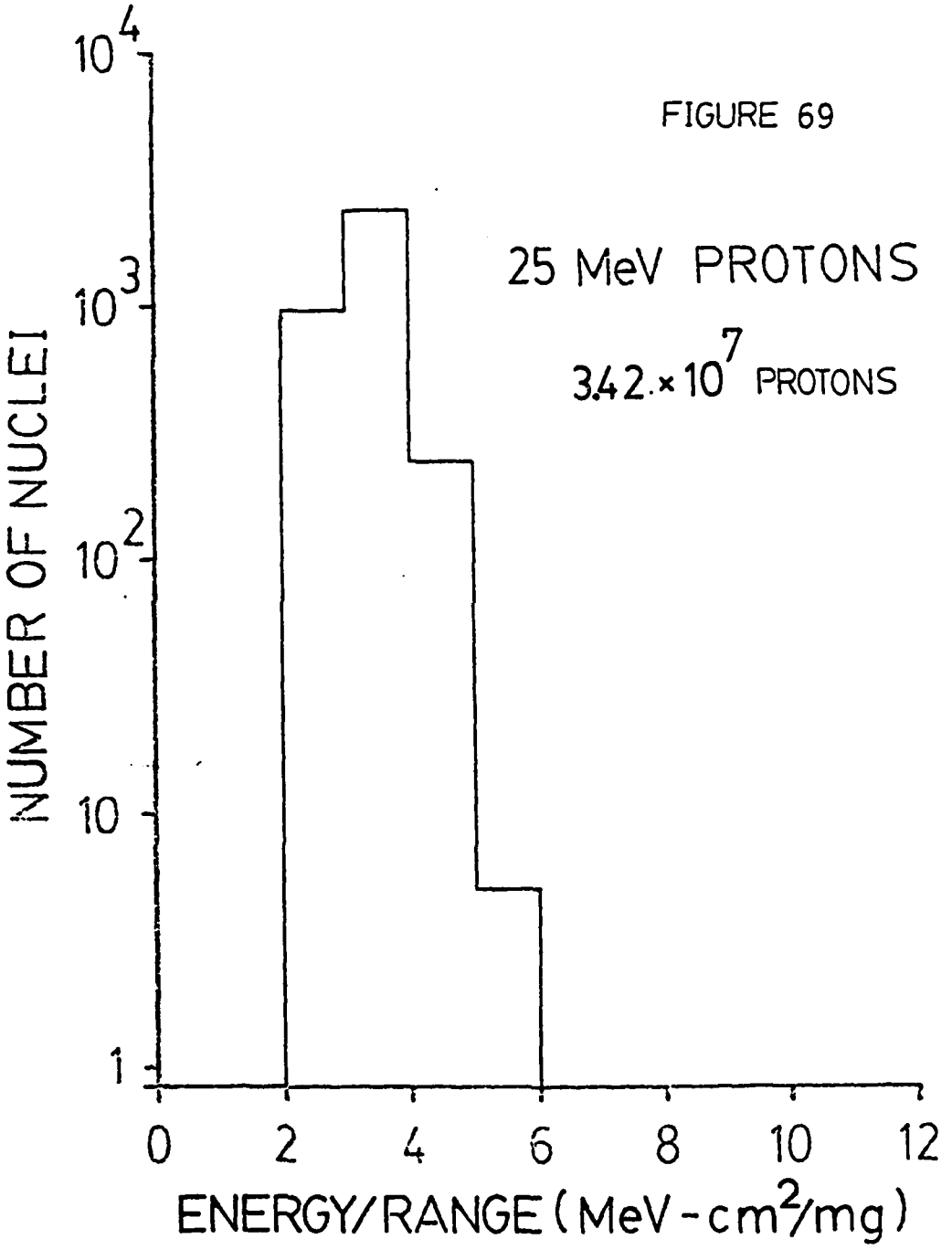
25 MeV PROTONS
3.42 × 10^7 PROTONS
NUMBER OF NUCLEI
10^4
10^3
10^2
10
1
0
2
4
6
8
10
12
ENERGY/RANGE (MeV - cm^2/mg)

FIGURE 70

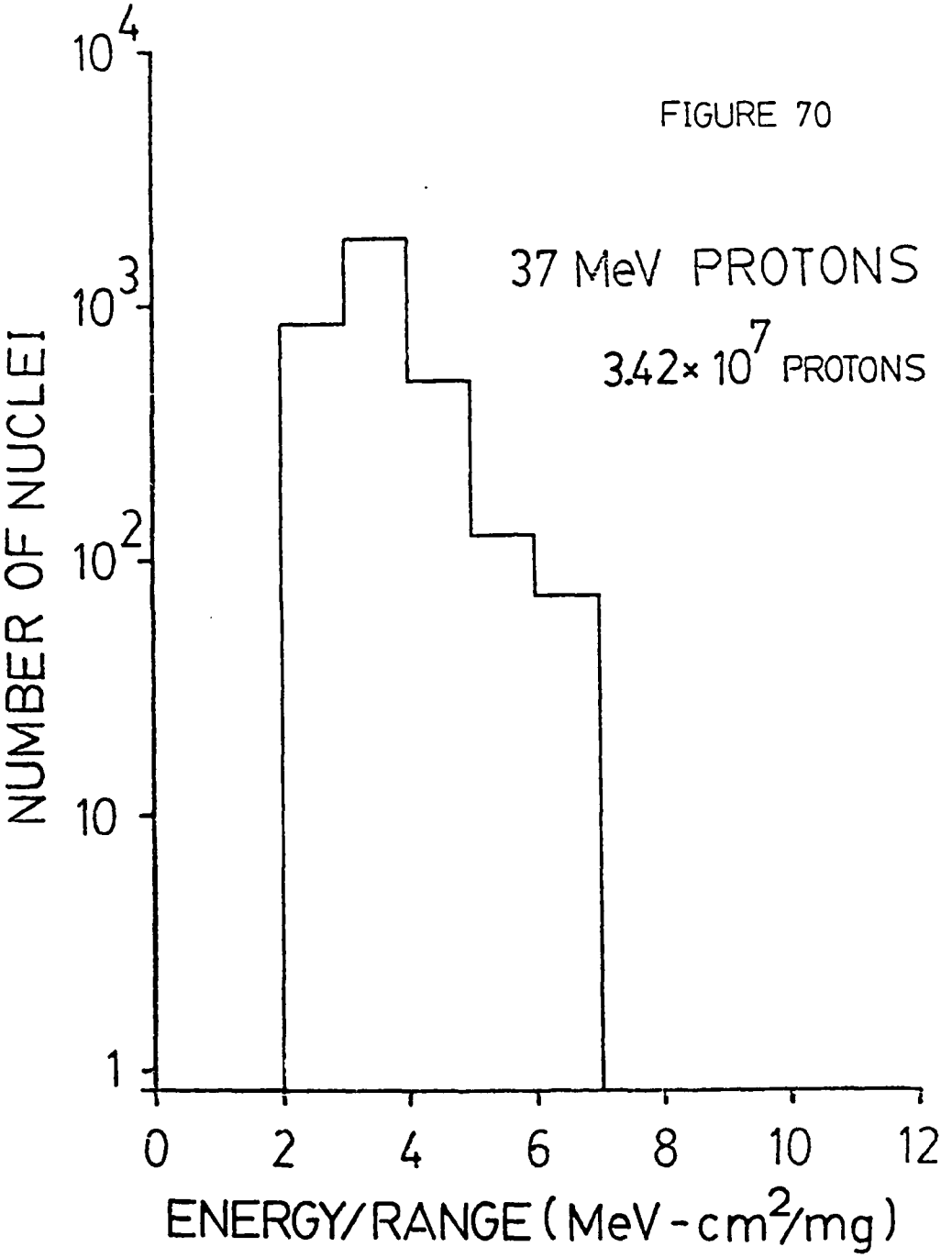
37 MeV PROTONS
3.42× 10^7 PROTONS
NUMBER OF NUCLEI
10^4
10^3
10^2
10
1
0
2
4
6
8
10
12
ENERGY/RANGE (MeV - cm^2/mg)

FIGURE 71

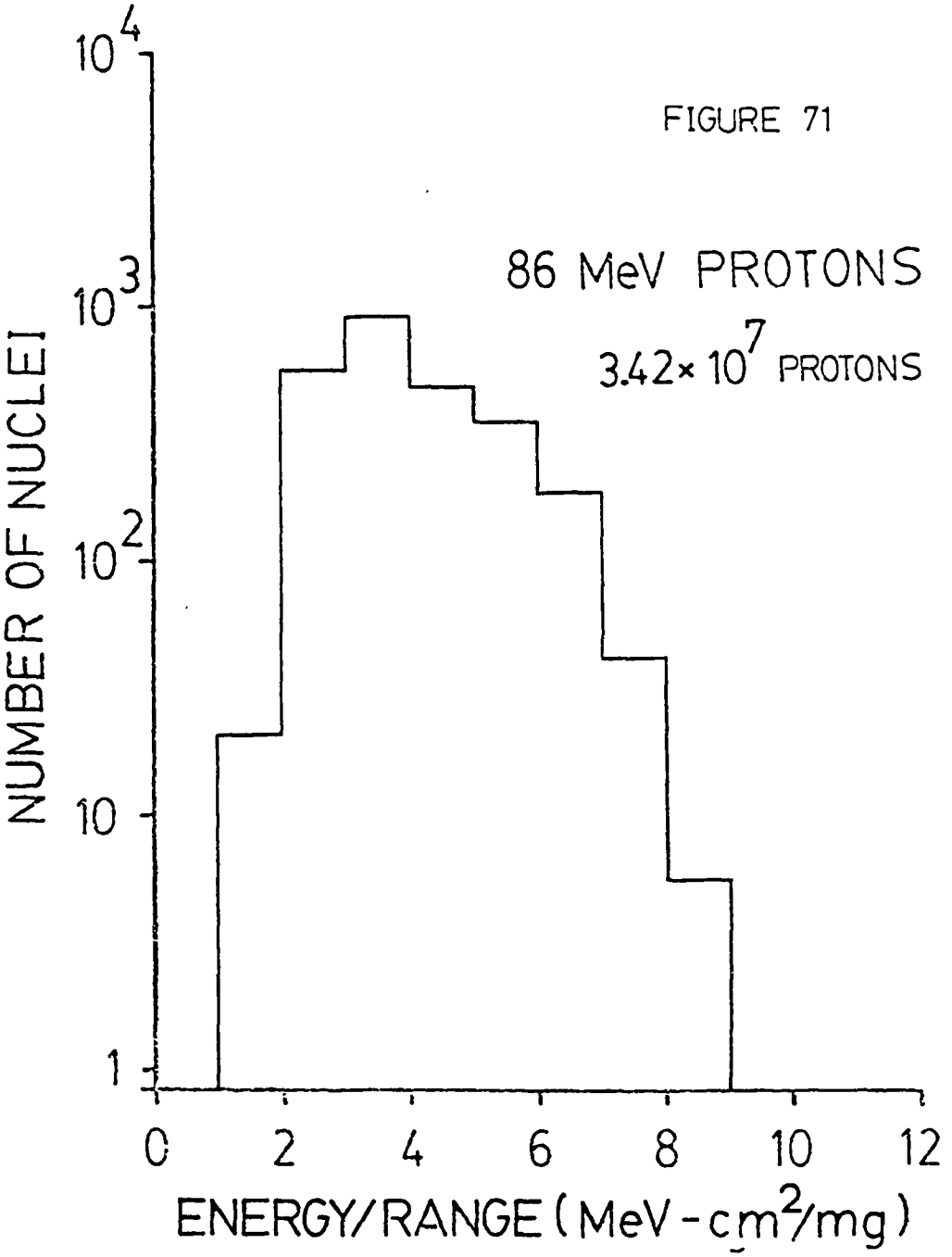
86 MeV PROTONS
3.42× 10^7 PROTONS
NUMBER OF NUCLEI
10^4
10^3
10^2
10
1
0
2
4
6
8
10
12
ENERGY/RANGE (MeV - cm^2/mg)

FIGURE 72

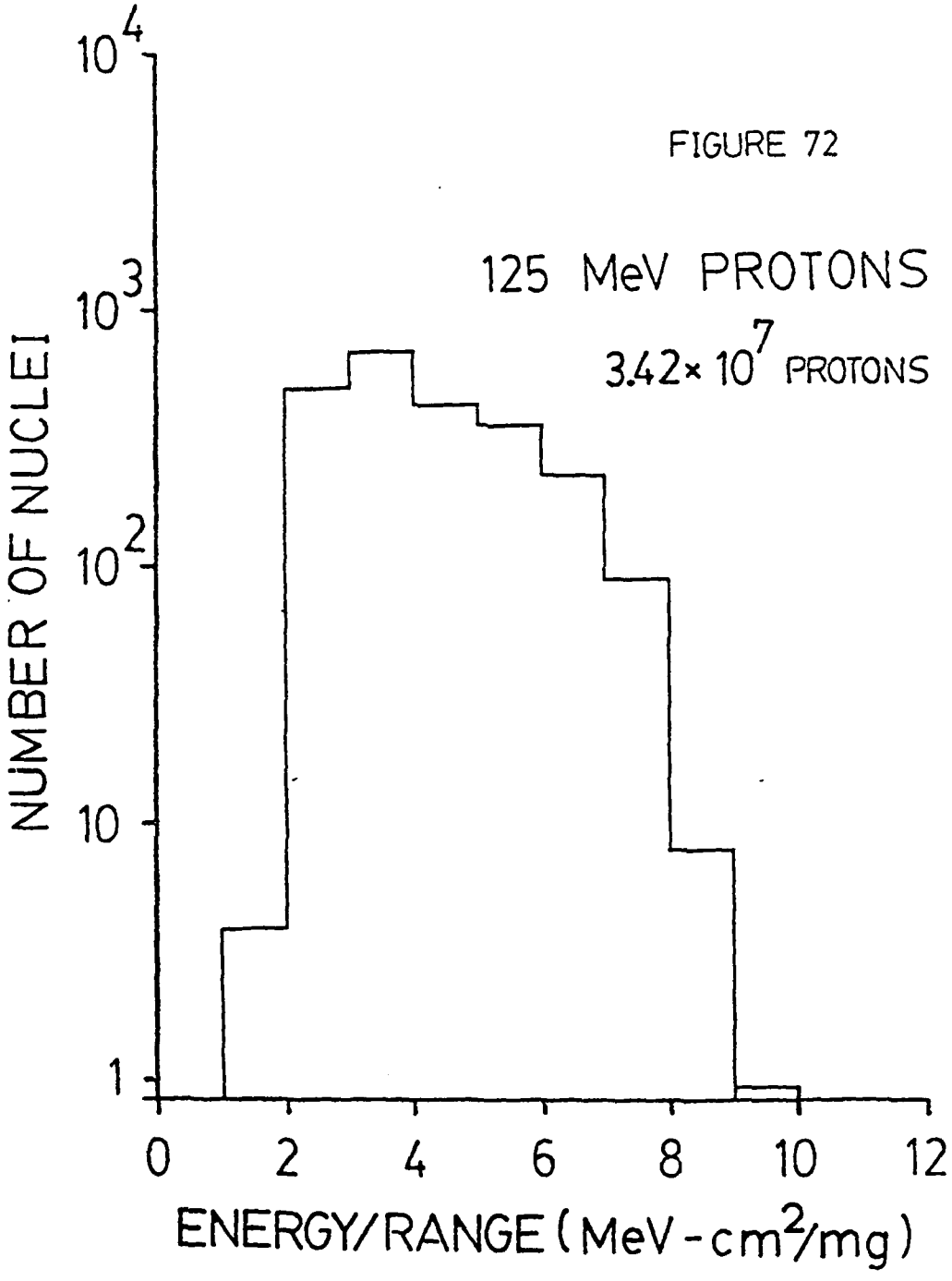
125 MeV PROTONS
3.42× 10^7 PROTONS
NUMBER OF NUCLEI
10^4
10^3
10^2
10
1
0
2
4
6
8
10
12
ENERGY/RANGE (MeV-cm^2/mg)

FIGURE 73

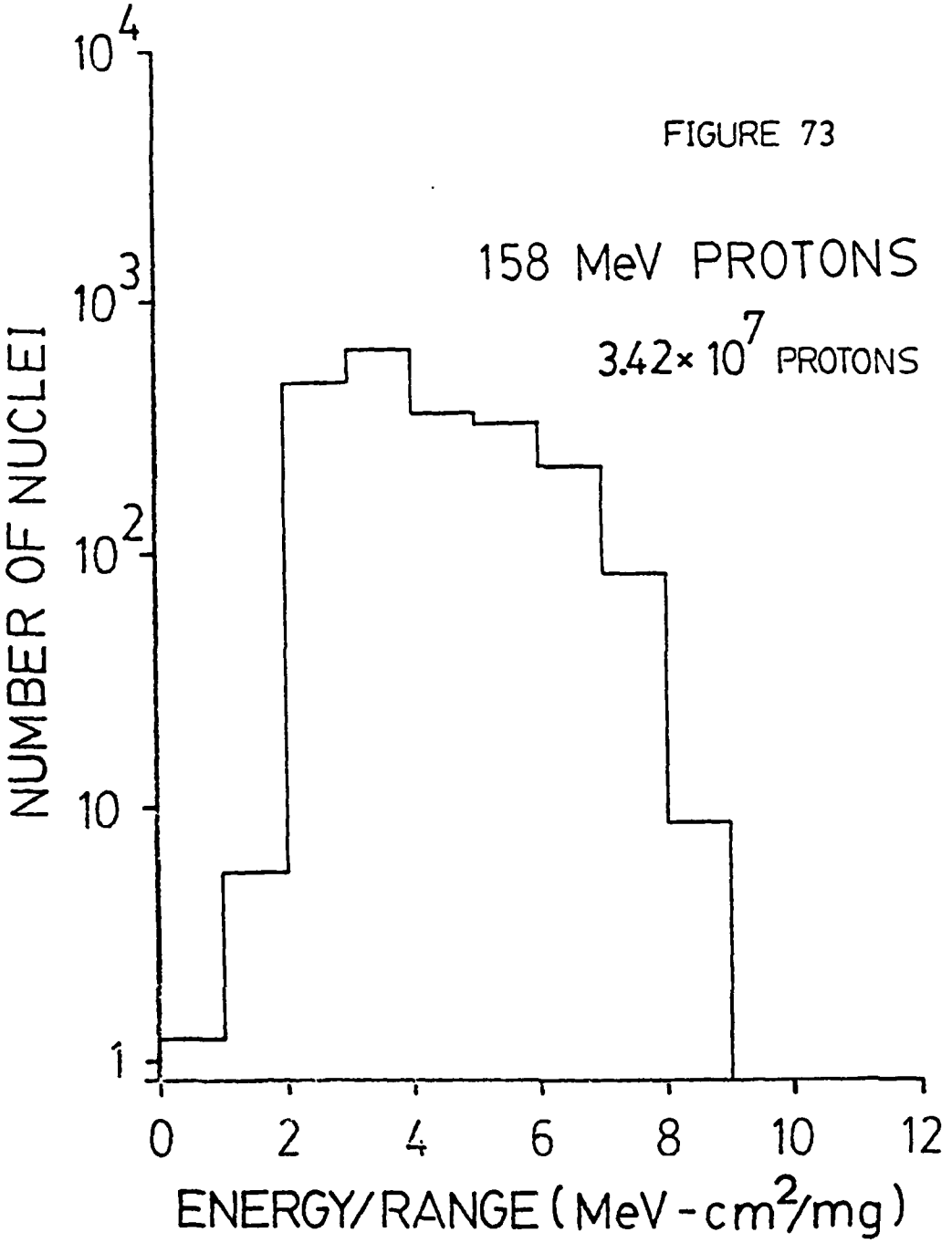
158 MeV PROTONS
3.42× 10^7 PROTONS
NUMBER OF NUCLEI
10^4
10^3
10^2
10
1
0
2
4
6
8
10
12
ENERGY/RANGE (MeV - cm^2/mg)

FIGURE 74

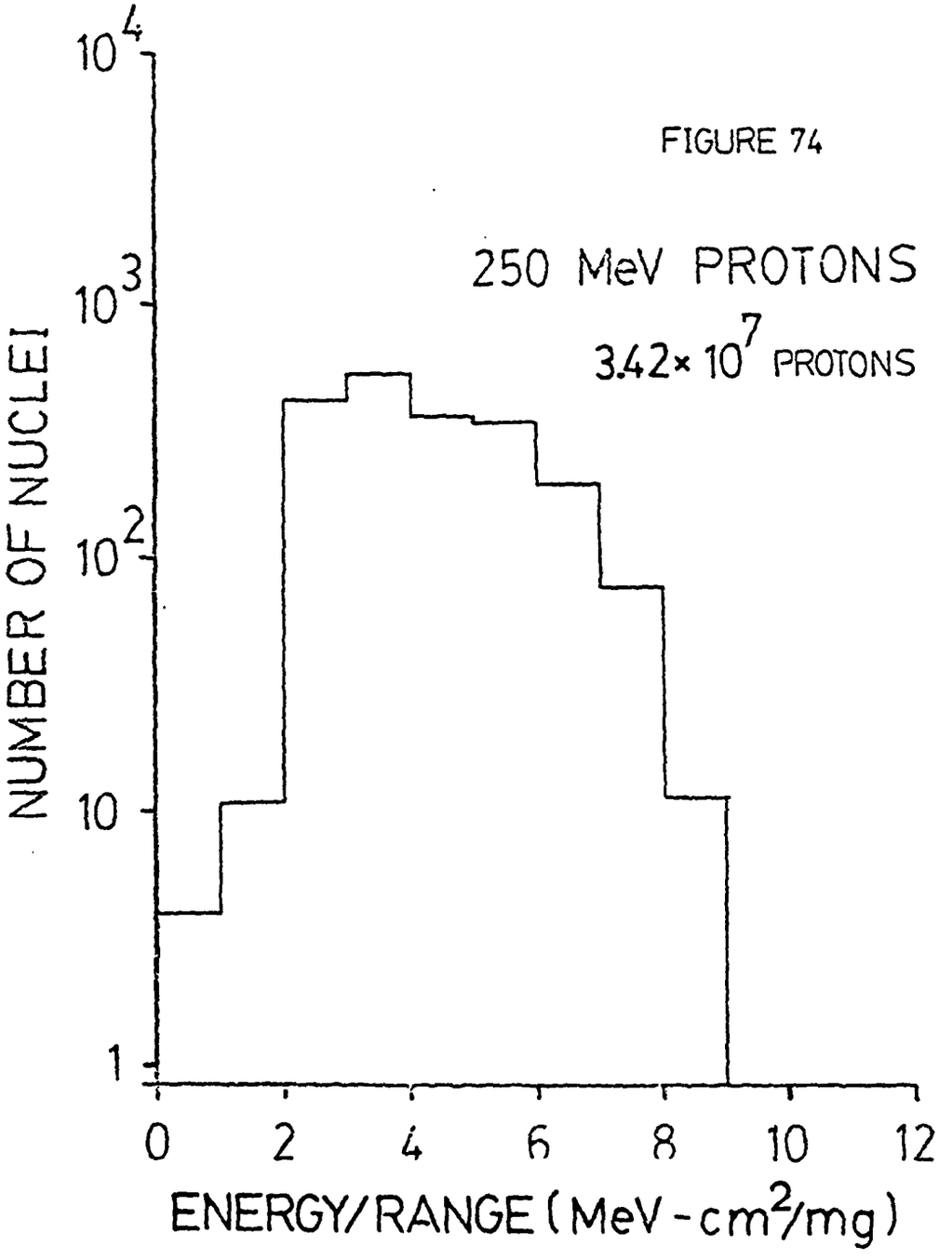
250 MeV PROTONS
3.42× 10^7 PROTONS
NUMBER OF NUCLEI
10^4
10^3
10^2
10
1
0
2
4
6
8
10
12
ENERGY/RANGE (MeV - cm^2/mg)

FIGURE 75

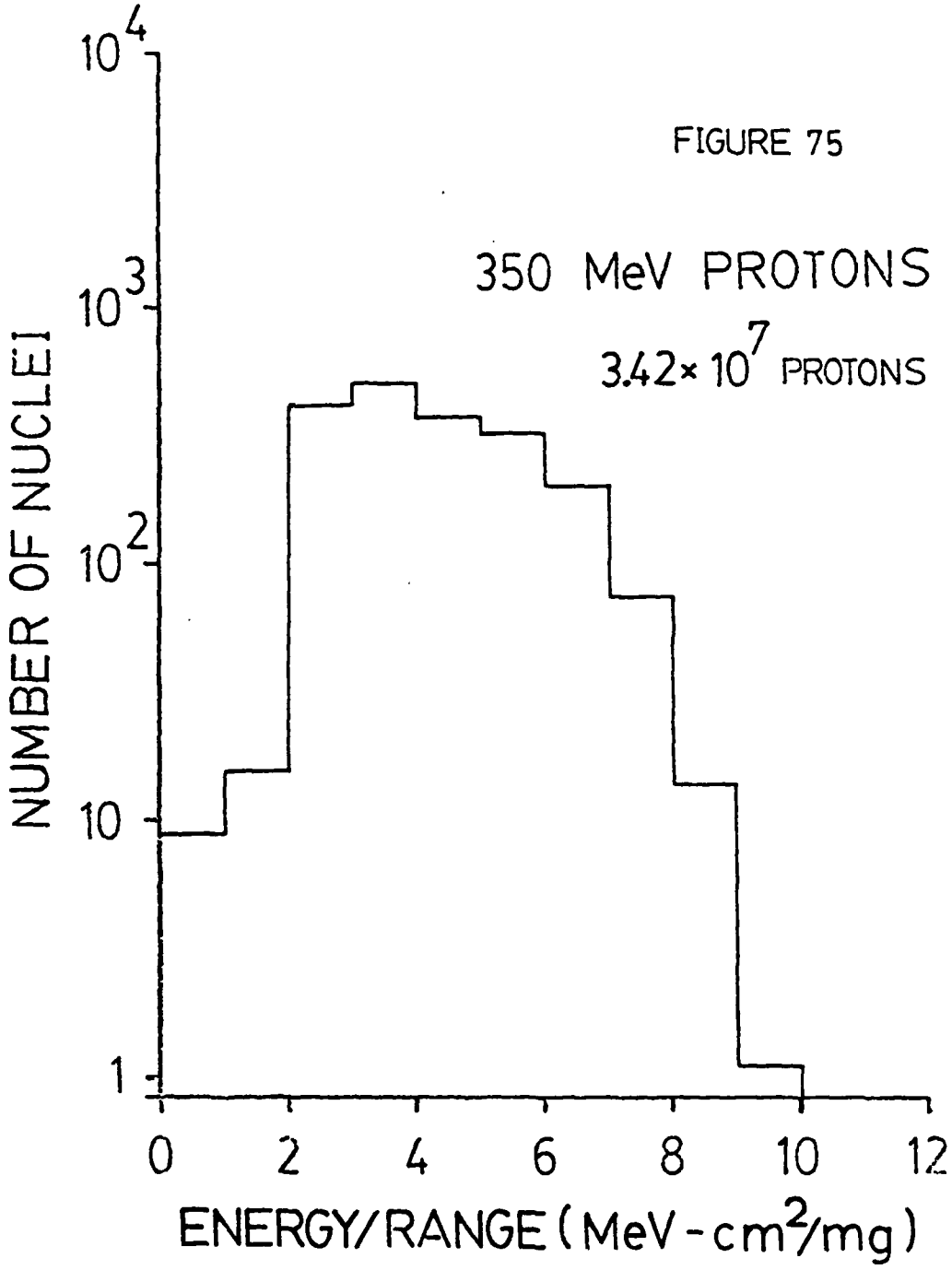
350 MeV PROTONS
3.42× 10^7 PROTONS
NUMBER OF NUCLEI
10^4
10^3
10^2
10
1
0
2
4
6
8
10
12
ENERGY/RANGE (MeV - cm^2/mg)

In Figures 76-79 the effects of the material surrounding the sensitive volume are examined. In Figures 76 and 77 a 10 um x 10 um x 2.5 um sensitive volume is at the center of a 30 um x 30 um x 30 um large volume. Figure 76 shows the energy deposition spectrum for a monoenergetic beam of 125 MeV protons, and Figure 77 shows the energy deposition spectrum for a proton energy distribution used to model a region of the Earth's radiation belt known as the SAA (South Atlantic Anomaly).

Figures 78 and 79 show the energy deposition spectra in a 10 um x 10 um x 2.5 um sensitive volume with no surrounding material. Figure 78 is for a 125 MeV proton beam, and Figure 79 is for the SAA distribution.

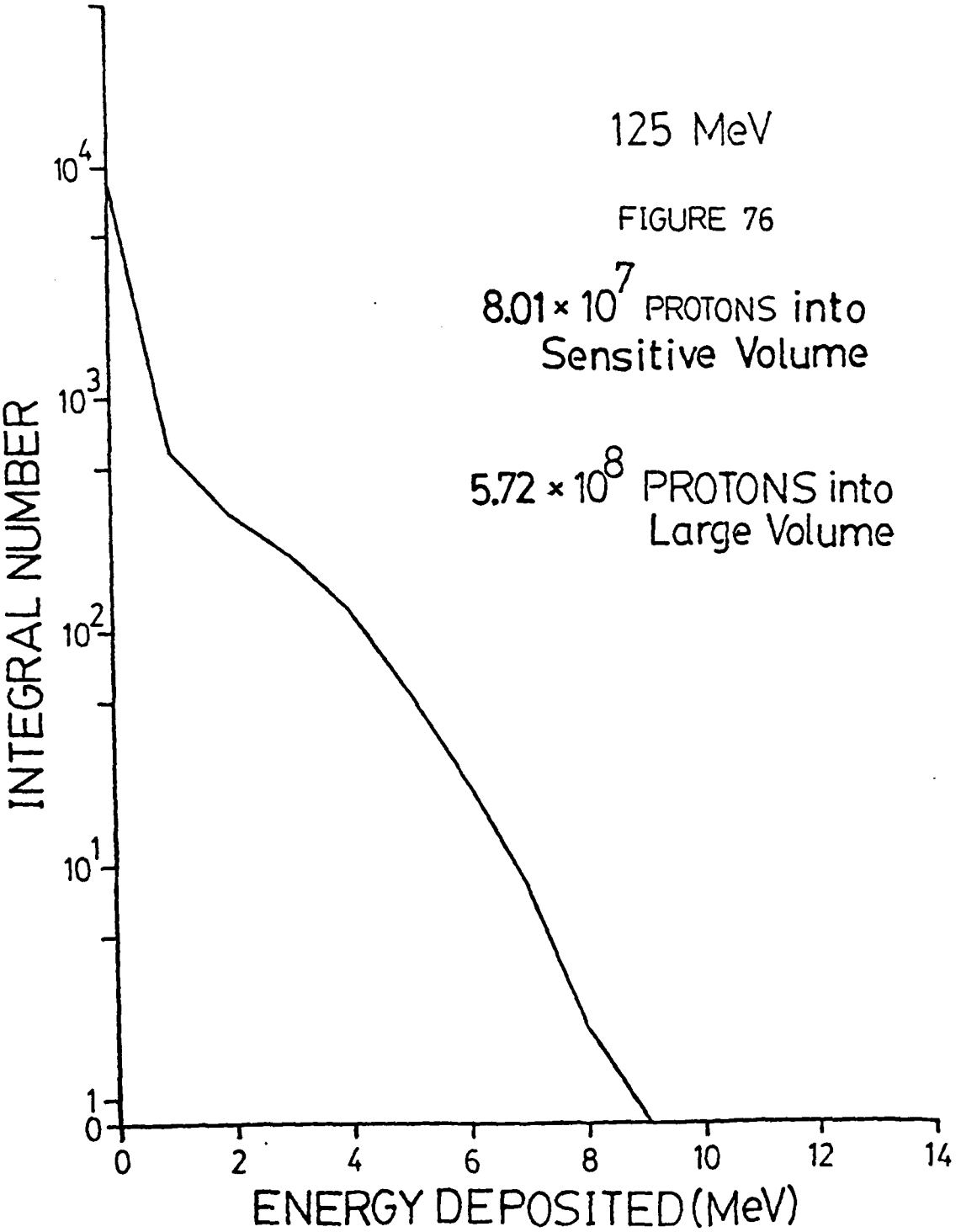
125 MeV
FIGURE 76
8.01 × 10^7 PROTONS into Sensitive Volume
5.72 × 10^8 PROTONS into Large Volume
INTEGRAL NUMBER
10^4
10^3
10^2
10^1
1
0
0
2
4
6
8
10
12
14
ENERGY DEPOSITED (MeV)

FIGURE 77

SAA

8.96×10^7 PROTONS into Sensitive Volume

5.52×10^8 PROTONS into Large Volume

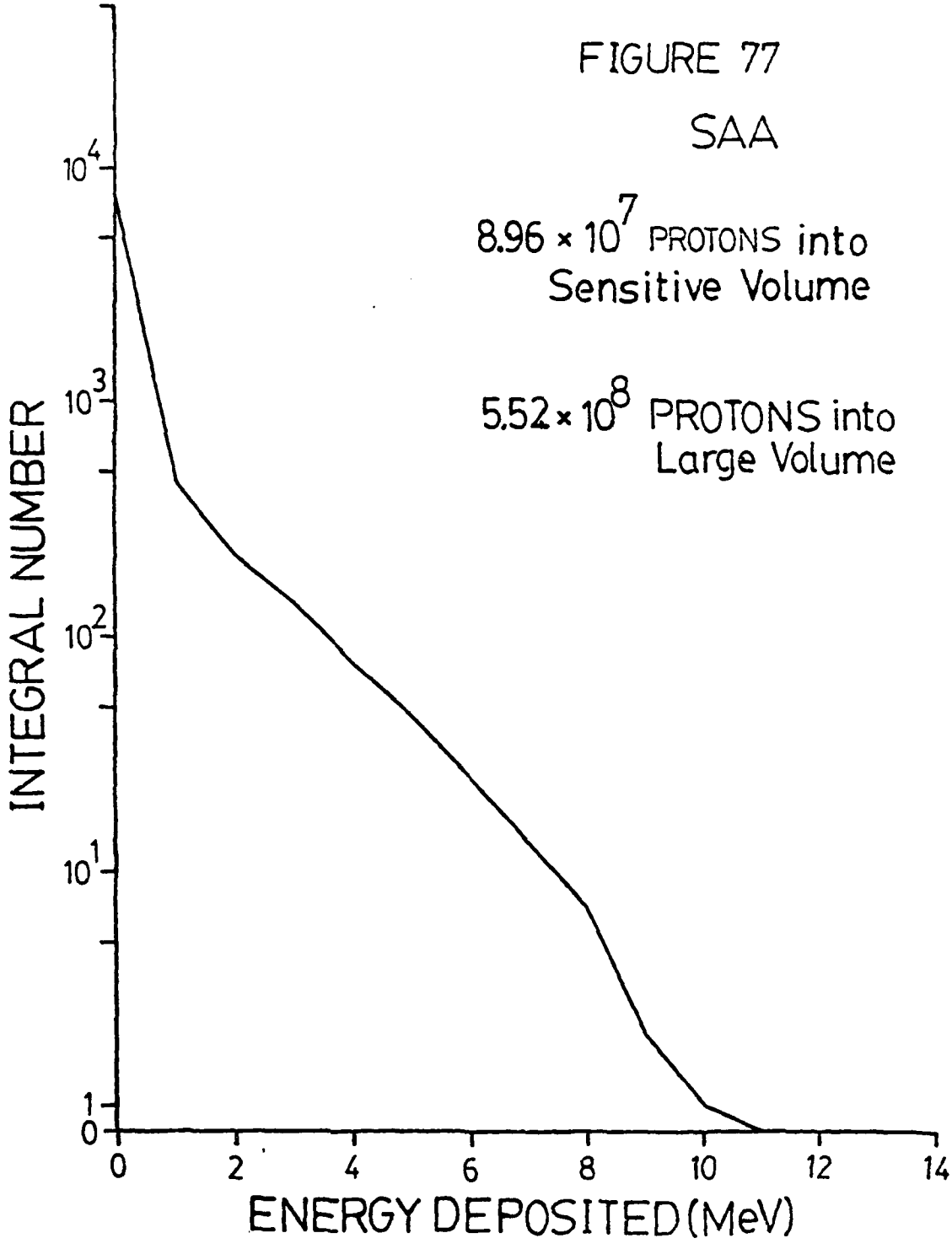

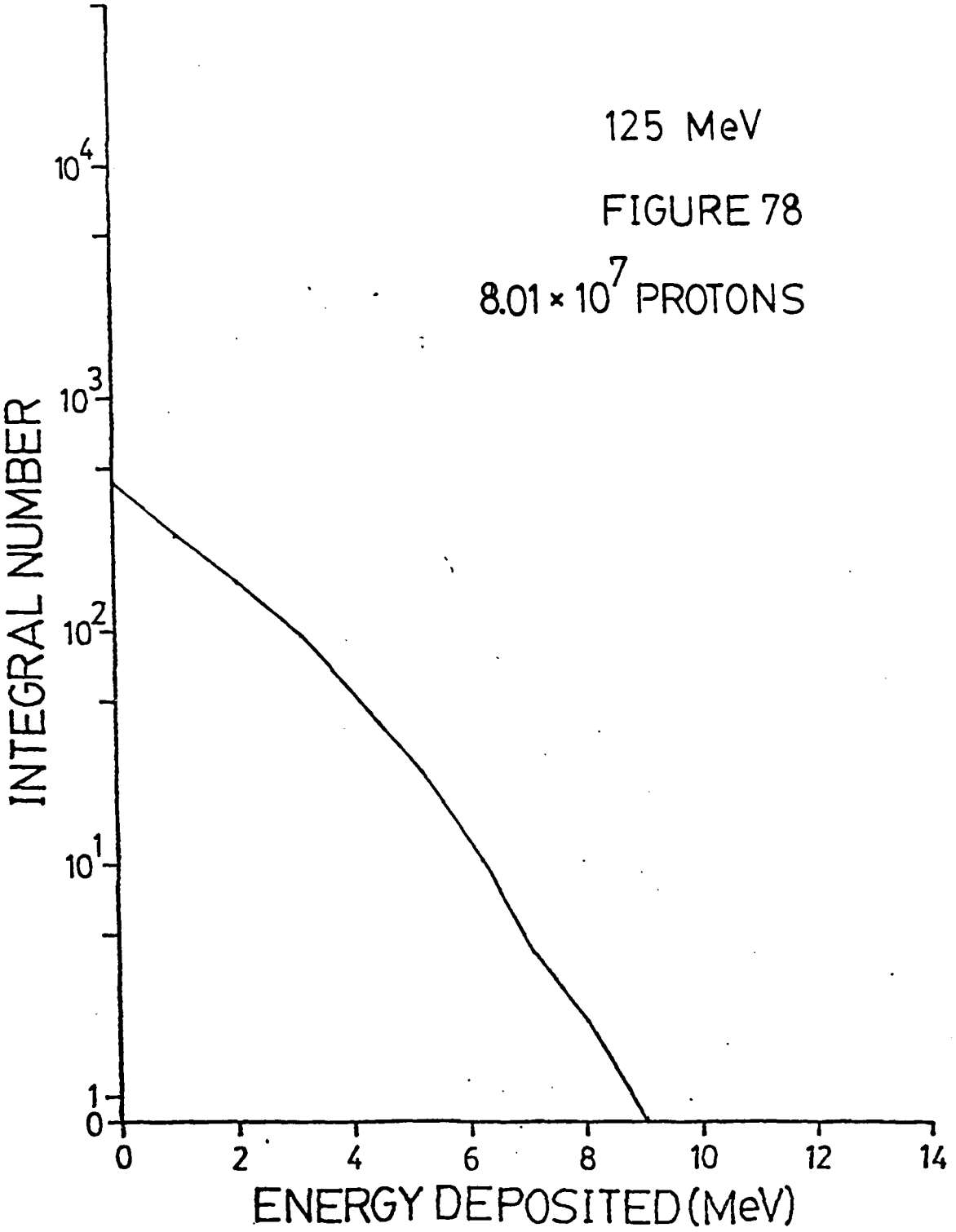
125 MeV
FIGURE 78
8.01 × 10^7 PROTONS
INTEGRAL NUMBER
10^4
10^3
10^2
10^1
1
0
0
2
4
6
8
10
12
14
ENERGY DEPOSITED (MeV)

FIGURE 79

SAA

8.96×10^7 PROTONS

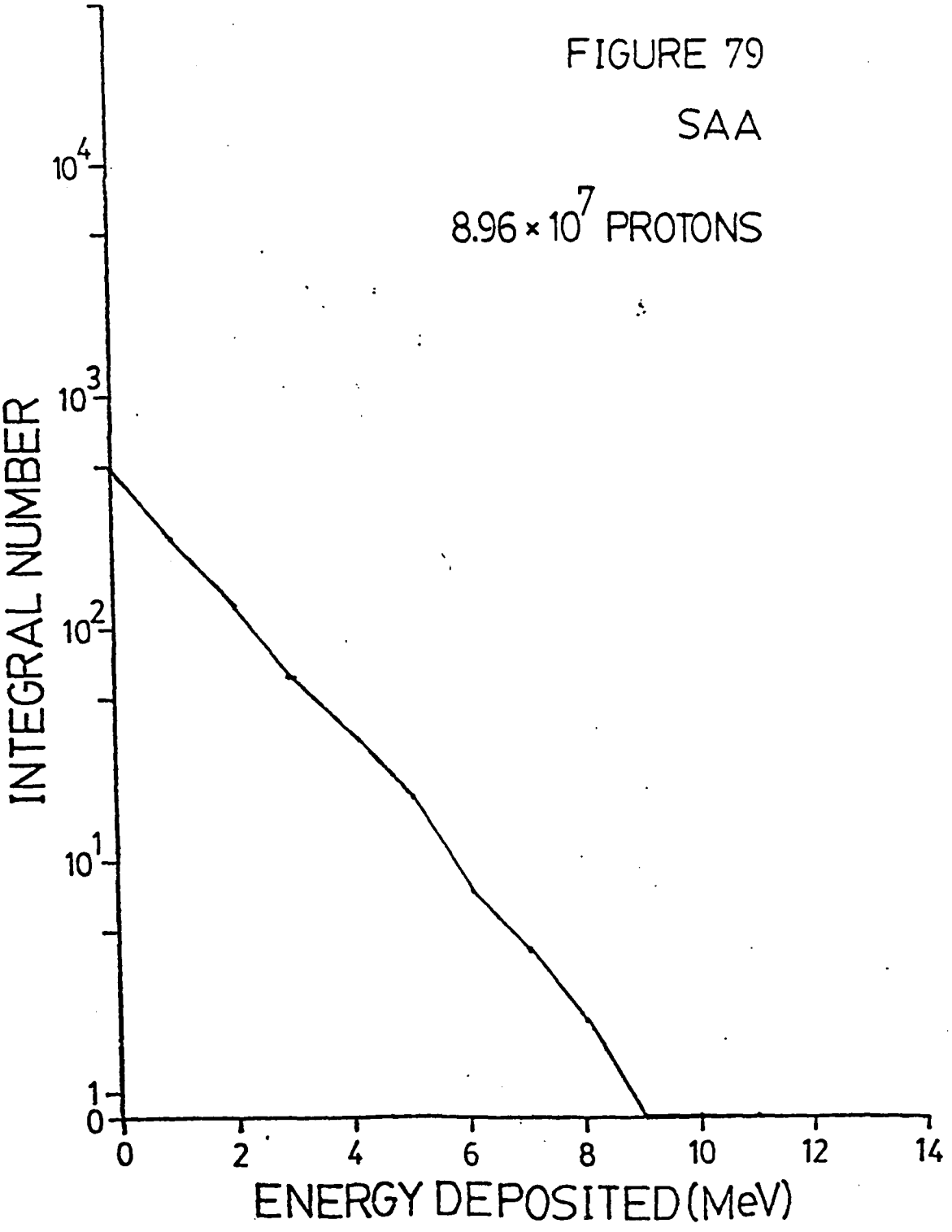

VII. SUMMARY

A computer simulation has been developed which calculates the spectrum of energy deposited in a small volume by nuclear interactions. The results have been compared to experiments run at the Harvard Cyclotron, and predictions of the nuclear model used in the simulation have been compared to other models and other experiments.

The most important conclusion involves the heavy recoiling nucleus that results from a nuclear interaction. For certain small volumes the energy deposition is dominated by this fragment. This has been overlooked by previous investigators of the microelectronics soft error problem.

Comparisons between this computer simulation and other models and experiments are reasonable. The existing codes differ substantially among themselves. There is some indication from the detector experiments that the enhanced energy deposition predicted by the pre-equilibrium model is in fact occurring.[102]

The silicon detector experiments agree well with the simulation over detector thickness sizes from 2.5 um to 97 um, and an energy range of 51 MeV to 158 MeV. The thinner detectors have thicknesses in the size range of LSI devices, indicating that the model is applicable to microelectronics.

Given the dimensions of the sensitive volume on a device, together with the critical charge for an upset, the

model can predict the soft error rate. This has particular importance for devices flown in space. Given the dimensions of a retinal receptor, the model can predict the rate at which light flashes will be seen. The model can also be applied to the field of radiation induced mutations.

BIBLIOGRAPHY

1. T.C. May and M.H. Woods, IEEE Transactions on Electron Devices ED-26, 2 (1979).
2. J.T. Wallmark and S.M. Marcus, Proceedings of the IRE 50, 286 (1962).
3. D. Binder, E. Smith, and A. Holman, IEEE Transactions on Nuclear Science NS-22, 2675 (1975).
4. J.N. Bradford, IEEE Transactions on Nuclear Science NS-25, 1144 (1978).
5. J.C. Pickel and J.T. Blandford, Jr., IEEE Transactions on Nuclear Science NS-25, 1166 (1978).
6. R.N. Noyce, Scientific American 237, 62 (1977).
7. J.N. Bradford, Journal of Applied Physics 50, 3799 (1979).
8. J.N. Bradford, IEEE Transactions on Nuclear Science NS-27, 942 (1980).
9. D.S. Yaney, J.T. Nelson, and L. Vanskike, IEEE Transactions on Electron Devices ED-26, 10 (1979).
10. R.P. Capece, Electronics, p. 85, March 15, 1979.
11. J.N. Bradford, Expected Contributions to LSI/VLSI RAM Soft Error Rates by Solar and Cosmic Protons -- Some Implications for Beam Weaponry, Technical Memorandum RADC-TM-79-ES-02, March 1979.
12. S. Kirkpatrick, IEEE Transactions on Electron Devices ED-26, 1742 (1979).
13. J.F. Ziegler and W.A. Lanford, Science 206, 776 (1979).
14. R.C. Wyatt, P.J. McNulty, P. Toumbas, P.L. Rothwell,

and R.C. Filz, IEEE Transactions on Nuclear Science NS-26, 4905 (1979).

15. P.J. McNulty, R.C. Wyatt, G.E. Farrell, R.C. Filz, and P.L. Rothwell, pp. 413-433 in Space Systems and Their Interactions with Earth's Space Environment, Edited by H.B. Garrett and C.P. Pike, American Institute of Aeronautics and Astronautics, New York 1980.
16. L.L. Sivo and J.C. Peden, IEEE Transactions on Nuclear Science NS-26, 5042 (1979).
17. R.N. Hamm, J.E. Turner, H.A. Wright, and R.H. Ritchie, ibid., NS-26, 4892 (1979).
18. G.J. Brucker, W. Chater, and W.A. Kolasinski ibid., NS-27, 1490 (1980).
19. W.A. Kolasinski, J.B. Blake, J.K. Anthony, W.E. Price, and E.C. Smith, ibid., NS-26, 5087 (1979).
20. C.S. Guenzer, E.A. Wolicki, and R.G. Allas, ibid., NS-26, 5048 (1979).
21. J.C. Pickel and J.T. Blandford, Jr., ibid., NS-27, 1006 (1980).
22. P.J. McNulty, G.E. Farrell, R.C. Wyatt, P.L. Rothwell, R.C. Filz, and J.N. Bradford, ibid., NS-27, 1516 (1980).
23. W.E. Price, D.K. Nichols, and K.A. Soliman, ibid., NS-27, 1506 (1980).
24. E. Peterson, ibid., NS-27, 1494 (1980).
25. J.N. Bradford, ibid., NS-27, 1480 (1980).
26. G.J. Brucker, W. Chater, and W.A. Kolasinski, ibid.,

NS-27, 1490 (1980).

27. A.B. Campbell and E.A. Wolicki, ibid., NS-27, 1509 (1980).

28. C.S. Guenzer, R.G. Allas, A.B. Campbell, J.M. Kidd, E.L. Petersen, N. Seeman, and E.A. Wolicki, ibid., NS-27, 1485 (1980).

29. C.M. Hsieh, P.C. Murley, and R.R. O'Brien, IEEE Electron Device Letters EDL-2, 103 (1981).

30. P.J. McNulty, G.E. Farrell, and W.P. Tucker, IEEE Transactions on Nuclear Science NS-28, 4007 (1981).

31. R.N. Hamm, M.L. Rustgi, H.A. Wright, and J.E. Turner, ibid., NS-28, 4004 (1981).

32. W.E. Price, J.C. Pickel, T. Ellis, and F.B. Frazee, ibid., NS-28, 3946 (1981).

33. C.S. Guenzer, A.B. Campbell, and P. Shapiro, ibid., NS-28, 3955 (1981).

34. D.K. Myers, W.E. Price, and D.K. Nichols, ibid., NS-28, 3959 (1981).

35. J.C. Pickel and J.T. Blandford, Jr., ibid., NS-28, 3962 (1981).

36. E. Petersen, ibid., NS-28, 3981 (1981).

37. W.A. Kolasinski, R. Koga, J.B. Blake, and S.E. Diehl, ibid., NS-28, 4013 (1981).

38. A.R. Knudson and A.B. Campbell, ibid., NS-28, 4017 (1981).

39. J.P. Woods, D.K. Nichols, and W.E. Price, ibid., NS-28, 4022 (1981).

40. C. Hu, IEEE Electron Device Letters EDL-3, 31

(1982).

41. G.E. Farrell and P.J. McNulty, IEEE Transactions on Nuclear Science NS-29, 2012 (1982).

42. F.B. McLean and T.R. Oldham, ibid., NS-29, 2018 (1982).

43. G.C. Messenger, ibid., NS-29, 2024 (1982).

44. S.E. Diehl, A. Ochoa, Jr., P.V. Dressendorfer, R. Koga, and W.A. Kolasinski, ibid., NS-29, 2032 (1982).

45. J.L. Andrews, J.E. Schroeder, B.L. Gingerich, W.A. Kolasinski, R. Koga, and S.E. Diehl, ibid., NS-29, 2040 (1982).

46. W.A. Kolasinski, R. Koga, J.B. Blake, G. Brucker, P. Pandya, E. Petersen, and W. Price, ibid., NS-29, 2044 (1982).

47. J.C. Pickel, ibid., NS-29, 2049 (1982).

48. E.L. Peterson, P. Shapiro, J.H. Adams, Jr., and E.A. Burke, ibid., NS-29, 2055 (1982).

49. W.E. Price, D.K. Nichols, P.R. Measel, and K.L. Wahlin, ibid., NS-29, 2064 (1982).

50. A.B. Campbell and A.R. Knudson, ibid., NS-29, 2067 (1982).

51. P. Shapiro, A.B. Campbell, E.L. Petersen, and L.T. Myers, ibid., NS-29, 2072 (1982).

52. D.K. Nichols, W.E. Price, and J.L. Andrews, ibid., NS-29, 2081 (1982).

53. J.M. Bradford, ibid., NS-29, 2085 (1982).

54. R. Magno, M. Nisenoff, R. Shelby, J. Kidd, and A.B.

Campbell, ibid., NS-29, 2090 (1082).

55. L.S. Pinsky, W.Z. Osborne, J.V. Bailey, R.E. Benson, and L.F. Thompson, Science 183, 957 (1974).

56. L.S. Pinsky, W.Z. Osborne, R.A. Hoffman, and J.V. Bailey, Science 188, 928 (1975).

57. J.H. Fremlin, New Scientist 47, 42 (1970).

58. C.A. Tobias, T.F. Budinger, and J.T. Lyman, Nature 230, 596 (1971).

59. P.J. McNulty, Nature 234, 110 (1971).

60. T.F. Budinger, H. Bichsel, and C.A. Tobias, Science 172, 808 (1971).

61. P.J. McNulty, V. Pease, V.P. Bond, W. Schimmerling, and K.G. Vosburgh, Science 178, 160 (1972).

62. P.J. McNulty, V.P. Pease, and V.P. Bond, Science 189, 453 (1975).

63. P.J. McNulty, V.P. Pease, and V.P. Bond, Journal of the Optical Society of America 66, 49 (1976).

64. P.J. McNulty, V.P. Pease, and V.P. Bond, Radiation Research 66, 519 (1976).

65. P.J. McNulty, V.P. Pease, and V.P. Bond, Science 201, 341 (1978).

66. R. Madey and P.J. McNulty, Proceedings of the National Symposium on Natural and Manmade Radiation in Space, edited by E.A. Warman, pp. 757-766, January 1972.

67. P.J. McNulty and R. Madey, Proceedings of the National Symposium on Natural and Manmade Radiation in Space, edited by E.A. Warman,

pp. 767-772, January 1972.

68. C.A. Tobias, T.F. Budinger, and J.T. Lyman, Proceedings of the National Symposium on Natural and Manmade Radiation in Space, edited by E.A. Warman,pp. 757-766, January 1972.

69. P.L. Rothwell, R.C. Filz, and P.J. McNulty, Science 193, 1002 (1976).

70. P.J. McNulty, V.P. Pease, V.P. Bond, R.C. Filz, and P.L. Rothwell, Radiation Effects 34, 153 (1977).

71. A.M. Kellerer and H.H. Rossi, Current Topics in Radiation Research Quarterly 8, 85 (1972).

72. P.J. McNulty, private communication.

73. CCC-156/MECC-7 Code Package, RSIC Computer Code Collection, Oak Ridge National Laboratory, Oak Ridge, Tennessee.

74. K. Chen, Z. Fraenkel, G. Friedlander, J.R. Grover, J.M. Miller, and Y. Shimamoto, Physical Review 166, 949 (1968).

75. A.S. Goldhaber, Physics Letters 53B, 306 (1974).

76. R. Silberberg and C.H. Tsao, Astrophysical Journal Supplement 25, 315 (1973).

77. R. Serber, Physical Review 72, 1114 (1947).

78. V.F. Weisskopf, Physical Review 52, 295 (1937).

79. M.L. Goldberger, Physical Review 74, 1268 (1948).

80. G. Bernardini, E.T. Booth, and S.J. Lindenbaum, Physical Review 85, 826 (1952).

81. N. Metropolis, R. Bivins, M. Storm, A. Turkevich, J.M. Miller, and G. Friedlander, Physical Review

110, 185 (1958).

82. K. Chen, G. Friedlander, and J.M Miller, Physical Review 176, 1208 (1968).

83. K. Chen, G. Friedlander, G.D. Harp, and J.M. Miller, Physical Review C4, 2234 (1971).

84. H.W. Bertini, Physical Review 131, 1801 (1963).

85. H.W. Bertini, Physical Review 171, 1261 (1968).

86. H.W. Bertini, Physical Review 188, 1711 (1969).

87. H.W. Bertini, Physical Review C6, 631 (1972).

88. H.W. Bertini, A.H. Culkowski, O.W. Hermann, N.B. Gove, and M.P. Guthrie, Physical Review C17, 1382 (1978).

89. I. Dostrovsky, Z. Fraenkel, and G. Friedlander, Physical Review 116, 683 (1959).

90. H. Hurwitz and H.A. Bethe, Physical Review 81, 898 (1951).

91. A.G.W. Cameron, Canadian Journal of Physics 36, 1040 (1958).

92. A.G.W. Cameron, Canadian Journal of Physics 35, 1021 (1957).

93. L. Dresner, ORNL-TM-196, Oak Ridge National Laboratory, Oak Ridge, Tennessee (1961).

94. M.P. Guthrie, ORNL-4379, Oak Ridge National Laboratory, Oak Ridge, Tennessee (1969).

95. M.P. Guthrie, ORNL-TM-3119, Oak Ridge National Laboratory, Oak Ridge, Tennessee (1970).

96. R.W. Peelle and P.M. Aebersold, ORNL-TM-1538, Oak Ridge National Laboratory, Oak Ridge, Tennessee

(1966).

97. G.J. Mathews, B.G. Glagola, R.A. Moyle, and V.E. Viola, Jr., Physical Review C25, 2181 (1982).

98. M. Blann, Annual Review of Nuclear Science 25, 123 (1975).

99. V.S. Barashenkov, H.W. Bertini, K. Chen, G. Friedlander, G.D. Harp, A.S. Iljinov, J.M. Miller, and V.D. Toneev, Nuclear Physics A187, 531 (1972).

100. J. Jastrzebski, H.J. Karwowski, M. Sadler, and P.P. Singh, Physical Review C22, 1443 (1980).

101. L.C. Northcliffe and R.F. Schilling, Nuclear Data, Tables, A7, pp. 233-463 (1970).

102. K. Kwiatkowski, S.H. Zhou, T.E. Ward, V.E. Viola, Jr., H. Breuer, G.J. Mathews, A. Gokmen, and A.C. Mignerey, preprint, Indiana University Cyclotron Facility, January 1983.

103. J.F. Janni, Atomic Data and Nuclear Data Tables 27, p. 176 (1982).